2015-03-01

Advancing Biomechanical Research Through a Camelid Model of the Human Lumbar Spine

Dean K. Stolworthy
Brigham Young University - Provo

Advancing Biomechanical Research Through a Camelid Model of the Human Lumbar Spine

Dean Keith Stolworthy

A dissertation submitted to the faculty of
Brigham Young University
in partial fulfillment of the requirements for the degree of

Doctor of Philosophy

Anton E. Bowden, Chair
Larry L. Howell
David T. Fullwood
Laura C. Bridgewater
Beverly L. Roeder

Department of Mechanical Engineering

Brigham Young University

March 2015

ABSTRACT

Advancing Biomechanical Research
Through a Camelid Model of the
Human Lumbar Spine

Dean Keith Stolworthy
Department of Mechanical Engineering, BYU
Doctor of Philosophy

The increasing incidence of disc degeneration and its correlation with lower back pain is an alarming trend in modern society. The research of intervertebral disc degeneration and low back pain would greatly benefit from additional methods to study its etiology and possible treatment methods. A large animal model that maintains the biological and mechanical environment that is most similar to the human lumbar spine could provide substantial improvements in understanding and resolving the problem of intervertebral disc related low back pain.

This dissertation presents my doctoral work of investigating the potential for the camelid cervical spine to serve as a suitable animal model for advancing biomechanical research of low back pain and intervertebral disc degeneration in the human lumbar spine. Specifically, this work identifies the cellular, morphological and biomechanical characteristics of the camelid cervical spine and intervertebral disc as compared to the human lumbar spine. My results demonstrate that there are remarkable similarities in all aspects. Many of the similarities with respect to the cellular environment of the intervertebral disc are a consequence of the camelid status as a large mammal. Additional testing of the cellular makeup of the camelid intervertebral disc cells revealed that many human qRT-PCR primers associated with disc degeneration are suitable for use in alpacas without modification. From a biomechanics standpoint, the camelid cervical spine also has a vertically oriented spinal posture and is unsupported near the end in an open kinetic chain, providing a mechanical parallel with the human lumbar spine. The camelid cervical intervertebral disc size is closer to the human lumbar intervertebral disc than all other currently used animal models available for comparison in the literature. Average flexibility (range of motion) of a camelid spinal motion segment showed similarities in all modes of loading. Based on magnetic resonance imaging and radiologic grading of the intervertebral disc, almost 90% of elderly camelids exhibited advanced degeneration (Pfirrmann grade 3 or higher) in their cervical spine, and about half of aged camelids have developed severe degeneration (Pfirrmann grade 4 or higher) in at least one or more of their cervical segments, most commonly within the two lowest cervical segments (e.g. c6c7 and/or c7t1). Thus, while there remain differences, the remarkable similarities between the camelid and human spine strengthen the case for using camelids as a model for human disc degeneration, normal and pathological biomechanics and fluid transport, and potentially as a pre-clinical model for investigating the efficacy of novel spinal devices.

Keywords: animal model, spine, intervertebral disc, disc degeneration, biomechanics, orthopaedics, camelid

ACKNOWLEDGEMENTS

I would first like to thank all those on my committee. Each one has served as a technical, professional, and personal example, throughout this whole experience. Dr. Bowden especially has been a great mentor. I have been very blessed by the advice and support that he has given to me from the first time I spoke to him. I am extremely grateful for the opportunity I have had to study at this institution, Brigham Young University (BYU) as I am continually amazed and inspired by the faculty, staff, and fellow students that I associate with at BYU. One faculty member (not on my committee) who really went out of the way to make this research possible is Dr. Todd Robinson. I appreciate all of his contributions with my research.

I'd like to thank Dr. Bridgewater and the research assistants from her lab, especially Loyd Christensen, and Jake Holland. They taught me a lot about proper MMBio lab protocol. I appreciate the time provided by Steve Barber from the RIC-facility while training me to use the fluorescent microscope. The BYU MRI Research Facility was excellent to work with; specifically, Dr. Bangerter, Michelle Nash, and Merry Taylor. Their technical expertise was critical to this research. I appreciate the clinical expertise offered by Dr. John Wendel and Dr. Susanne Stiegar-Vanegas; they provided their time and contributions in regards to the MRI research. I am grateful for the time that Dr. Eggett spent reviewing my statistical analysis methods and SAS code. I would also like to thank all of the past and present research assistants of Dr. Bowden's BABEL group and Dr. Fullwood's nano-composite research group; the genuine friendships and comradery experienced here will last forever.

I am most grateful for all of my family, extended and immediate, especially my wife and my three (we currently only have three) favorite kids. I hope to be able to always support them in chasing their goals and dreams as well as they have supported me. Finally, I know there are a lot of other people, powers, and influences that have made this dream possible. The best way I feel that I can express my appreciation here is to continue moving forward, and continue being better each day.

TABLE OF CONTENTS

LIST OF TABLES

LIST OF FIGURES

1 INTRODUCTION

The human spine is a complex moveable structure, with biology and mechanics that simultaneously work together to maintain its health and function [1, 2]. Analogous with all mechanical devices, the probability of failure increases with the number of moving parts and joints. The human spine follows this standard as it consists of multiple intervertebral disc (IVD) joints that allow motion while also being implicated with low back pain, which affects 80% of the population, with 15% of the United States suffering from chronic low back pain [3]. While the cause of low back pain is often uncertain, it is most often attributed to degeneration of the IVD [4-7].

The lack of understanding for low back pain and intervertebral disc degeneration (IVDD; also referred to as degenerative disc disease, DDD) is due, at least in part, to the lack of available tissue for study. With few healthy tissue samples from humans to compare with unhealthy tissue samples, much effort has been devoted to the study of DDD in other species; however, the spine and IVD of these animals are often dissimilar to the respective human anatomy. Animals rarely experience DDD naturally, and several other important differences in regards to the cellular, morphological, and biomechanical environment of the spine, make them unfit for comparison. Ultimately, understanding the differences and specifically identifying the relevant similarities is key to finding a viable animal model for intervertebral disc degeneration. If there exist specific characteristics that predispose a human to develop DDD, then these characteristics might also predispose an animal to develop a similar condition. Likewise, if particular characteristics

combat DDD, then these should also be considered with future animal studies and should be considered when selecting an animal for future studies.

The discovery of a clinical paper that identified DDD in the lower cervical spine of a mature llama [8] prompted this research and hypothesis that camelids, specifically llamas and alpacas, often experience IVDD in their lower cervical spine due to similarities with the human lumbar spine, in regards to the cellular, morphological, and biomechanical environment. As such, the camelid cervical spine and intervertebral disc would be a good animal model to represent intervertebral disc degeneration in the human lumbar spine.

1.1 Motivation

The growing global problem of chronic low back pain is often correlated with DDD [9] and is one of the top-five reasons for hospital admissions, activity limitations, surgical procedures, and physician visits for people under 45 years of age in the United States [4, 10-13]. A large percentage of the aging human population is afflicted with this seemingly irreversible condition [11, 70], with approximately 40% of people under 30 years of age and upwards of 90% of people 55 years of age or older that reportedly suffer with moderate-to-severe levels of DDD in their lumbar IVDs [70].

In the United States alone, the economic impact of low back pain approaches upward of $625 billion [14, 15], in regards to medical costs, lost wages/taxes, disability claims, and workman's compensation. The concern with this growing problem is that the current solution of lumbar spinal fusion is reportedly ineffective for half of the patients [16, 17] as revisions surgeries are often required, and the validation process for future solutions is inadequate. Following the first spinal fusion surgery, approximately 60% never return to work, and 80%

never return to work after multiple fusions. They become functionally classified as permanently disabled [14, 15, 18, 19].

Our understanding of the potential mechanical causes of LBP and disc degeneration is primarily limited due to the difficult nature of obtaining and testing appropriate, live human material [20]. IVD research is most often destructive, and destructive tests require large sample sizes to verify statistical significance. There is simply not enough healthy IVD tissue to compare against unhealthy IVD tissue, Thus, much of our current understanding of the intervertebral disc has been obtained from cadaveric, ex-vivo testing methodologies [21-24]. Recently, in-vitro models have emerged that use human or animal tissue that is sustained using advanced bioreactors and cell culture techniques [25-27]. These techniques hold great promise, but are currently limited in scope (e.g., a single spinal disc without adjacent tissue or bone), mechanics (e.g., simple loading conditions), and availability (e.g., only a few specialized sites have demonstrated long-term survival of human discs) [28].

While past research has greatly enhanced our knowledge and understanding of the spine, the development of novel treatments is largely hampered because the research community lacks an appropriate model for testing and study. Current ex-vivo testing methodologies have provided exceptionally useful information. For example, numerical analysis studies help analyze nutrient flow and mechanical flexibility; biomechanical spine simulators may provide boundary conditions for the numerical studies or benchmark flexibility data for future orthopaedic devices; benchtop testing protocols using cadaver specimen increase our confidence in devices prior to FDA approval; and bioreactors allow the testing of some cellular therapies. However, none of these models can demonstrate efficacy of treatments in vivo, thus the design-prototype-test-cycle that is common to engineers is limited by the burdensome regulatory processes required for

human testing. A validation and testing platform is needed to address the dynamic, functional requirements of the human lumbar spine. In order to accelerate the development of better treatments for low back pain, a more readily accessible and characteristically similar model of the human condition is required, and this is most likely to occur with an animal model [20, 29]. Identifying a more accurate animal model is the most-likely approach to accelerating research and forging breakthroughs for disc degeneration and lower back pain [20, 30].

1.2 Objective

The objective of this work was to examine the hypothesis that the camelids (specifically llamas and alpacas) will naturally develop intervertebral disc degeneration due to similarities in the cellular, morphological and biomechanical environment, and therefore would be a good animal model for intervertebral disc degeneration in the human lumbar spine. Relevant background information is provided for the vertebral column and for other large animal models that are commonly used in orthopaedic research. Characteristics of the human spine, and an explanation for why these particular characteristics are important to capture in a potential animal model, are presented as desired characteristics for animal models of DDD. As intervertebral disc degeneration has proven to contain both biological and mechanical correlations, and considering that mammalian biology is extremely similar within all mammals, this research focuses primarily on the mechanical similarities of the alpaca and llama cervical spine to the human lumbar spine; specifically, morphological and biomechanical evaluations of the camelid cervical spine were performed for benchmark comparison with other animal models that are commonly used in spinal research, in addition to comparison with the human lumbar spine. The hypothesis is tested by determining the prevalence of intervertebral disc degeneration in several alpacas.

1.3 Document Organization

The contents of this dissertation come from multiple publications that were accepted or submitted for publication and are organized to present the findings in a clear and logical manner. Relevant background information is included; although, this is not considered a comprehensive review of animal models and intervertebral disc degeneration. Additional background and methodology information may also be found in my master's thesis [31].

Characteristics for a good animal model of DDD can be found in Chapter 3, and the separate research for the camelid animal model is found in Chapter 4 through Chapter 7. Chapter 4 describes the morphology of the alpaca and llama cervical IVD in regards to the shape and size. Alpaca and llama morphology were compared with published benchmark data from other large animal models, and the human cervical and lumbar intervertebral disc. Chapter 5 is focused on the biomechanical posture and flexibility of the alpaca and llama cervical spine, and includes comparisons with human cadaveric lumbar biomechanics, also obtained from my master's research, in addition to published values for the human cervical spine and other animal models. Chapter 6 describes the MRI study performed on 20 live alpacas to investigate the prevalence of intervertebral disc degeneration in the alpaca cervical spine, which was also compared to published values for the human spine. Chapter 7 contains a brief review of some preliminary research on the development of an intervertebral disc bioreactor, which is ongoing; Chapter 8 describes another ongoing project for tracking in vivo biomechanics using high-displacement nano-composite strain gauges. A summary of my doctoral work, conclusions, and recommendations for continuing this body of research can be found in Chapter 9.

1.4 Acknowledgements

This work was all made possible from the contributions and collaborations of many people and sources. I am grateful for the opportunity to use the equipment and work with the people at the BYU MRI Research Facility, RIC Facility, Bridgewater's Lab, Dr. Bowden's BABEL lab, and Dr. Fullwood's Nano-composite's lab, at Brigham Young University. Research funding for this work was provided by the National Science Foundation (NSF CMMI-0952758 and NSF CMMI-1235365). I appreciate the vast amounts of funding that is provided for scientific research, particularly in the academic environment.

Chapter 4 and Chapter 5 comprise portions of a paper that has been published in the Journal of Orthopaedic Translation [32]. These chapters describe the select aspects of the camelid cervical spine and intervertebral disc morphology and biomechanics. Coauthors for this paper include Tyler M. Merrell, R. Amy Fullwood, Anton E. Bowden, and Laura C. Bridgewater, all from BYU.

Chapter 6 is part of a paper that has been submitted for publication to the Journal of Orthopaedic Research. This chapter reports on the incidence rate of an imaging-based diagnosis of intervertebral disc degeneration in the alpaca cervical spine. Coauthors for this paper include Anton Bowden, Beverly Roeder, Todd Robinson, Jacob Holland, Loyd Christensen, Amanda Beatty, Laura Bridgewater, and Dennis Eggett, from BYU; John Wendel with Diversified Radiology (Denver, CO); and Susanne Stieger-Vanegas with Oregon State University (Corvallis, OR).

The work described in Chapter 7 has been included in multiple abstracts and presentations at research conferences. I initially began this work with the intent of developing an IVD bioreactor to sustain the life of the IVD cellular biology. This research is continued with

the master's research of Amanda Beatty in her development of a dynamic intervertebral disc bioreactor.

The collaborative work outlined in Chapter 8 has resulted in several presentations and publications, with several more potential publications in development. The section on high-displacement nano-composite strain gauge research includes background information that was used for gaining approval for tests on live, human subjects; portions of this section were presented as a conference paper at the Society of the Advancement of Material and Process Engineering [33] in addition to work that has been submitted for publication to the Journal of Applied Biomechanics. This work was directed by Taylor Remington, with support from Jake Merrell, Adam Bilodeau, David Fullwood, Anton Bowden and myself, all from BYU. Additional work is continued at BYU through the master's research of Dan Baradoy and others.

2 BACKGROUND

2.1 Vertebral Column

The primary purpose of the vertebral column, or spine, is to protect the spinal cord, while also providing an uninterrupted and flexible, structural element for the body. The spine consists of a series of interdependent joints that allow motion, while also providing support to those regions above each vertebral level. Based on location, the vertebral column is divided into different segments: the cervical segment in the neck, the thoracic segment in the chest (or upper back), the lumbar segment in the lower back, and the sacral region in the hips.

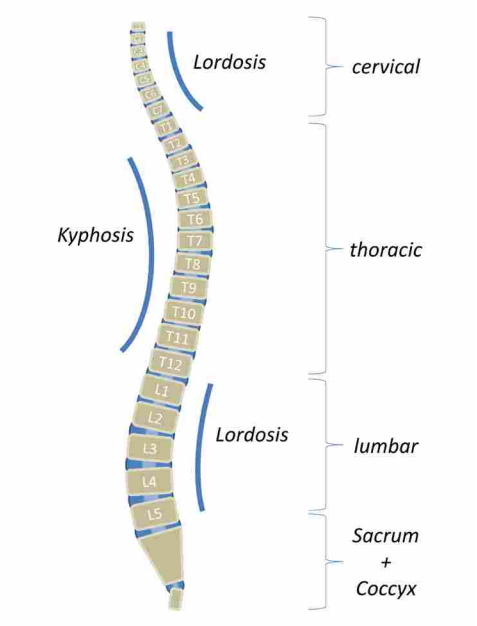

Figure 2-1: The human vertebral column shown with spinal sections, vertebrae, intervertebral discs, and curvature.

In order to maintain stability, the human vertebral column develops its characteristic "double s-shaped" curve in the sagittal plane. The direction of curvature is termed lordosis and kyphosis, which alternates between each segment: cervical—lordosis, thoracic—kyphosis, lumbar—lordosis, sacral—kyphosis. This is not necessarily the case though with quadrupeds. While most animals maintain a lordotic curvature in the cervical spine, some animals may display a curvature of primarily kyphotic in the thoracic and lumbar regions. However, there are some animals that may develop a lordotic curvature in both their thoracic and lumbar regions of the spine, and this may be influenced by environmental factors such as gait or external loads [34, 35].

While the purpose and anatomy of the spine may be similar for humans and other mammals, the relevant differences come into play with the mechanics and function. A big factor that changes the mechanics experienced throughout the spine involves the orientation of the particular segment with respect to gravity. Other inputs may also change the loading and mechanics of a specific spinal segment. For example, the vast majority of mammals walk using all four legs (quadrupeds), but humans only walk on two legs (biped). The vertebral column is actually a column in humans with its vertical orientation, whereas the quadruped spine is mostly horizontal and supported from the front and hind legs. However, the function of the cervical spine for all mammals (including humans) is to support and transfer the loads from the head. With the cervical spine only supported from the lower end, it functions in an open-kinetic chain, where the motion of a lower level affects the position of everything above. The dynamics of the cervical spine begin like an inverted pendulum, but grow increasingly more complicated with each additional joint, which is like stacking another inverted pendulum on the other. With quadrupeds, this dynamic dilemma is simplified as the front legs create a stable anchor point for

the cervical spine and close the kinetic chain for the lumbar and thoracic spine. For quadrupeds, the lumbar and thoracic spine work like a bridge—supported at both ends by the front and hind legs, the spine connects the two as it runs mainly horizontal to span the distance while supporting the gravitational loads, with a direction that is near perpendicular to the spine. However, the vertebral structure of humans continues the open kinetic chain for the entire length of the spine. The thoracic spine supports the loads from the cervical region, in addition to the loads from the arms and chest; the lumbar region in the lower back supports the loads from the thoracic and cervical regions, plus the additional loads from the abdomen; and the sacral region in the hips serves as the base of the vertebral column and bilaterally transfers the load from the rest of the spine to the os coxae (hip bones) via the sacroiliac joint. With each descending level, the load from above that needs to be supported grows.

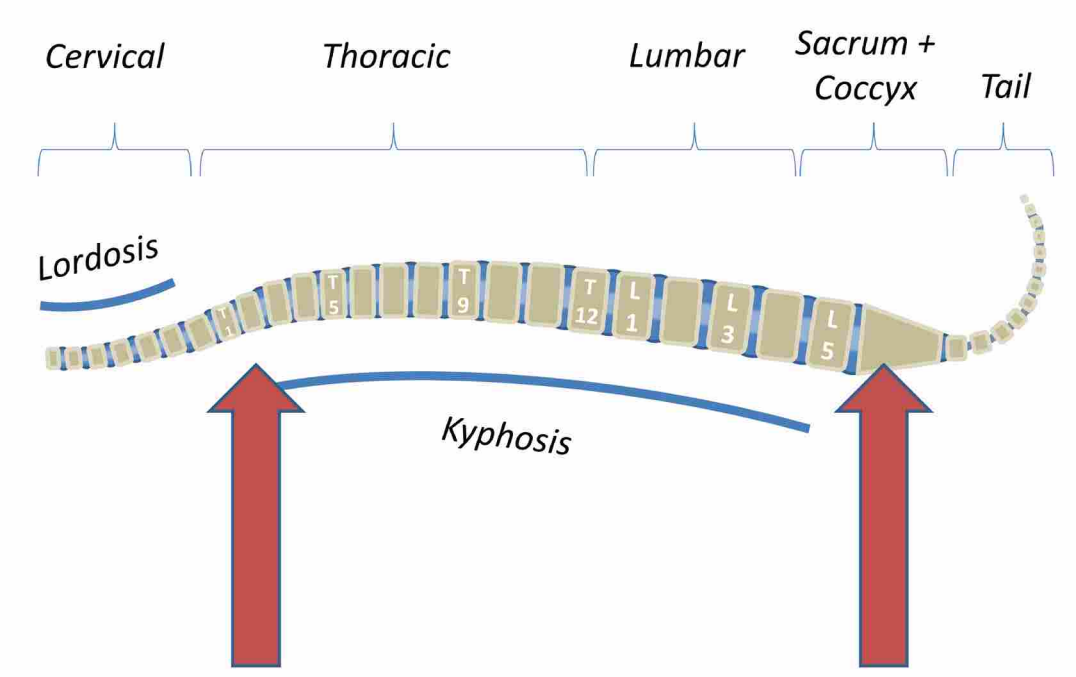

Figure 2-2: Quadruped animal spine is supported by the front and hind legs.

2.2 Intervertebral Disc

The vertebrae of the cervical, thoracic, and lumbar regions are all separated by a thick cartilaginous pad called the intervertebral disc, which is the motion-enabling component within the spine [36]. The IVD acts as a mechanical spring-damper [37, 38]. The hydrostatic pressure that is caused by the vertical loading of the vertebral column translates to tensile stresses in the collagen fibers of the annulus fibrosus. While allowing motion, the intervertebral disc also provides stiffness and damping (or shock absorption), which is associated with the size of the disc: the level of shock absorption is determined by the disc height, and the stiffness depends on a mixture of the disc height, and transverse sectional geometry. IVD size varies greatly among individuals, depending on the individuals' size (e.g., height and weight) and lifestyle (e.g., sedentary or active), in addition to other factors such as gender, race/ethnicity, and genes. The intervertebral disc size also varies within an individual based on the location (e.g. spinal region and superior/inferior), which is largely correlated with function. In humans, cervical IVDs are smaller diametrically, which allow for a greater segmental range of motion while supporting a smaller load. Likewise, the lumbar IVDs are larger diametrically, which may reduce the segmental range of motion, but it also allows more weight to be supported for the same stress level [39-43].

2.2.1 Intervertebral Disc Structure

The IVD is composed of three distinct regions: a nucleus pulposus (NP) core that hydrostatically transfers the compressive loads along the spine through each adjacent vertebra. This is accomplished as the disc is compressed, and the NP pushes out on the cross-linked collagen fibers of the annulus fibrosus (AF). The arbitrarily oriented collagen fibers of the NP contribute to their viscous response. While the two regions are easy to distinguish, the change

from one to the other is a continuous transition such that it is difficult to distinguish a distinct line between the two, especially when viewing this transition zone under a microscope. Likewise, the NP and AF rapidly and continuously transition into the vertebral endplates (EP), which enclose the disc, superiorly and inferiorly, and regulate nutrient and waste exchange between the adjacent vertebrae and the disc.

2.2.1.1 Nucleus Pulposus

The NP is a gelatinous, hydrogel-like composite of randomly oriented collagen fibers that are embedded in a proteoglycan-rich extracellular matrix [11]. The proteoglycans (mainly aggrecan) bind to long chains of hyaluronic acid, which are highly charged chains of glycosaminoglycan (GAG) that form a viscous substance to attract and retain water, therefore enabling the NP to distribute the axial compressive loads as it pressurizes the IVD and increases disc height [44].

2.2.1.2 Annulus Fibrosus

The AF is composed of 7-25 concentric lamellar bands of fibrocartilage with highly organized and cross-linked collagen fibers that are oriented at alternating oblique angles with each successive band [45, 46]. The AF bands effectively resist the tensile forces produced from the NP pushing outwards during loading of the spinal column [37, 38, 46, 47]. The AF is often further segmented into an inner- and outer-annulus due to compositional and associated biomechanical differences between the two regions. The outer annulus consists of high concentrations of type-I collagen (90%) relative to total collagen content, whereas the inner-annulus has an increasing composition of type-II collagen and proteoglycans as it transitions into the NP [6, 45, 48].

2.2.1.3 Cartilaginous End Plates

Similar to the articular cartilage of other joints in the body, the cartilaginous end plate (CEP) is made of hyaline cartilage; however, the function of the end plate is remarkably different than that of articular cartilage. The primary function of the end plate involves enclosing, maintaining, and protecting the NP while regulating nutrient transport between the NP and the available blood supply in the neighboring vertebral body. The cartilage cells of the end plate are oriented to facilitate both functions, as it transitions into bone.

2.2.2 Nutrition

Although small vessels do exist in the vertebral endplates and outer rings of the AF, the IVD is generally accepted to have no direct nerve or vascular supply [5, 11, 49-51]. Due to the largely avascular structure of the IVD, the health of the disc is largely associated with its ability for nutrient and waste transfer [11, 47, 51-56]. As a result, nutrients are exchanged via two alternative mechanisms: long distance diffusion for smaller molecules and bulk fluid transport for larger molecules [52, 56]. Smaller molecules include oxygen, amino acids, water, and glucose. Larger molecules include growth factors, proteases, and macromolecules that are generated in the cells. Diffusion is greatly enhanced by bulk fluid transport. The metabolic activities are dependent on receiving nutrients (such as glucose) and disposing of metabolic byproducts (e.g. lactic acid).

2.2.3 Intervertebral Disc Biology

The environment of each region of the disc (and all connective tissue) is maintained by the respective cell of that tissue. For example, the fundamental cell of bone is the osteocyte, or for cartilage is the chondrocyte. Likewise, the nucleus pulposus is maintained by the NP cells,

which are similar to the chondrocyte, such that the extracellular matrix that is produced by the cells is rich in proteoglycans--predominantly aggrecan and collagen. The NP consists of randomly oriented (primarily Type-II) collagen fibers. The increased concentrations of aggrecan contribute to the viscous amorphous consistency of the NP. The apparently disorganized collagen structure is due to the hydrostatic stress distribution within the NP. NP cells are unique as they have adapted to a low-oxygen environment as there is no direct blood supply to the NP, yet they are able to survive [1, 57-60].

The cells in the annulus fibrosus (AF-cells) are like fibroblasts as they create an extracellular matrix rich with collagen. The strength and rigidity of the tissue is largely determined by the concentrations and organization of the different types of collagen, which are aligned with the stress field that is experienced throughout the respective tissue. The AF concentration of aggrecan is lower than that of the NP; however, when combined with the high-degree of organization of the (primarily Type-I) collagen fibers, the tissue forms a strong mesh to support the pressurized NP [1, 57-60].

2.2.4 Development of the Intervertebral Disc

The mammalian disc is unique such that it develops from cells of two distinct embryonic origins: the notochord and the somite [36]. As the embryo matures, the notochord is surrounded by somites, which develop into sclerotome cells and trigger the notochord to separate into distinct clusters as the notochord retreats from within the sclerotome, the somites transition to the AF, and the notochord groups into the future NP. The AF and NP cells further develop to begin forming the IVD structure and extra-cellular matrix [61-65]. The origins and the progressive formation of the cartilaginous endplate are currently unknown [47].

An interesting phenomenon with the nucleus pulposus concerns the absence of notochord cells in the adult human disc. The post-natal nucleus pulposus becomes increasingly more populated by chondrocyte-like NP cells, which may originate and migrate from the cartilaginous endplates and the inner annulus fibrosus [63], but recent studies found the NP cells primarily originate from the notochord, with select occurrences of non-notochordal origins found near lesions of the annulus fibrosus or cartilaginous end plate [66].

The notochord cells most-likely transdifferentiate into NP cells as the increased pressurization and decreased oxygen and nutrient supply of the IVD [61], or possible other items, trigger adaptation of the cells to prevent apoptosis and survive in a low-oxygen (hypoxic) and high mechanical-stress environment. Notochord cells are more potent than the chondrocyte-like NP cells in synthesizing proteoglycans, but also have a higher, metabolic demand that is unsustainable in the mature human intervertebral disc. Notochord cells may remain present in the post-natal nucleus pulposus, but most are triggered to phenotypically change to chondrocyte-like NP cells for maintaining the collagen of the extra-cellular matrix of the tissue. Their disappearance and replacement by the chondrocyte-like NP cells will lead to a transformation of a fluid-like nucleus pulposus into a more solid cartilaginous one [67]. However, while humans experience drastic changes to the NP by adulthood [7], with undetectable amounts of notochordal cells as early as 4-10 years of age [67], similar results do not transcend with most animals, which maintain notochord cells throughout their life. Notochord cells are particularly important with the investigation of disc degeneration and regeneration because of their potential metabolic demand and ability to produce aggrecan.

2.2.5 Intervertebral Disc Degeneration and Dysfunction

The human lumbar intervertebral disc operates under a mechanically harsh environment and plays a significant role in the development of DDD [3, 43, 68, 69]. Intervertebral disc degeneration is difficult to characterize because it is broadly defined and arguably impossible to distinguish from the natural changes associated with aging [3, 10, 67, 70, 71]. According to Smith,

> "[Intervertebral disc] degeneration is perhaps best defined as a cascade that begins with changes to the cellular microenvironment within the substructures of the disc that progress over decades to structural breakdown and functional impairment" [36].

Adams more concisely defined disc degeneration as "an aberrant cell-mediated response to progressive structural failure" [3]. While degeneration affects a large portion of young individuals in the industrialized world between 20-40 years of age, many older individuals do not have disc degeneration. So, while age is correlated with degeneration, the two are not synonymous. Other environmental and genetic factors must also be in play [36] that contribute to the structural breakdown and failure of the IVD, including nutrition, weight, and activity type, intensity and frequency [43].

Degeneration occurs when catabolic activity is greater than the anabolic processes, such that cell death occurs more rapidly than cellular proliferation. Both the NP and the AF are sparsely populated with cells [67, 72] making cell death an extremely significant occurrence. A single preliminary cause of disc degeneration has not been identified, however disc degeneration occurs when the biological remodeling balance between protein synthesis and protein catabolism is upset in favor of catabolism [73-75]. When mechanical fluid flow is reduced or interrupted, there is decreased cell function, increased acidity, and possibly cell death [48, 73, 76, 77].

While age-related IVD degeneration is a virtually universal condition for humans, it remains largely absent from most of the animal kingdom. Only a few breeds of animals are known to exhibit this condition: several species of "knock-out" mice [78-87], rats [88-90], dogs [91], and baboons [92-94]. Specific dog breeds (e.g., chondrodystrophic breeds such as daschunds, beagles, and bulldogs) develop DDD [95, 96] whereas non-chondrodystrophoid breeds rarely experience DDD. Of these, primates are obviously the most genetically similar to humans; however, their use as animals models is limited by ethical, regulatory, and cost considerations [28, 29].

2.2.5.1 Intervertebral Disc Related Low Back Pain

Pain is not an automatic precursor for IVDD, nor is the lack of pain a sign of disc health. While the intervertebral disc is often considered a source of low back pain, intervertebral disc degeneration is often present without pain. Pain can also be present without DDD. Other sources of low back pain may include the zygapophysial (facet) joints, spinal muscles and ligaments, or vertebral fractures [28, 97-101].

2.3 Animal Models of Intervertebral Disc Degeneration

Animals have been used for over 100 years [102] for research that has allowed significant advancements in the medical field. Specifically, biomedical research has utilized animals to investigate matters of disease [20, 29, 103], biocompatibility [104], function [105, 106], and therapeutics [20, 102], of various products, implants and procedures. Animal models have historically provided an appropriate benchmark for understanding human biology [107] and mechanics [108, 109], along with their relation to injury [110, 111], pathology [20, 69, 112, 113], and healing [41, 114].

Animals are an important part of biomedical research of the spine [20, 29, 115-118]. Current *in vivo* animal models used in spinal research include murines [119-121], leporids [122, 123], canines [91], porcines [124-126], ovines [127, 128], bovines [129, 130], macropodidae [131, 132], and caprines [133-135]. Each animal model has distinct advantages and disadvantages, yet no animal is capable of sufficiently replicating the environment of the human spine, and especially the degenerative pathology of the human IVD. Preparatory steps for human clinical trials may already include particular animal studies, but the animals and models that are used often do not adequately simulate the environmental conditions for human orthopaedic implants. As most animals will rarely naturally experience disc degeneration, they may hold the key to understanding different non-invasive, therapeutic methods that either discourage catabolism or further encourage metabolism.

The biology and mechanics of the IVD have been investigated using several methods, including *in vivo* and *ex vivo* studies using human cadaver and animal specimen. While much has been learned from existing disc models, each has its limitations, and the perfect model for the human disc does not exist. The extreme difficulties that are often experienced while advancing an orthopaedic device to the point of human clinical studies may prevent many reasonably good devices from realizing the destined application. At the same time, there is a lot of information and knowledge that remains unknown because these devices are never implemented. For this reason, the development of spinal orthopaedic devices would greatly benefit from an intermediate step that utilizes the biology and mechanics of animals.

Preparatory steps for human clinical trials of several orthopaedic devices may already include specific animal studies, but the animals and models that are used often do not adequately

simulate the environmental conditions for the human lumbar spine. Therefore, there exists a need to discover a reasonable and applicable animal model for human spine orthopaedics.

2.4 Camelids

Preliminary research had sparked interest to investigate camelid animals (i.e., llamas and alpacas) for use as a viable animal model for intervertebral disc degeneration. During related research of intervertebral disc degeneration, a published clinical report was found claiming that a llama naturally developed pathology of the cervical intervertebral disc [8], so our interest turned to whether llamas naturally experienced disc degeneration, as humans do.

Despite an elongated vertebra, several similar characteristics were identified with initial inspections, including the spinal curvature, moment arm, and vertical weight-bearing. Specifically, the camelid cervical spine maintains a characteristic lordotic curvature and supports a vertical load through a series of multi-faceted joints in an open kinetic-chain. Whereas the other segments (thoracic, lumbar) of the spine on quadruped animals are bound by front- or hind-legs the camelid cervical spine moves freely, which resembles the bipedal motion of the human lumbar spine [136].

Llamas and alpacas were also available for study as several alpaca and llama ranches were nearby, in addition to several local abattoirs that slaughtered the animals for their meat and hide. The bones and especially the cervical spine were often discarded. A fresh llama neck was obtained from the abattoir, and the cervical region was dissected, the IVDs removed and visual inspection of the discs confirmed that the llama IVD was at least similar, if not larger, in size to current large animal intervertebral discs. Also observed during this dissection was the significant role that the supporting musculature and large bifurcated nuchal ligament must play in

stabilization of the neck. As camelids are large animals, it was also suspected that the NP of the mature IVD would be absent of notochord cells, which is also typical of other large animals [62, 65, 137].

There are several species of camelids (six shown in Table 2-1), and they all may provide a unique perspective for studying the spine. The dromedary and bactrian camel are attractive due to their age. A large animal that lives over 40 years old is probably more likely to develop an age-correlated pathological condition than an animal that only lives a few years. Their weight also would require larger IVDs, which might be subjected to increased stresses. However, camels would be difficult to obtain as they are only accessible in particular parts of the world. Vicugna and guanaco are most often found in the wild in South America but are unavailable as they are protected under various conservation laws in several countries.

Table 2-1: General Characteristics of Camelid Species [138]

Common (*Scientific*) Name	**Life Span**	**Adult Weight**	**Height at Shoulder**	**Load Bearing Capacity**
Dromedary Camel (camelus dromedaries)	40-50 years	450–540 kg (1000–1200 lb)	180–210 cm (6–7 ft)	150-230 kg (350-500 lb)
Bactrian Camel (camelus bactrianus)	40-50 years	450–680 kg (1000–1500 lb)	180–210 cm (6–7 ft)	150-270 kg (350-600 lb)
Llama (lama glama)	20-30 years	130–200 kg (280–450 lb)	90-120 cm (3-4 ft)	30-50 kg (60-100 lb)
Guanaco (lama guanicoe)	20-25 years	70–90 kg (150-200 lb)	105–120 cm (3½–4 ft)	15-20 kg (30-50 lb)
Vicuna (vicugna vicugna)	20-25 years	35-65 kg (80-140 lb)	70–90 cm (2½–3 ft)	10-15 kg (20-30 lb)
Alpaca: Huacaya & Suri (vicugna pacos)	15-20 years	46-84 kg (100-185 lb)	90–120 cm (3–4 ft)	10-20 kg (20-50 lb)

The llama and alpaca are the most available for study: world-wide and locally. Llamas and alpacas are highly domesticated animals, which are raised for their wool and meat. They can easily be found at several ranches that are located nearby and throughout the world, and local abattoirs and ranches were able and willing to provide the neck for research purposes. Furthermore, the llamas and alpacas would be the desired animals to study as their weight range is similar to humans. In fact, comparing these two animals may yield some interesting data concerning the effects of weight.

Alpacas may live between 15-20 years and are typically skeletally mature by age 3. The cervical spine consists of 7 vertebrae, which are relatively long compared to their transverse geometry, although the atlas (C1) and C7-vertebra are noticeably shorter [136] (Figure 2-3). The extended lengths of the vertebral bodies of the cervical spine create a long moment-arm that further exacerbates the bending stresses, particularly in the lower segments [43, 68]. The cervical vertebrae also have noticeable differences from the human lumbar vertebrae; specifically, the camelid vertebrae have two sets of lateral masses: cephalic and caudal protrusions extend ventrally to protect the blood vessels, trachea, and esophagus. The vertebrae transverse-sectional geometry is smaller in the mid-transverse section and expands outward near the endplates. The cervical IVDs get larger with the lower segments, which is similar to the human lumbar spine [136] and is likely a response to elevated mechanical cell-signaling from the increased stresses [139] of supporting the head and upper cervical musculature. The facet joints of the camelid spine are similar in size to the human spine; however, the orientation is more vertical, and appears to act as a stabilizing guide during axial-rotation, rather than a hard-stop motion limiter during extension and/or lateral-bending motions, as seen in humans.

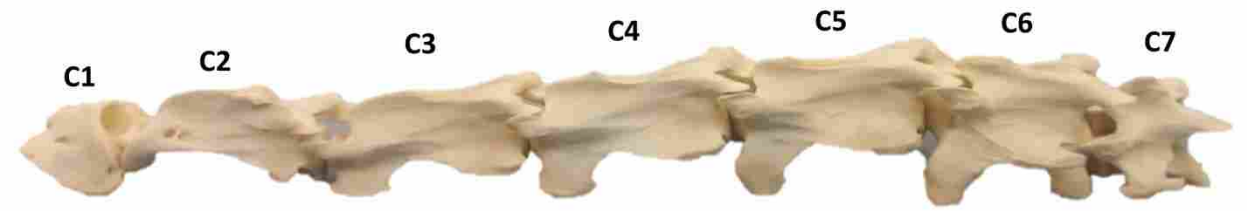

Figure 2-3: Alpaca cervical spine: cervical vertebra (C) #1 (C1, atlas), C2 (axis), C3 – C7. Note the differences in the shape of the atlas and axis, compared to the mid- to caudal-cervical vertebrae (C3 – C6): C3 is tall and thin, and C6 is shorter and wider.

The paper that initially prompted this research identified DDD in the lower cervical spine of a mature llama that showed clinical signs of pain [8]. While this was a single case of DDD in an animal, it was particularly interesting because of the potential for an animal that might also exhibit disc-related pain. Several questions were driven by this single case concerning whether this was a unique, solitary, or isolated, incidence of DDD in the animal kingdom; or, if it is common with this animal species. Not considering any potential genetic predisposition to DDD, there were other observed similarities between camelids and humans. Considering these options, and understanding how the spine research community lacked a viable animal model of DDD, a list of desired characteristics for an animal model of DDD in the human lumbar spine was compiled.

3 DESIRED CHARACTERISTICS FOR ANIMAL MODELS OF THE HUMAN LUMBAR SPINE

The desired characteristics for an animal model of the human lumbar spine and intervertebral disc are described in this chapter, with focus on the relevance and understanding of the applications and limitations. For example, shared characteristics of hair color are probably irrelevant for this application of identifying an animal model to describe an orthopaedic condition. Conversely, similarities in DDD incidence rates and mechanism would be highly relevant.

Each animal model has advantages and disadvantages, as well as its applications and limitations, when used to simulate any human condition. While a perfect animal-model match is impossible, the increased prevalence of relevant characteristic similarities often corresponds to a better model [20]. Not all criteria must be met to justify use as an animal model, but the differences and limitations should be understood for the results to be translated for applications to the human condition. Each aspect of the animal IVD that bears a close resemblance with that of the human IVD greatly simplifies translation of the test results from animals to human.

3.1 Availability

The most important characteristic for any model is the availability and the availability over time—or sustainability. An animal is not available for consideration if it is classified as extinct, near extinct (or endangered), protected, rare, or otherwise difficult to obtain. This is a

big reason why laboratory tests are most often performed with mice, rats, rabbits, and many other small mammals: there are lots of them, and they reproduce quickly. They are also easy to sustain by means of shelter, food, and hygiene requirements. Research utilizing non-mammalian animals (e.g. insects) have also been extremely successful with laboratory studies for these reasons. The number of animals available for study, as well as the simplicity to obtain animals for study must be a factor in identifying a viable, sustainable model.

Deviation from this requirement may not affect the quality of the animal model itself; however, it will limit the number of researchers that could work with the model, and therefore increase the time required for reaching a solution. It may also simultaneously encourage testing on an animal model that is near extinction, or pushed to extinction, which would greatly hamper the research efforts, despite the fact of being unethical. For this research, it was already understood that llamas and alpacas were available for study locally. As alpaca or llama farms are located throughout the world (including over 1,800 registered alpaca farms located throughout all regions of the US), the results presented here indicate exciting potential for using camelids as a model of human lumbar disc degeneration

3.2 Cellular

The second most important characteristic of an animal model of intervertebral disc degeneration concerns similarities in the cellular environment. The cellular environment contains much of the intimate pre-requisites for cellular health, and rather than simulating this via a bioreactor, or manipulating an animal surrogate to parallel the environment of the human lumbar intervertebral disc, a representative animal model would already capture these similarities. One of these requirements was already mentioned above in 2.2.4, regarding the

notochord cells of the nucleus pulposus. The presence of these cells may make an animal more robust to disc degeneration and may not accurately represent the adult human condition [20]. Notochord cells, therefore, should not be present in the IVDs of the mature animal since they are not present in mature human IVDs, and it has been shown that these cells play a factor in reducing the susceptibility of the disc to develop DDD. The presence of notochord cells is just one example of the cellular homology seen across species but more cellular requirements may exist, which may also be captured by using an animal with a similar cellular environment.

Other factors for comparison may be in regards to cell type and densities (e.g., 80% NP-cells vs 20% notochord cells, at 40 cells/cc), in addition to similarities in the extracellular matrix, such as the type and density of proteoglycans and collagen. Another factor for comparison may be tissue hydration. For the purposes of this research, the cellular environment was not studied. It was assumed that these items were similar enough between the camelid cervical and the human lumbar intervertebral disc, and this is what allowed the DDD to develop in the llama of the clinical paper [8].

3.3 Morphology

3.3.1 Shape

The shape of the cartilaginous end plates of the IVD may form convex or concave curves. Human lumbar IVDs are convex for both the upper (cranial) and lower (caudal) endplates, when viewed from the sagittal or frontal planes [20], which mate with the concave-shaped vertebral endplate (Figure 3-1). The double-convexity of the human lumbar endplate results in varying outcomes: the benefits of increased stability and contact area are overshadowed by the increased distance (and therefore difficulty) for nutrient and waste exchange. Also, while the increased

disc volume may provide more shock absorption, it also requires more maintenance through the NP and AF cells, and therefore more nutrition is required in an already nutrient-deprived location.

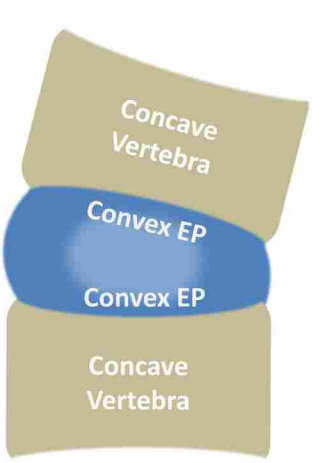

Figure 3-1: Sagittal cut representation of the human vertebrae-disc-vertebrae structure shows the shape of the endplate (EP) is convex on both the cephalic and caudal endplates.

The transverse planar shape of the human disc is often approximated as an ellipse; sometimes it more closely resembles an ellipse than any other shape; however, the human lumbar IVD is often found with a "lima-beam" shape as the mid-posterior portion provides spinal cord clearance (Figure 3-2). This unique shape provides increased surface area for nutrient diffusion and stress-dispersion during compressive loading, but it also creates high-stress concentration points in the posteriolateral regions of the disc during lumbar extension. This portion of the disc also coincides with the primary location of radial fissure and nuclear protrusion [3].

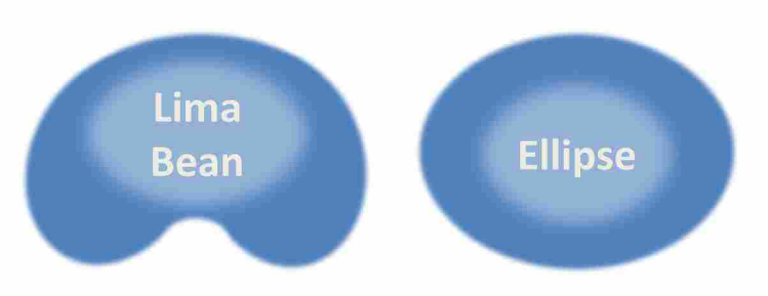

Figure 3-2: Transverse sectional view of the human IVD. In the transverse plane, the human disc may take on a more kidney bean (left) or elliptical shape (right), but the disc is most often represented as an ellipse.

3.3.2 Size

The IVD is a unique tissue as it is considered (by some) to be the largest avascular organ in the human body [61, 140]. Due to this lack of vascularity, nutrition in the disc is governed by diffusion (through the surface area in contact with blood vessels) and bulk fluid flow due to the biomechanical pumping effects of spinal motion. IVD size affects both the mechanics of the disc and the availability of nutrition and waste exchange. The transverse-cut cross-sectional dimensions (width and depth) and the height of the IVD, all of which would affect the mechanics, should be sufficiently similar to the human lumbar IVDs to maintain comparable static and dynamic mechanical stress levels between the animal and human lumbar IVD.

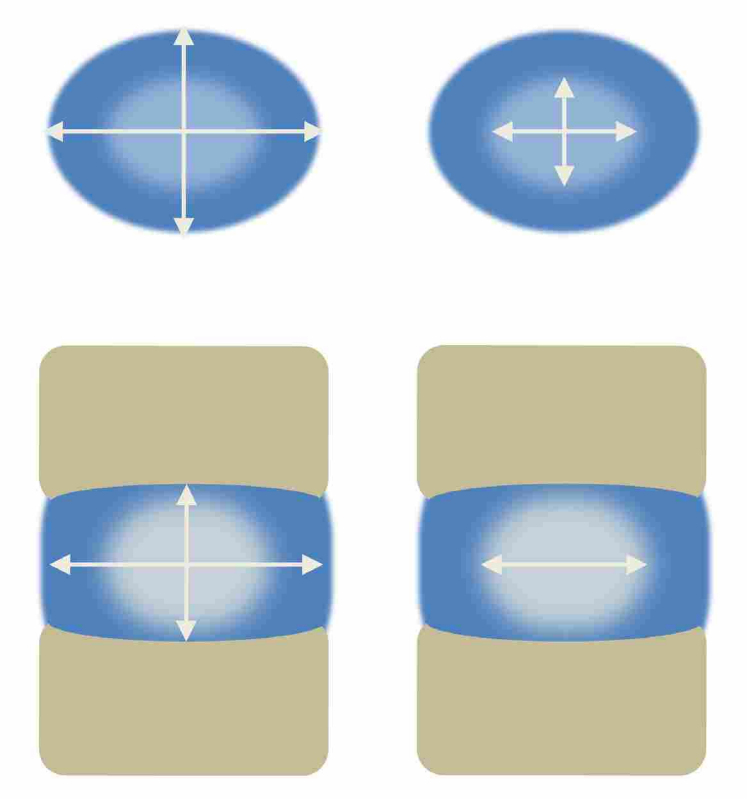

Figure 3-3: Measurements in the transverse sectional view of the whole disc (top-left) and the nucleus pulposus (top-right). Measurements of the IVD in the frontal (or sagittal) sectional view for the whole disc width and disc height (bottom-left) and the nucleus pulposus width (bottom-right).

3.4 Biomechanics

A characteristic that is closely related to disc size is that of biomechanics. Comparisons with the biomechanics and flexibility of the spine should also be normalized by the appropriate geometric parameters (disc size, weights, and applied torques and moments all contribute to mechanical stresses) in order to accurately transfer knowledge for pre-clinical tests of orthopaedic devices. A familiar example of this normalization process is that pressure is a normalization of the force by the cross-sectional area; however, a comparison of applied moment conditions, or the more physiologic applied moment plus compressive follower load conditions

[141, 142], are challenging to normalize. Just as pressure is the normalization of the force, the physiological loads may also be normalized to the resulting stress that is felt at the intervertebral disc. This may not be required though if the disc size and flexibility of the respective animal model matches the comparable human. If the static and dynamic stresses are similar in the form of magnitude, direction, or the time-dependant variations of the two, these factors may contribute to an increased likelihood of developing intervertebral disc degeneration.

The biomechanics of the spinal segment is also important as it captures the segmental motions that encourage nutrient dispersion, increased diffusion, and bulk fluid transport of nutrition and the evacuation of metabolic byproducts (waste). Flexibility studies of animal and cadaveric-human spines have proven exceptionally useful in evaluating IVD mechanics and biomechanical changes due to disc degeneration [20, 29]. The torque-rotation response correlates with the flexibility and strength properties of the soft tissue, and the compression/relaxation response correlates with the mechanical pumping required for bulk fluid flow with nutrient transport to the tissue, in addition to providing a measured parameter to begin to understand the stress levels experienced at various disc levels and locations. Similar to the benefits of having an animal with similar-sized IVDs, testing orthopaedic devices would not require as significant of alterations or translation of knowledge if the flexibility and stiffness of the spinal segments are more similar to that of the human spine.

3.5 Degeneration

A large difference with current animal models of intervertebral disc degeneration is that the animals do not naturally experience disc degeneration. While it may not be required, the ability of an animal to develop degeneration greatly increases the number of studies that are

possible with the model, including (especially) treatment studies. Some animal models of DDD use small animals and/or unnatural methods to artificially initiate the development and progression of DDD, which may not accurately resemble the human condition. Several animal models induce degeneration through puncture, overloading, or protease injection; the ideal animal model should naturally develop disc degeneration, similar to the human condition.

3.6 Summary

The desired characteristics for an animal model of the human lumbar spine were described in this chapter and are summarized in Table 3-1. While every animal shares various characteristics and traits, the applications and limitations of an animal model has advantages and disadvantages when used to simulate any human condition. A perfect match is impossible, but the increased prevalence of relevant characteristic similarities often corresponds to a better model.

Table 3-1: Desired Characteristics for Animal Models of the Human Lumbar Spine

Characteristic	Purpose
Availability	World-wide access to an animal model will accelerate and focus the research of the human lumbar spine and intervertebral disc
Cellular	Similarities in the cellular environment will capture the disc's susceptibility to developing DDD, and therefore allow mechanical effects to be manipulated and studied
Morphology	Nutrition requirements for the disc in addition to the discs ability to transfer nutrients and waste are heavily influenced by the disc morphology (size and shape) and biomechanical environment.
Biomechanics	
Degeneration	The best verification for an animal model of disc degeneration is for the animal to be able to naturally experience degeneration.

4 MORPHOLOGY OF THE CAMELID INTERVERTEBRAL DISC

Human lumbar intervertebral discs are wedge-shaped with convex cartilaginous endplates on both the cephalic and caudal ends when viewed from the mid-sagittal plane [20]. This convexity results in an increased transport distance and difficulty for nutrient and waste exchange with the vasculature in the adjacent vertebrae. Other functional effects of the size and shape of the IVD concern the disc biomechanics, cellular environment, and applicability of human-sized spinal interventions.

Pre-clinical animal models of the spine are regularly used to investigate safety and efficacy of spinal fusion hardware [118, 143-145], scoliosis instrumentation [146-149], artificial discs [150-155], or other spinal orthopaedic devices. However, current large animal models do not match the size of human lumbar spinal discs [156-162]. Thus, size incongruity of the disc limits applicability of observed efficacy data from these studies. Having an animal model with similar-sized IVDs would allow more straight-forward testing of orthopaedic devices as it would not require significant alterations or translation of knowledge if the morphology of the spinal segments more closely resembled that of the human spine.

Results from pre-clinical testing of biological approaches to disc repair and regeneration are similarly limited due to differences in nutrient diffusion rates which are highly, and nonlinearly, dependent on tissue dimensions [51, 52, 55, 61, 163-165]. The IVD sizes among the various animal models vary by orders of magnitude. Small-animal IVD models provide a

substantially different nutritional environment which "may be biased against the influence of nutritional or healing deficiencies that underlie human disc degeneration" [29]. Existing large animal models of the IVD (ovine, porcine, bovine) approach the size of the larger human IVD, but there remains room for improvement.

This chapter details the studies of the size, shape, and other qualitative aspects of the alpaca and llama cervical intervertebral disc morphology, such as disc structure and organization. Quantitative results were compared with published benchmark data for the human cervical and lumbar intervertebral disc, in addition to other large animal models, to gain insight into the benefits or faults of using the camelid cervical model of the human intervertebral disc.

4.1 Methodology

Morphological studies were performed on seventeen alpaca IVDs and nine llama IVDs, which were obtained from four alpacas: Alpaca1 (C3C4, C4C5, C5C6, C6C7); Alpaca2 (C2C3, C6C7); Alpaca3 (C2C3, C4C5, C5C6, C6C7, C7T1); Alpaca4 (C2C3, C3C4, C4C5, C5C6, C7T1); and three llamas: Llama1 (C2C3, C5C6); Llama2 (C2C3, C3C4, C4C5, C5C6); Llama3 (C2C3, C3C4, C4C5). Cervical segments were transected and imaged to compare disc morphology, including the disc shape and size. The disc shape was observed in the transverse and sagittal planes, with the focus on the curvature of the cephalic and caudal endplates of the IVD. The disc size was measured using calibrated optical photogrammetry of the mid-transverse and mid-sagittal sections of the disc using MATLAB® (The MathWorks, Inc.; Natick, MA) Image Processing Toolbox to quantify the size (Figure 4-1).

Three researchers with experience in IVD anatomy each made three measurements of the respective disc anatomy shown in Figure 4-1. Analysis of these measurements showed no

significant difference ($p<0.05$) between observations (intra-observer reliability) or researchers (inter-observer reliability) using a mixed model analysis. Reported results represent an average of all the measurements taken and a pooled standard deviation.

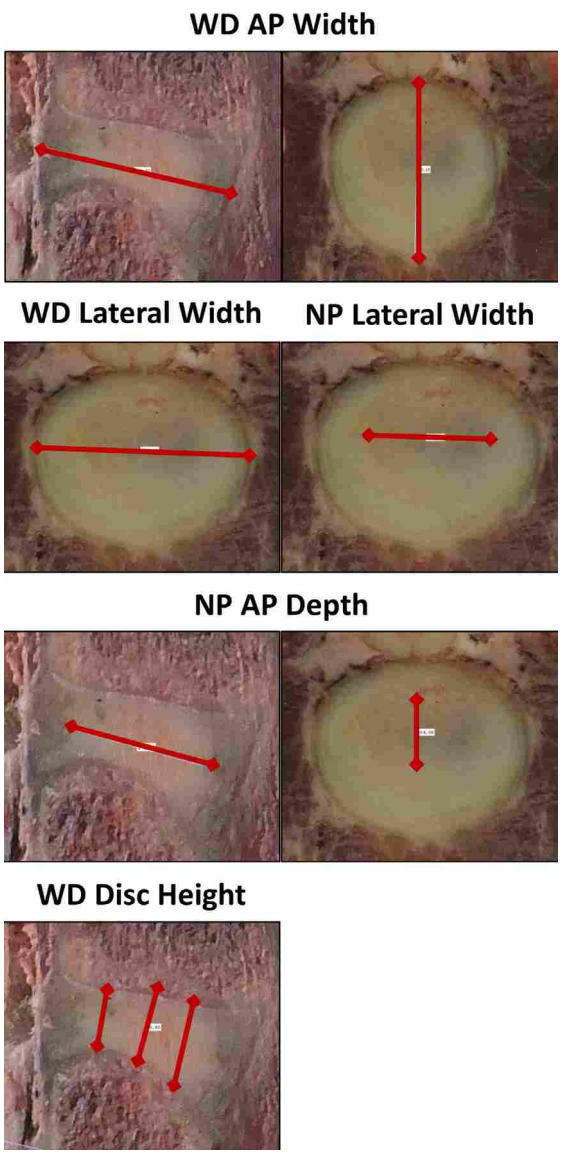

Figure 4-1: Measurements of IVD anatomy for the camelid (alpaca and llama) cervical IVD. WD = Whole Disc; AP = Anterior Posterior; NP = Nucleus Pulposus.

Whole disc (WD) anterior-posterior (AP) width was measured as the maximum straight-line distance from the middle anterior to the middle posterior annular region, including the annular and nuclear regions. WD lateral width was measured as the maximum straight-line distance from the middle left lateral to middle right lateral region, which also included the annular and nuclear regions. Nucleus pulposus (NP) AP width was measured as the maximum straight-line distance from the middle anterior to the middle posterior nuclear region, not including the inner annulus. NP lateral width was measured as the maximum straight-line distance from the middle left lateral to the middle right lateral annular region, not including the inner annulus. Annulus fibrosus (AF) AP width was calculated as the difference between the whole disc AP width and the NP AP width. AF lateral width was calculated as the difference between the whole disc lateral width and the NP lateral width. Disc height was estimated as the average distance between the cranial and caudal endplates within the bounds of the NP. Disc shape will be evaluated in the mid-sagittal section, according to concavity of the cephalic and caudal endplates, and mid-transverse sections, according to the elliptical axes, which are captured by the AP width and lateral width.

Finally, a qualitative anatomical review of the alpaca intervertebral disc was performed to study the tissue structure of the whole IVD and the individual sections of the IVD, including the cartilaginous endplate, nucleus pulposus, and annulus fibrosus. This was accomplished using a fluorescent-microscopy live/dead cell-staining method, which stains the IVD tissue for brighter contrast under fluorescent light. Results are presented in this chapter as it relates to the disc morphology; however, the methodology and other applications of live/dead cell-staining are described in greater detail in chapter 7.

4.2 Results

A qualitative review of the alpaca intervertebral disc gross anatomy, morphology and extracellular environment confirmed the expectation for similarities, while also identifying some contrasting characteristics in regard to shape and size. On average, the size of the alpaca and llama cervical IVD approached the size of the human lumbar IVD (Figure 4-2) and cervical IVD (not shown), while still maintaining a significantly smaller size and elliptical shape.

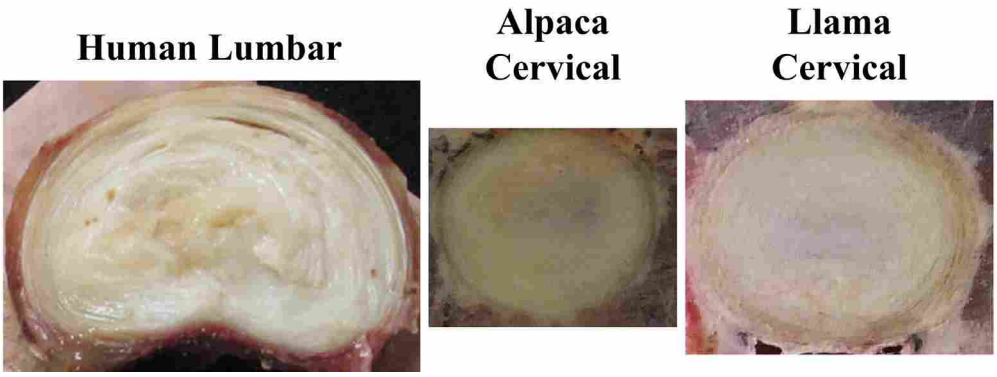

Figure 4-2: Relative intervertebral disc size/shape comparison of the human lumbar (left), alpaca cervical (middle) and llama cervical (right). A consistent scale was maintained for all images.

Figure 4-3: The camelid cervical IVD presents the lordotic wedge shape in the sagittalplane (left) with the adjacent vertebrae maintaining a planar cephalic endplate and a concave caudal endplate. The shape in the transverse plane (right) was elliptical.

In the mid-sagittal section, the lordotic-wedge shape (Figure 4-3) of the camelid cervical IVD differed from the human lumbar IVD as the cartilage endplates were planar-concave, with the cephalic endplate maintaining a pseudo-planar surface and the caudal endplate maintaining a concave surface, where the center of the disc may reside closer to the endplate, as shown in Figure 4-4, where a disc is being prepped for fluorescent microscopic inspection and a transverse planar microtome cut of the caudal end of a frozen IVD reveals the rings of the annulus fibrosus with the cartilaginous-endplate still visible in the center. This differed from the human condition of convex-convex and may result in a decreased likelihood of degeneration due to a lack of nutrition-supply because the diffusion distance is reduced for the NP cells to transfer nutrients and waste to the vasculature in the adjacent vertebrae.

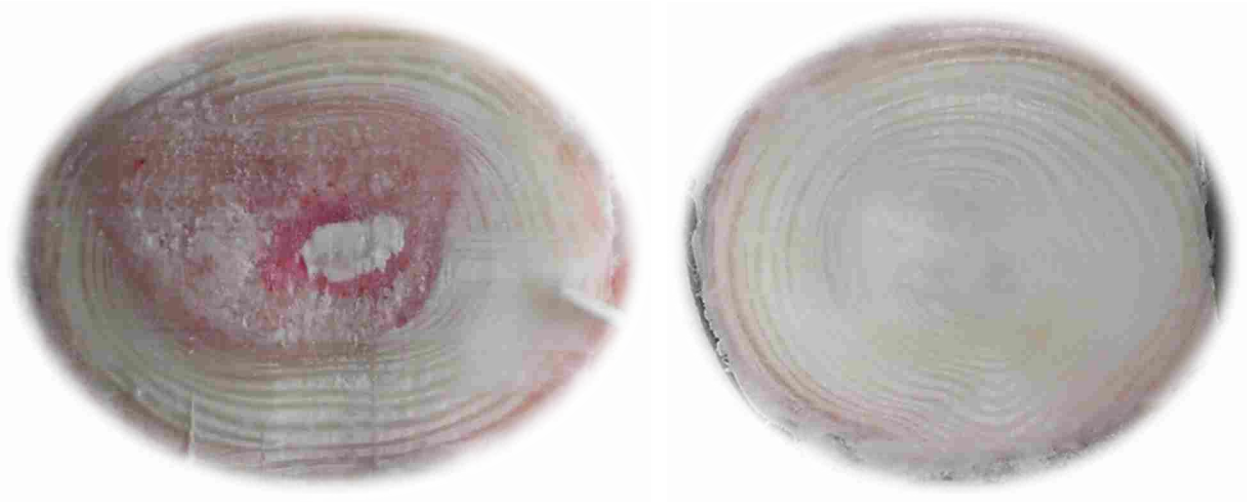

Figure 4-4: In a transverse planar section of the intervertebral disc, the convex portion of the caudal alpaca vertebra is shown in the center (pink/white), surrounded by the annular rings (left). As the cuts go deeper, the endplate is removed and the nucleus pulposus and annulus fibrosus are apparent (right).

Figure 4-5 shows two images obtained using 10X magnification with fluorescent microscopy. The nucleus pulposus is visible on the left with randomly oriented collagen fibers (green clouds) with living (green) and dead (red) NP-cells scattered throughout the nucleus pulposus. The annulus fibrosus on the right shows the alternating orientation of the collagen fibers (green hue) and the increased AF-cell density between the adjacent layers. More information on fluorescent microscopy can be found in Chapter 7.

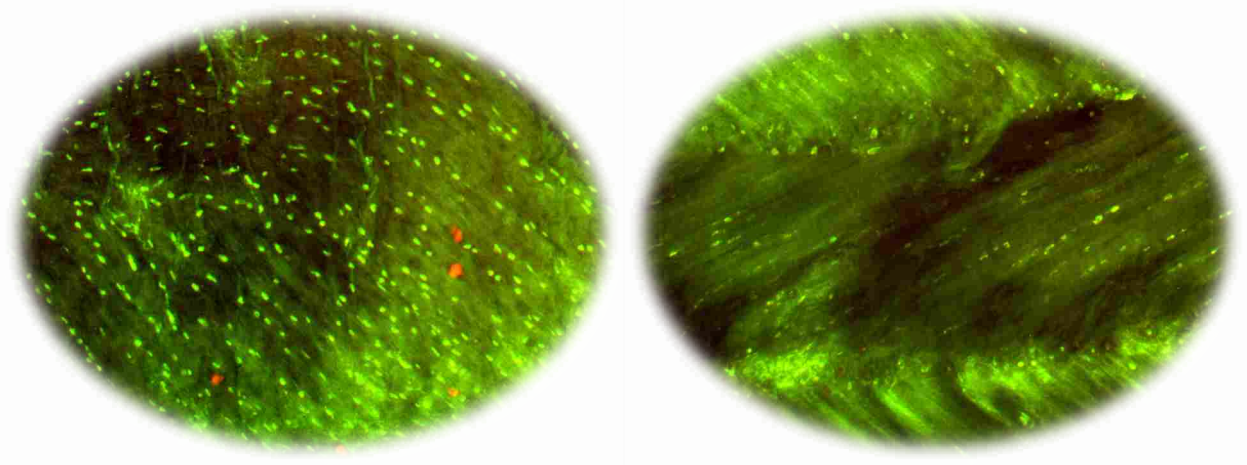

Figure 4-5: Nucleus pulposus (left) and annulus fibrosus (right) of the alpaca intervertebral disc during fluorescent microscopic imaging using 10X magnification.

However, when compared to other large animal models commonly used in spinal orthopaedic research, the alpaca and llama cervical IVDs were closest in whole disc size to the human cervical and human lumbar intervertebral disc (Figure 4-6, Table 4-1), in regards to the measured whole disc dimensions of AP width and lateral width, and also in regards to the calculated transverse area, which is calculated as the area of an ellipse, using the measured AP width and lateral width as the major and minor axes, according to the following

$$AREA_{elipse} = \frac{\pi}{4} \cdot a \cdot b, \quad \begin{matrix} a = WD\ AP\ width \\ b = WD\ lateral\ width \end{matrix}.$$

The alpaca and llama cervical IVD transverse area were approximately 48% and 53% of the transverse area of the human lumbar IVD, with the next closest size comparison coming from the porcine lumbar IVD transverse area of 43% of the human lumbar IVD.

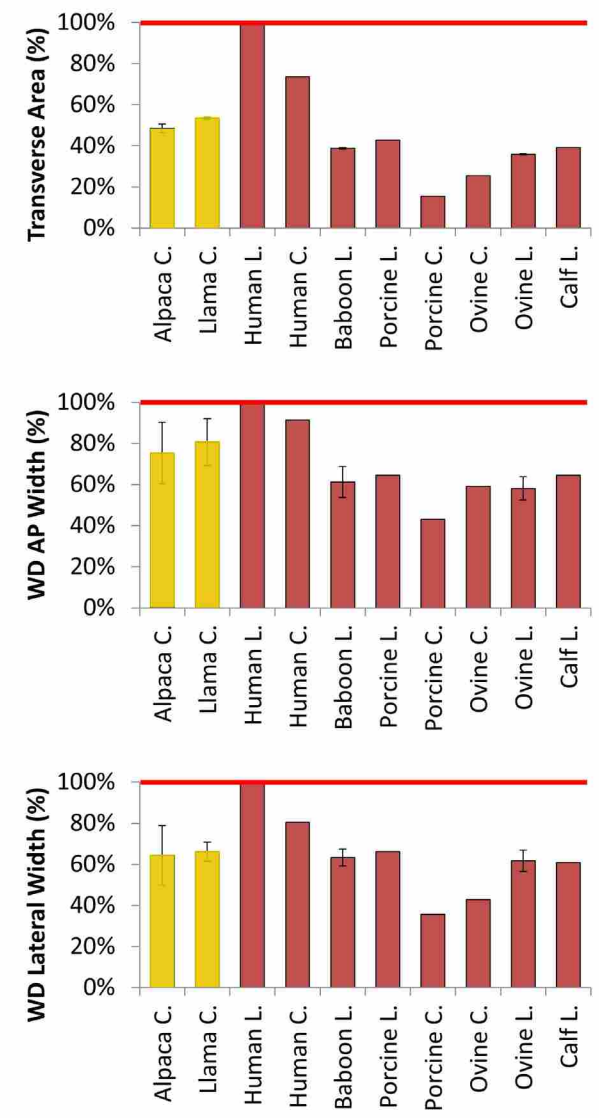

Figure 4-6: IVD size (area, depth, width) comparison between alpaca, llama and large animal spine segments (C=cervical, L=Lumbar) [159-161, 166, 167], as a percentage of human lumbar [22, 58, 160, 166, 168], which is represented with the horizontal reference line. Standard deviations are shown where available. AP = Anterior Posterior.

Table 4-1: Large Animal Intervertebral Whole Disc Size Comparisons:
AP=Anterior Posterior, L.=Lumbar, C.=Cervical, T.=Transverse.

DIMENSION	AP Width (mm)	% Human L.	L. Width (mm)	% Human L.	T. AREA (mm)	% Human L.	Source
Alpaca C.	28	75%	36	64%	792	48%	original
Llama C.	30	81%	37	66%	872	53%	original
Human L.	37	100%	56	100%	1630	100%	[58, 159, 161]
Human C.	34	91%	45	81%	1200	74%	[58, 161]
Baboon L.	23	61%	35	63%	634	39%	[159, 161]
Porcine L.	24	65%	37	66%	697	43%	[161, 166]
Porcine C.	16	43%	20	36%	251	15%	[161, 166]
Ovine L.	22	58%	35	62%	585	36%	[159, 161]
Ovine C.	22	59%	24	43%	415	25%	[159, 161, 169]
Calf L.	24	65%	34	61%	641	39%	[161]

The intervertebral disc is more than just a single cartilaginous pad, and requires the proper function of all of its anatomical parts, including the nucleus pulposus, and annulus fibrosus, and their interactions as the disc is compressed and deformed. Comparable benchmark data was not widely available in the literature for anything other than the human IVD. Considering all of these factors, the camelid IVD also showed similarities in regards to the AP depth of the whole disc, NP, and AF depth, as well as the AF width, (Figure 4-7, Table 4-2).

The alpaca and llama discs proved to be similar in size to each other, with the alpaca disc anatomy generally being smaller except in regards to the AF. The alpaca AF was thicker in both the anterior-posterior depth and the lateral width (Figure 4-7, Table 4-2). Camelid IVD height was shorter than human lumbar IVD (Figure 4-7, Table 4-2). In the transverse plane, the shape of the disc consistently appeared elliptical, with no observed deviations in the posteriolateral

regions of the disc; therefore, by capturing the disc depth and width, the transverse planar shape can be accurately captured as the minor and major axes of an ellipse. In the sagittal/frontal planes, alpaca and llama cervical discs are approximately planar on the cranial end plate and concave on the caudal end plate.

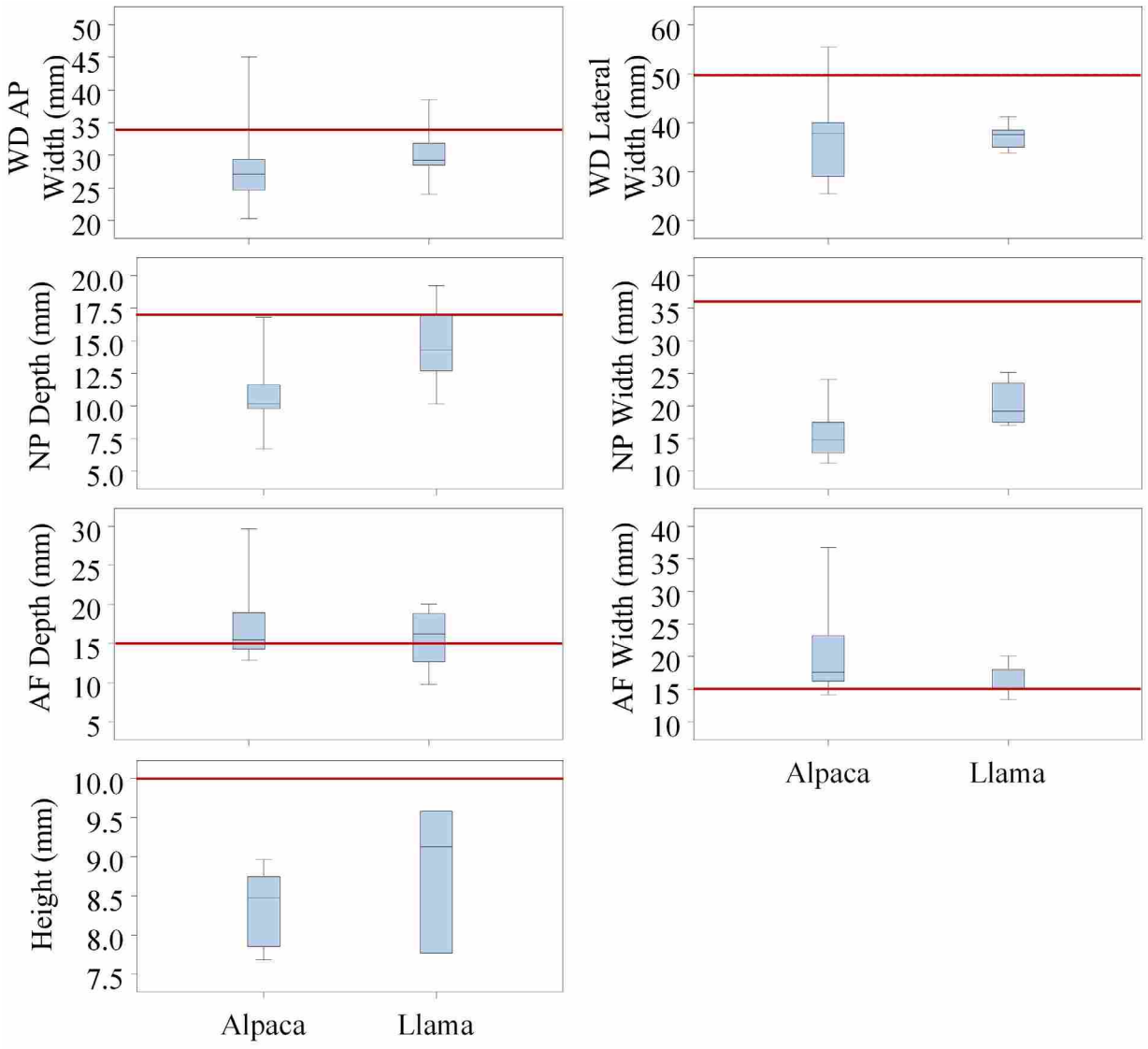

Figure 4-7: Alpaca (left box) and llama (right box) cervical IVD size comparison with the human lumbar IVD (reference line shown as average of human data in Table 4-2).

Table 4-2: Alpaca and llama cervical IVD size (measured in mm) comparison with the human lumbar IVD. AP = Anterior-Posterior; SD = Standard Deviation.

Measured in mm		Alpaca Cervical		Llama Cervical		Human Lumbar	
		N	Mean (SD)	N	Mean (SD)	Mean (SD)	Source
Whole Disc	Height	5	8.3 (0.56)	2	8.8 (0.94)	8.1 (1.7) 11.3 (0.3)	[2] [38]
	AP Width	16	28.1 (5.58)	8	30.2 (4.23)	34.4 (1.1) 35.8 (1.7) 37.2 (4.7	[1] [2] [38]
	Lateral Width	11	36.2 (8.11)	5	37.3 (2.63)	47.1 (1.2) 49.0 (3.7) 55.9 (9.4)	[1] [2] [38]
Nucleus Pulposus	AP Width	16	11.1 (2.67)	8	14.6 (3.26)	20.8 (2.0)	[38]
	Lateral Width	11	16.0 (4.32)	5	20.2 (3.31)	27.3 (3.2)	[38]
Annulus Fibrosus	AP Width	16	17.0 (4.29)	8	15.7 (3.72)	16.4 (3.6)	[38]
	Lateral Width	11	20.3 (6.46)	5	17.1 (2.40)	28.6 (7.0)	[38]

4.3 Discussion

Llama and alpaca cervical discs are similar in shape as the human lumbar discs while consistently exhibiting a more elliptical shape in the transverse plane and portraying the common lordotic wedge shape when viewed in the sagittal plane. However, the curvature of the cartilaginous endplates is not consistent with the human condition as the camelid discs have a pseudo-planar cephalic endplate and a concave caudal endplate. These shared characteristics strengthen the applicability of the camelid cervical model with potential for testing various

physical, cellular, or surgical treatments, which may be more rapidly translated to viable treatments for LBP in humans.

Pre-clinical animal testing of spinal instrumentation is often viewed as an extended biocompatibility test, rather than providing valid functional data. Our results demonstrate that llama and alpaca discs are significantly closer in size to human discs than other animal models, and thus have greater potential to provide a more direct comparison of treatment options for discogenic back pain, intervertebral disc repair and regeneration.

In summary, the results provided in this chapter show that a camelid IVD model sufficiently mimics the human lumbar IVD in regards to intervertebral disc size, shape, and cellular anatomy. Of the large animal models included in this chapter for benchmark comparison, the alpaca and llama included in this study were larger than any other model. From these results and the information presented previously, the larger disc has an increased demand for oxygen, nutrition, and waste exchange in order to sustain the life of the camelid IVD cells, and therefore the disc is more susceptible to degeneration.

5 BIOMECHANICS AND FLEXIBILITY OF THE CAMELID CERVICAL SPINE

The purpose of this chapter is to report on our findings for the biomechanics of the camelid cervical IVD in the context of providing an animal model of the human lumbar IVD. This chapter describes the studies on the biomechanical posture and flexibility of the alpaca and llama cervical spine, and includes comparisons with human cadaveric lumbar biomechanics, which was obtained from my master's research, in addition to other published values for the human cervical spine and other animal models.

Animal models of the spine have proven exceptionally useful in evaluating IVD mechanics and biomechanical changes due to disc degeneration [20, 29, 133]. However, there are fundamental differences in the biomechanical loading observed in the spine of most quadrupeds as compared with that of humans [34, 35, 170]. Those animals that are currently used in spinal research have a horizontal spine orientation for the thoracic and lumbar spine while standing; however this is vertical in humans [170, 171]. The passive compression provided by spinal musculature in the thoracic and lumbar spine is unlikely to capture the kinetic/kinematic effects of gravity and loading when the rostral and caudal ends are supported by the front and hind limbs.[171] However, in all animals, the cervical spine is loaded in an open-kinetic chain and more vertically oriented than the thoracic and lumbar regions. In fact, the posture of the cervical spine directed over the front legs of a quadruped is markedly similar to the bipedal structure of the human (see Figure 5-1).

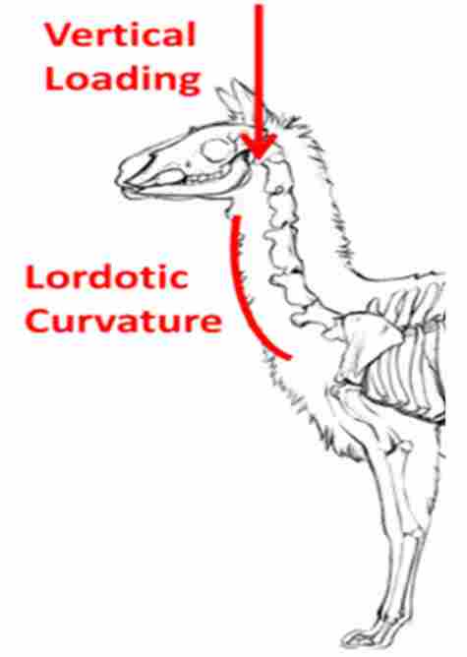

Figure 5-1: The camelid cervical spine maintains a characteristic lordotic curvature and is vertically loaded.

Oriented resistance to gravity loading is a fundamental loading condition associated with erect posture and ambulation in humans, and most quadruped spines lack this characteristic, particularly in the lumbar spine. Both humans and quadrupeds exhibit additional compressive loading due to the intermediate and deep muscle loading and pre-strain in passive stability elements (i.e., ligaments and fascia) of the spine, which varies by location [20, 141, 172], but the human lumbar spine exhibits a characteristic lordotic curvature that is in stark contrast to the kyphotic curvature in the lumbar region of quadrupeds. This difference in curvature also contributes to a different loading condition and biomechanical motion profiles [34, 173, 174] for the IVD.

5.1 Methodology

Biomechanical flexibility tests were performed on camelid cervical spines (Figure 5-1), which included 10 alpaca and 3 llama cervical segments. Test specimen were obtained from 4 Alpacas: Alpaca1 (C3C4, C4C5, C5C6); Alpaca2 (C4C5, C6C7); Alpaca3 (C3C4, C4C5, C5C6); Alpaca4 (C4C5, C7T1); and a single llama: Llama1 (C2C3, C3C4, C5C6). Human samples used for statistical comparison were obtained from 7 lumbar segments that were obtained from 4 human cadavers: Human1 (L1L2, L3L4, L5S1); Human2 (L1L2); Human3 (L2L3, L4L5); Human4 (L3L4) [31].

Spinal segments were cleansed of all extraneous muscle and adipose tissue, and used for biomechanical flexibility testing of the functional spinal unit (FSU). The bilateral nuchae ligament was also removed from each camelid FSU due to attachment difficulties during biomechanical testing of a single level FSU. The nuchae ligament plays a large role in the support of the cervical spine and would greatly resist flexion, and stabilize against left and right lateral-bending. The removal of the nuchae ligament was expected to result in increased ROM and decreased stiffness in the flexion-extension and lateral-bending loading directions.

Remaining specimen preparation and testing followed published protocols using the flexibility method [22-24, 31, 58, 175-179], where the resulting motion is measured and correlated with an applied load. Each specimen was sprayed with phosphate buffered saline [180] at 5 minute intervals to maintain hydration during dissection and testing. Each FSU was potted using a two-part polyester resin (Bondo 265, 3M; St. Paul, MN) [181-183] and secured in the test chamber, which maintained room temperature (20±3 ˚C).

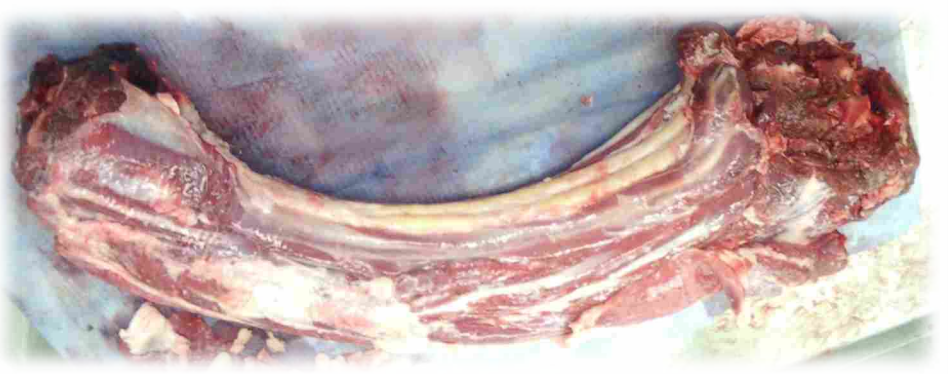

Figure 5-2: Sample camelid cervical spine prior to dissection.

Pure moment loads were applied in axial rotation, flexion-extension, and lateral bending, using a quasi-static, dynamic loading protocol with a continuous speed of 1-deg/sec [23, 31, 32]. A custom spine simulator [23, 24, 31] applied a symmetric ±4-Nm applied torque-limit in each loading direction to achieved the near-maximum segmental range of motion without damaging any soft-tissue [109, 157, 184, 185]. This torque-limit was determined during exploratory flexibility studies on a single C6C7 cervical spinal segment: the sigmoidal torque-rotation curve approached the segmental limits of motion, where large changes in applied torque had little effect on the observed motion, and the torque-rotation curve approached a horizontal asymptote (see Figure 5-3). This exploratory testing indicated that ±4-Nm was a reasonable limit in all modal loading directions in the absence of a compressive follower-load. Each FSU was preconditioned to this torque-limit for a minimum of 20 cycles, when a repeatable torque-rotation response was observed [23, 24, 31]. Multiple cycles of each testing condition were then recorded.

5.1.1 Data Analysis

Segmental rotations in each of the primary modes of loading were computed from the 3D kinematic data. The sigmoidal torque-rotation response of each segment was centered about the range of motion (ROM) and and fit with a pair of dual-inflection-point Boltzmann (DIP-Boltzmann) equations [23, 24], which are of the form

$$\theta = \frac{ROM}{2} \cdot \left[1 - \frac{1}{1 + e^{\alpha_1(T-m_1)}} - \frac{1}{1 + e^{\propto_2(T-m_2)}}\right].$$

The dependent variable, θ, represents the overall rotation of the upper vertebra with respect to the lower vertebra. *ROM* is the segmental range of motion, *T* is the applied torque (independent variable), m_1 and m_2 identify the location of the inflection points, and α_1 and α_2 are associated with the exponential growth rate near m_1 and m_2.

The full nonlinear, viscoelastic response of the segment was captured using the two DIP-Boltzmann equations to model the torque-rotation response (1 upper, 1 lower: unloading→loading, with an average coefficient of determination of 99%) for each test, as well as to easily calculate several FSU flexibility parameters (range of motion, neutral zone, hysteresis, and neutral-zone stiffness) in Table 5-2, which describe the viscoelastic torque-rotation according to [23, 24, 186]. These flexibility parameters were calculated numerically in order to reduce subjective results. Additional explanation of the flexibility parameters or the DIP-Boltzmann equation can be found in my master's research [23, 24, 31, 186].

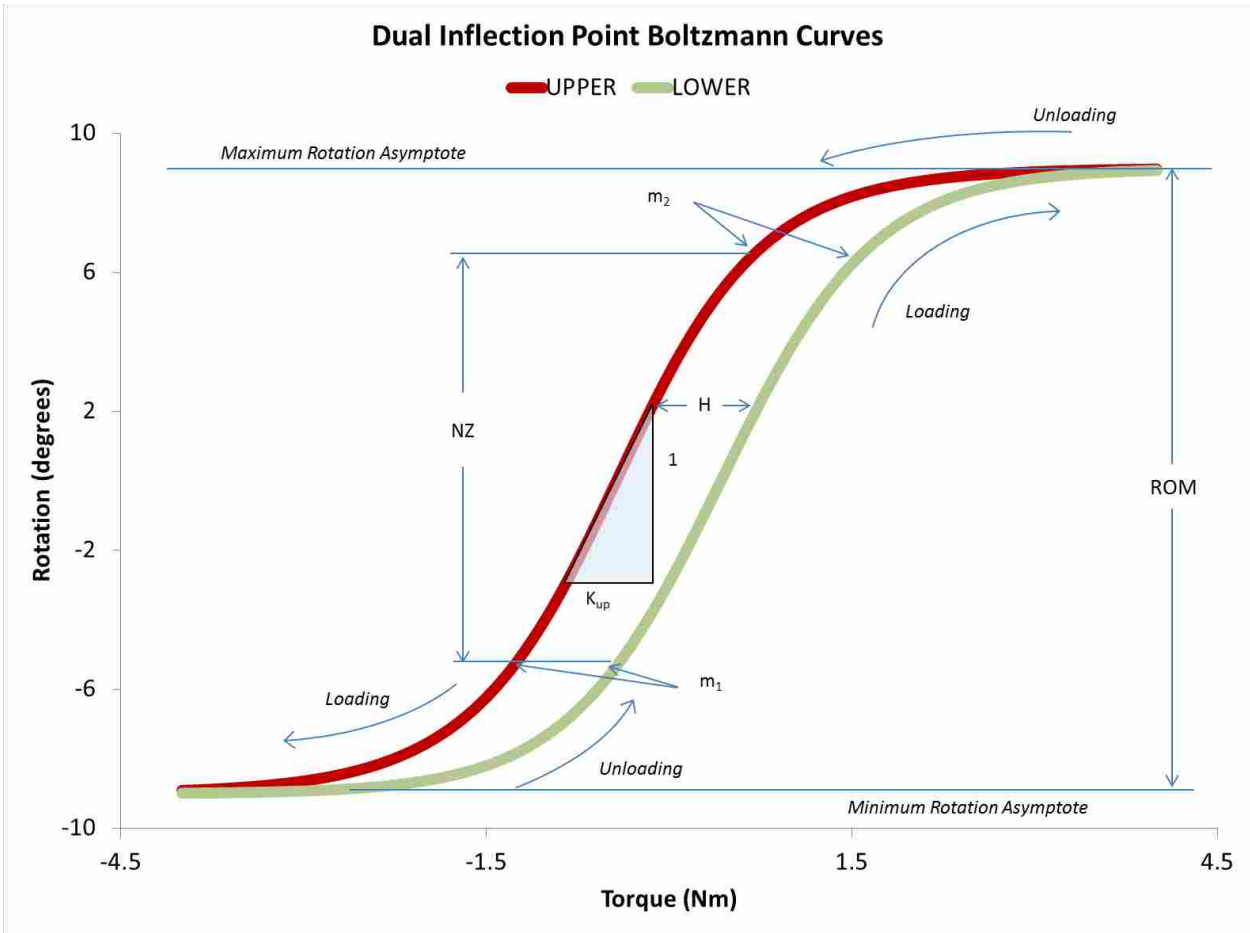

Figure 5-3: Generalized DIP-Boltzmann curve-fit.

Collected data was analyzed using a mixed model analysis of variance (ANOVA) test corresponding to loading direction (axial-rotation, flexion-extension, and lateral-bending), specie (alpaca, llama, human), and blocking on the randomized test specimen. Human lumbar data used for statistical comparison was obtained from published test data using the same testing protocols and spine tester, according to [24, 31], and the human data used was limited to healthy IVDs (Thompson grade degeneration less than 2) that came from published data on seven human lumbar IVDs [31]. Descriptive statistics (mean and standard deviation) were calculated for the observed/calculated flexibility parameters, and are presented for comparison between species.

Table 5-1: Flexibility parameters of the spine.

	Definition
ROM	**Range of motion (deg)** The amount of segmental rotation experienced during testing
NZ	**Neutral zone (deg)** A portion of the ROM where small changes in load result in large changes in rotation
K	**Stiffness of neutral-zone (Nm/deg)** The amount of torque required to cause one degree of rotation within the near constant-slope neutral-zone region
H	**Hysteresis (Nm)** The horizontal spread of the upper and lower torque-rotation curves within the neutral zone

5.2 Results

5.2.1 Postural Similarities

A qualitative inspection of the camelid identified four anatomical characteristics that enforce a similar biomechanical loading condition in the alpaca and llama cervical spine to that experienced in the human lumbar spine: 1) their natural posture aligns the loading of their cervical vertebrae vertically to resist gravity loading in an open kinetic chain, 2) the gravity load supported by the lower portion of the spine is magnified due to the extended (moment-arm) length of the neck, 3) the cervical vertebrae exhibit a lordotic curvature similar to that of the human lumbar spine (Figure 5-4), and 4) the lordotic curvature presents itself secondary to weight bearing in the upright position, whereas the primary (embryonic) curvature is kyphotic.

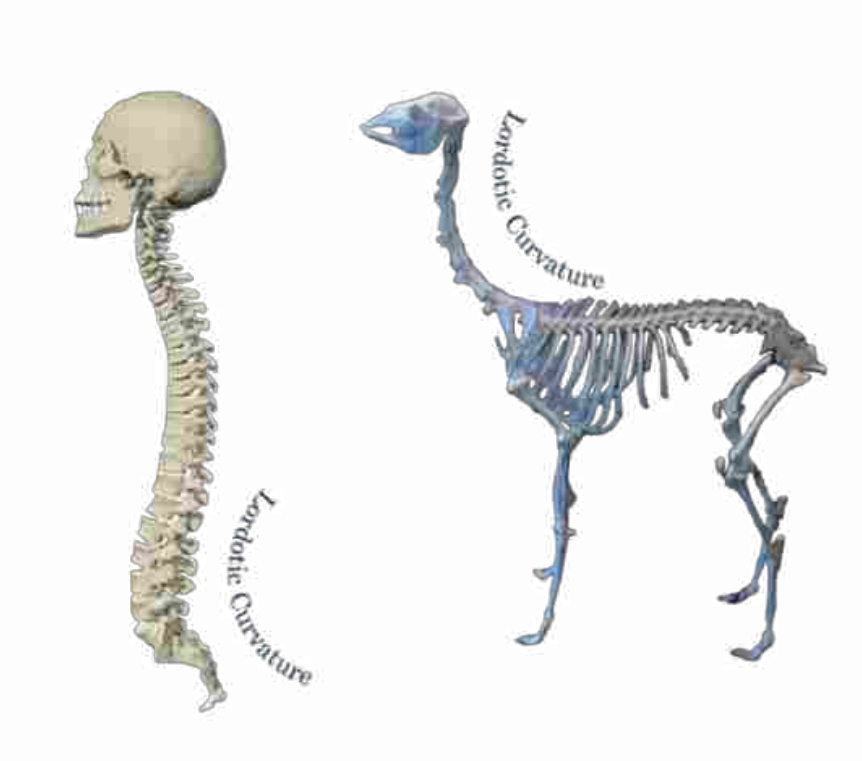

Figure 5-4: The camelid cervical spine (right) has biomechanical similarities to the human lumbar spine (left).

The role of the large bifurcated nuchae ligament was evident during preliminary dissection studies of the alpaca neck. With all musculature removed, the caudal base of the neck was manually held to the dissection table, and the cephalic portion of the neck oriented vertically to simulate the in-vivo condition. The cervical spine remained stable with its constant lordotic curvature. The neck would always return to this stable position following small and large perturbations in flexion, extension, and lateral-bending. By applying an increasing load up to approximately 25 pounds for flexion motion, the cervical spine lied flat on the dissection table. When released, the spine sprung back to its stable position as before. Also, despite regular misting with the PBS solution, the nuchae ligament appeared to desiccate as the nuchae ligament shortened and the radius of curvature decreased with time. This same effect occurred after

freezing an intact cervical spine. These observations confirmed that the nuchae ligament played a significant part in the stiffness and stability of the cervical spine in flexion and lateral-bending motions. As the nuchal ligament was on the posterior surface, it would not have affected the extension motion.

5.2.2 Biomechanics and Flexibility

Segmental biomechanics and flexibility parameters in the 3 primary modes of loading were captured through the torque-rotation response which exhibited the expected sigmoidal shape (Figure 5-5) that is consistent with human spine biomechanics [23, 24].

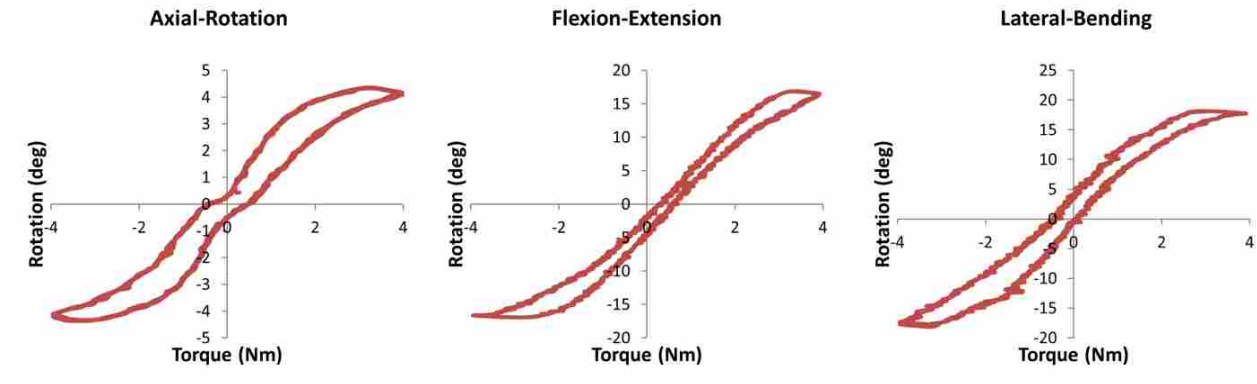

Figure 5-5: Flexibility tests captured the torque-rotation response of alpacas and llamas in the three modal axes of loading: axial-rotation (left), flexion-extension (middle), and lateral bending (right), as represented with these exemplar torque-rotation curves from one of the tests.

Available flexibility data in published literature was mostly limited to ROM, with some also reporting NZ. When comparing the ROM of alpaca, llama, and other large animal models used for human lumbar spine biomechanics testing, the llama and alpaca presented the expected results that they had a comparable ROM as the human lumbar spine or the other large animal models (Figure 5-6). The increased ROM observed in flexion-extension and lateral-bending was

expected due to the removal of the large nuchal ligament from the posterior spine, thereby greatly decreasing the passive stiffness of the segment.

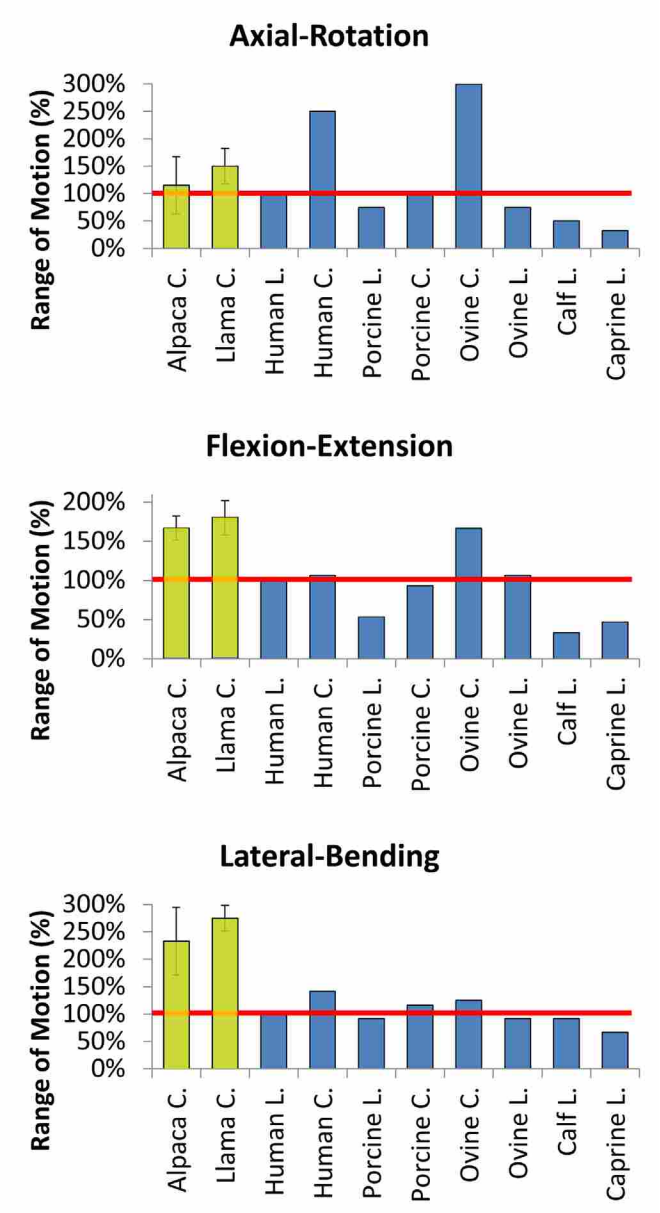

Figure 5-6: Approximate range of motion (ROM) of several large animal spine segments (C=cervical, L=Lumbar) in axial-rotation, flexion-extension, and lateral-bending, as a percentage of human lumbar ROM [41, 58, 109, 133, 185], which is represented as the horizontal reference line. References for provided benchmark data are as follows: Human L. [31, 58, 179, 183], Human C. [187], Porcine L. & C. [185], Ovine L. & C. [109], Caprine L. [133], Calf L. [41].

Flexibility parameters of ROM, NZ, K, and H, were determined from the DIP-Boltzmann torque-rotation curves and are shown in Table 5-2 with published human lumbar and cervical parameters. Boxplots of the range of motion (ROM) and other flexibility parameters (NZ, K_{NZ}, and H) show no significant difference between the alpaca and llama (Figure 5-7) found for any of the flexibility parameters (ROM, NZ, H, K) between alpacas and llamas. In axial rotation, the camelid ROM was nearly identical with the human lumbar spine. In flexion-extension and lateral bending however, the camelid segments were significantly more flexible than the human lumbar spine ($p<0.01$) and closer to data reported for the human cervical spine [58]. Regardless, multiple similarities with the human spine were observed with neutral zone, hysteresis, and neutral-zone stiffness (Figure 5-7). Significance levels for the various flexibility parameters and their differences across species can be found in Table 5-3.

Previously published human lumbar biomechanics data obtained using the same spine tester and a similar test protocol [24] was used for comparison. In axial rotation, the human cervical ROM lies within the range measured for camelids. In flexion-extension and lateral bending, however, the camelid segments were significantly more flexible ($p<0.001$) and closer to data reported for the human cervical spine [58]. This increased flexibility was expected due to the testing procedure used, which removed the large nuchae ligament from the posterior spine, thereby greatly decreasing the passive stiffness during flexion. Additional biomechanics and flexibility data presented in Figure 5-7 and Table 5-2 demonstrate similarities with the human spine in regards to neutral zone, hysteresis, and neutral-zone stiffness.

Table 5-2: Comparative flexibility parameters of the alpaca and llama cervical spine segments. ROM = Range of Motion; NZ = Neutral Zone; K_{NZ} = Neutral-Zone Stiffness; H = Hysteresis. Dir = Direction; AR = Axial-Rotation; FE = Flexion Extension; LB = Lateral-Bending.

Specie	Dir	N	Statistic	ROM	NZ	K_{NZ}	H
Alpaca	AR	10	Mean	4.6	0.9	1.5	1.1
			Std Dev	2.1	0.3	0.8	0.4
			Min	2.2	0.5	0.5	0.6
			Max	8.7	1.6	2.8	1.8
	FE	7	Mean	25	2.9	0.2	0.5
			Std Dev	2.3	0.3	0	0.1
			Min	21.4	2.3	0.1	0.4
			Max	27.2	3.3	0.2	0.6
	LB	9	Mean	28.4	4	0.2	0.6
			Std Dev	7.4	2	0.1	0.2
			Min	13.3	1.8	0.1	0.4
			Max	36.4	8	0.3	0.9
Llama	AR	3	Mean	6	1	0.9	0.9
			Std Dev	1.3	0.2	0.3	0.1
			Min	4.5	0.8	0.7	0.9
			Max	7.1	1.2	1.2	1
	FE	3	Mean	27.3	3.2	0.2	0.5
			Std Dev	3.3	0.4	0	0.1
			Min	23.6	2.8	0.1	0.4
			Max	29.6	3.6	0.2	0.6
	LB	3	Mean	32.8	5.4	0.1	0.7
			Std Dev	2.8	1.9	0	0.2
			Min	29.7	3.8	0.1	0.5
			Max	35	7.5	0.2	1

Table 5-3: Significance levels for species effects and the biomechanical flexibility parameters. ROM = Range of Motion; NZ = Neutral Zone; KNZ = Neutral-Zone Stiffness; H = Hysteresis.

Significance Levels (p-values)

Species	ROM	NZ	H	K_{NZ}
H. Lumbar vs Alpaca	<0.005	0.28	0.48	0.09
H. Lumbar vs Llama	<0.005	0.14	0.70	0.08
Alpaca vs. Llama	0.18	0.25	0.81	0.29

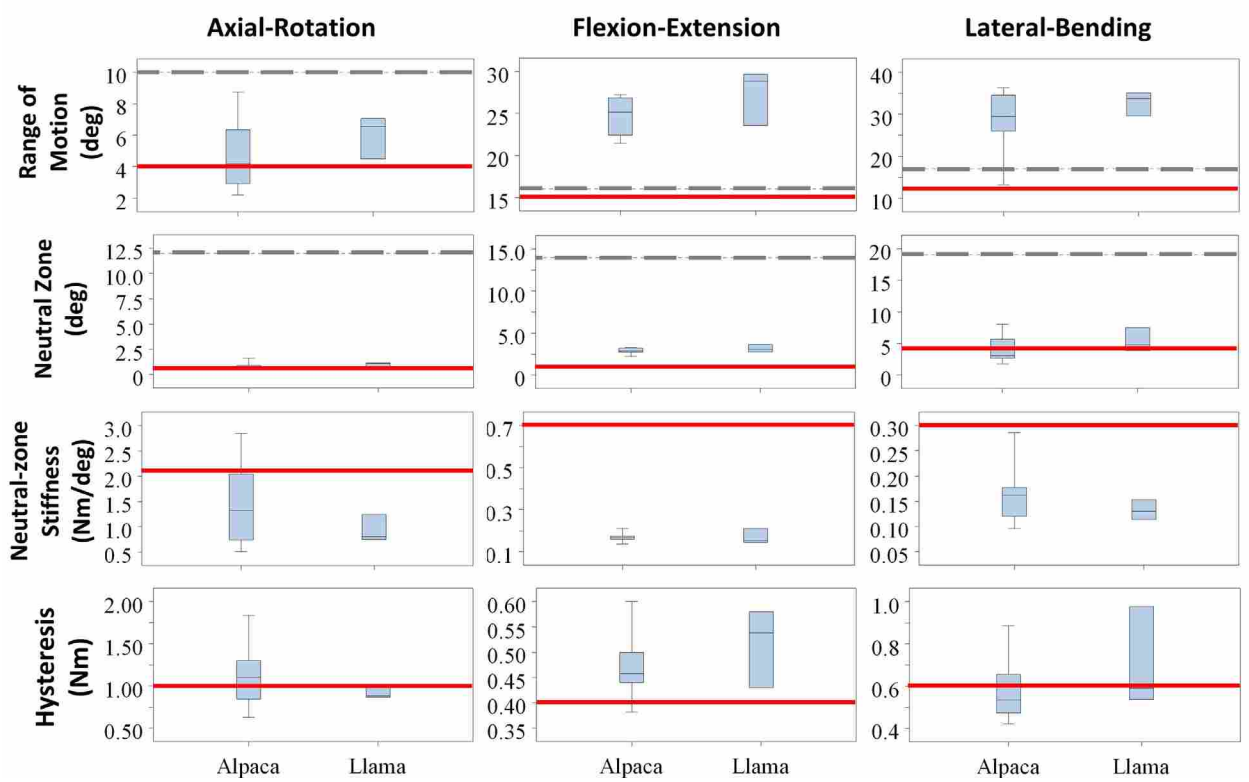

Figure 5-7: Flexibility parameter comparison of ROM, Range of Motion; NZ, Neutral Zone; K, Neutral-zone stiffness, H, Hysteresis. Reference lines shown represent comparable values for human lumbar (–) [24, 31, 58] and human cervical (- - - -, not shown for neutral-zone stiffness and hysteresis) [58, 176, 177] spine.

A two-way ANOVA of the data grouped by species subgroups showed that the effect of animal species was significant ($p<0.05$) between the human lumbar ROM and the alpaca and llama ROM, with no other significant differences noted between the various groups (Table 5-3). When looking specifically at the biomechanical differences between the alpaca and llama, the two are statistically similar.

5.3 Discussion

Published reports of painful disc bulging and herniation in a middle-aged llama [8] prompted the authors' theory that the camelid cervical IVD would make a good animal model of

the human lumbar IVD, and the present work showed substantial similarities in regards to spinal posture, biomechanics, and IVD size. These shared characteristics present a unique model with potential for testing various physical, cellular, or surgical treatments, which may be more rapidly translated to viable treatments for LBP in humans.

The camelid cervical segments appeared to be more flexible than the human lumbar segments in flexion-extension and lateral-bending; however, this increased flexibility may be attributed to the methodological procedure of removing the bilateral nuchal ligaments, which are assumed to significantly increase the stiffness and resistance to the flexion and lateral-bending motions. However, this increased ROM may also be attributed to the different orientation of the facets. Preserving all ligaments for future ex vivo studies is encouraged, and in vivo uses of a camelid spine model with intact nuchal ligaments may yield flexion-extension and lateral-bending motions that are more consistent with the human lumbar spine and could determine whether the facets' orientation significantly affect the range of motion. As the authors expected, with llamas being taller and heavier, their cervical spine segments were slightly larger in size than the alpaca segments, however the effects on biomechanical motion did not show any statistical significance. The limited number of available llama specimens used may have limited the statistical resolution of this study.

In summary, the authors believe the results provided in the present chapter show that a camelid IVD model sufficiently mimics the human lumbar IVD in regards to spinal posture and flexibility, which may be correlated with the development of intervertebral disc degeneration. The results presented here indicate exciting potential for using camelids as a model of human lumbar disc degeneration.

6 PREVALENCE OF INTERVERTEBRAL DISC DEGENERATION IN THE ALPACA CERVICAL SPINE

The purpose of the present work was to characterize the prevalence and severity of intervertebral disc degeneration in the alpaca cervical spine with hopes of identifying a large animal model to better understand this pathology in the human lumbar spine. If alpacas develop spontaneous disc degeneration with a similar prevalence and graded severity as humans, the case is strengthened to further investigate the camelid family to better understand their limitations in regards to the types and mechanisms of DDD. This study will potentially open the way for future research using camelids to study DDD and for pre-clinical testing of spinal implants and other therapeutics [28, 102, 112, 188].

6.1 Methodology

Twenty clinically normal, pasture-raised, female alpacas (*Vicugna pacos*) (Figure 6-1) were randomly chosen from a herd of 175 alpacas and transported to the imaging facility. Each alpaca was observed at a normal walking pace prior to MR imaging by the study veterinarian (BLR) to assess its gait for symmetry and lateral sequence to detect any neurologic or orthopedic abnormality. All alpacas were deemed to be in good health based on clinical assessment by the caretaker (TFR) and examination by the study veterinarian (BLR). All animals had a normal gait with no clinical signs of pain. Demographic information for the alpacas included in this study is shown in Table 6-1. All study parameters were approved by the Institutional Animal Care and Use Committee.

Figure 6-1: Alpaca 4 (aka “Dona”) relaxes before sedation.

All alpacas were fasted for 18 hours and had no access to water for 12 hours prior to the imaging study to minimize the risk of regurgitation, aspiration, and bloating, during sedation and imaging. Following a physical exam, each alpaca was sedated using 1ml/18.2kg intramuscular (IM) BKX solution. BKX was prepared by adding 1-ml of butorphanol (10-mg/ml; made in Germany for Merck Animal Health; Summit, NJ, USA) and 1-ml of xylazine (100-mg/ml; Putney; Portland, ME, USA) to a 10-ml vial of ketamine (100-mg/ml, Putney; Portland, ME, USA); BKX solution was dosed at of 0.04-mg/kg butorphanol, 4 – 5-mg/kg ketamine, and 0.4 – 0.5-mg/kg xylazine combined in a single syringe and administered by IM injection to induce recumbency within 3 - 8 minutes and to achieve up to 45 minutes of sternal recumbency. Alpaca of the Suri breed received an additional 0.5-ml of BKX solution, as recommended in the literature [189-191].

Figure 6-2: Silhouette of a young alpaca in the kushed position.

Immediately after administration of the BKX sedative, aseptic preparation of a jugular venipuncture site was performed prior to placement of an intravenous (IV) catheter to provide access for additional sedation during the MRI scan (if needed). Following sedation, alpacas were placed in a kushed position (sternal recumbency, as shown in Figure 6-2) on the MRI table. The vital signs of each alpaca, including rectal body temperature, heart rate (HR), respiratory rate (RR), capillary refill time (CRT), color of mucous membranes (CMM), and reflexes (jaw tone, palpebral, panniculus, pinnae, tail), were monitored at 5 min intervals during sedation and until the animal was conscious, exhibiting purposeful movements, and lifting its head up while in sternal recumbency, then every 15-minutes until it was standing in the trailer. The sedated alpacas maintained a normal respiratory rate of 15-30 breaths/minute breathing supplemental oxygen via nasal insufflation at a rate of 5-L/min during the MRI procedure. If the animal portrayed spontaneous movement of the ventral eyelid, which is correlated with insufficient anesthesia depth, during the MRI scan, additional sedation was administered IV using 0.125-mg/kg diazepam (Hospira, Inc,; Lake Forest, IL, USA) and 0.3 mg/kg ketamine (Putney; Portland, ME, USA) [189-192].

Table 6-1: Demographic Information for Alpacas in this Study.

Alpaca	Age (yrs)	Age Subgroup	Weight (kg)	Breed
Alpaca 1	3	Young	49.9	Huacaya
Alpaca 2	5	Young	63.5	Huacaya
Alpaca 3	5	Young	48.5	Huacaya
Alpaca 4	5	Young	52.2	Huacaya
Alpaca 5	6	Young	59.9	Huacaya
Alpaca 6	10	Old	69.4	Huacaya
Alpaca 7	10.8	Old	61.7	Huacaya
Alpaca 8	12	Old	55.3	Huacaya
Alpaca 9	11.9	Old	63.5	Huacaya
Alpaca 10	12	Old	62.1	Huacaya
Alpaca 11	12	Old	54.4	Huacaya
Alpaca 12	12	Old	64.9	Huacaya
Alpaca 13	12.7	Old	56.2	Suri
Alpaca 14	13	Old	72.1	Huacaya
Alpaca 15	13	Old	67.6	Huacaya
Alpaca 16	13.6	Old	56.7	Suri
Alpaca 17	13.8	Old	54.9	Huacaya
Alpaca 18	15	Old	51.7	Huacaya
Alpaca 19	17	Old	63.5	Suri
Alpaca 20	18	Old	68.0	Suri

Magnetic resonance (MR) imaging (Figure 6-3) of the cervical spine was performed using a 3.0-T MR unit (Siemens 3T Trio System; Siemens Healthcare, Erlangen, Germany) with an 8 channel spine array and a 4 channel neck coil to acquire sagittal T2-weighted Turbo Spin Echo images [Scan 1 (C1-C3): repetition time (TR) = 3500-ms, echo time (TE) = 111-ms; Scan 2 (C3-C5): TR = 4000-ms TE = 87-ms; Scan 3 (C5-T1): TR = 3500-ms TE = 99-ms] (Figure 3). DDD was evaluated using the Pfirrmann grading system [193], which is a 5-point grading scale for classification of degeneration of the intervertebral disc where a Pfirrmann grade of "1 (one)" is

healthy and “5 (five)” is severely degenerated. The Pfirrmann grade is based on disc structure, distinction between the nucleus pulposus and annulus fibrosus, MR signal intensity, and disc height [193]. Each intervertebral disc in each alpaca was evaluated independently by a board-certified veterinary radiologist (SMS) and a board-certified human radiologist (JDW).

Figure 6-3: Example magnetic resonance image of the lower cervical spine of an 18 year old alpaca.

6.1.1 Data Analysis

The alpacas were divided into two subgroups according to age. The younger subgroup (3 – 6 years) consisted of 5 alpacas (mean age 4.8±1.1 years; mean body weight 54.8±6.6-kg), and the older subgroup (10 – 18 years) consisted of 15 alpacas (mean age 13.1±2.2 years; mean body weight 61.5±6.3-kg). The alpaca in this study included 4 Suri, and 16 Huacaya; each of the younger subgroup was Huacaya, with the 4 Suri being in the older subgroup (Table 6-1). The

effects of IVD level (e.g., C3 – C4) and the age subgroup were analyzed for statistical significance using a mixed-model analysis of variance with α=0.05 blocking on the randomized alpaca group, which was nested with the age subgroup. Least-square means values were calculated to demonstrate the combined effect of age and IVD level, and linear trendlines were determined according to the sum of least-squares methods.

The radiologists were assumed to not be a factor with Pfirrmann grading, and both observations were weighted equally for analysis and determination of least-squares effects. Pfirrmann grades for each intervertebral disc (Figure 6-4) were determined as the average between the two observations, and rounded to the nearest integer-value Pfirrmann grade. The alpaca breed was also assumed to not be a factor with the incidence of DDD and was not taken into account.

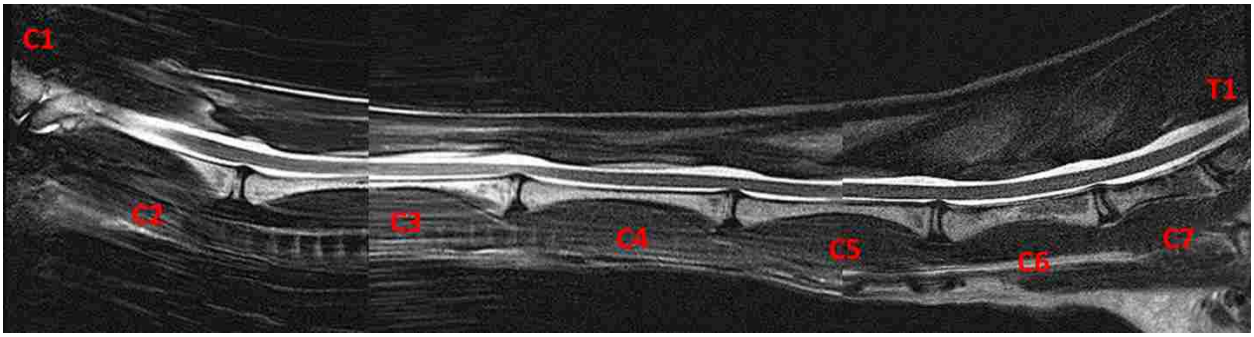

Figure 6-4: Composite MRI of a 12 yr alpaca cervical spine with vertebrae labeled.

6.2 Results

Each alpaca was observed to have a symmetrical gait with a lateral sequence footfall pattern when walking that was assessed to be sound, clinically normal, and not suffering from any orthopedic disease [35]. Young alpacas without DDD and aged alpacas with advanced DDD, as evidenced by MR imaging in our study, were asymptomatic and did not exhibit pain or abnormality of gait or neck movement. Several IVDs presented decreased water content (MR signal intensity) and had visible defects associated with the disc structure, including disc protrusions (n=9), disc prolapse (n=5), spinal cord impingement (n=1), and mild spinal cord deviation (n=3). An item that is particularly interesting is the observation that all the alpacas in this study were asymptomatic and did not exhibit clinical signs of pain or abnormality of gait.

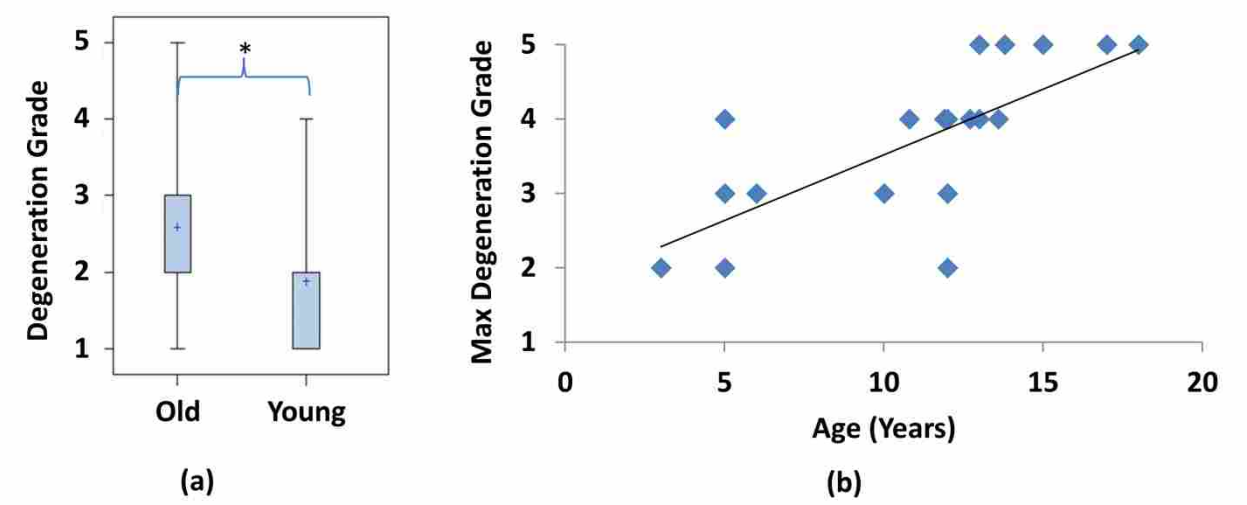

Figure 6-5: (a) A boxplot comparison of the Pfirrmann grades between the old and young subgroups, with the mean indicated by the marker inside the box, which indicates the first and third quartiles. Whiskers indicate the range of data. The asterisk (*) indicates that the two groups are significantly different (p=0.0042). (b) The maximum Pfirrmann-grade for each alpaca is plotted with the animal age. The maximum degeneration in the alpaca spine is positively correlated with age, as indicated by the linear trendline.

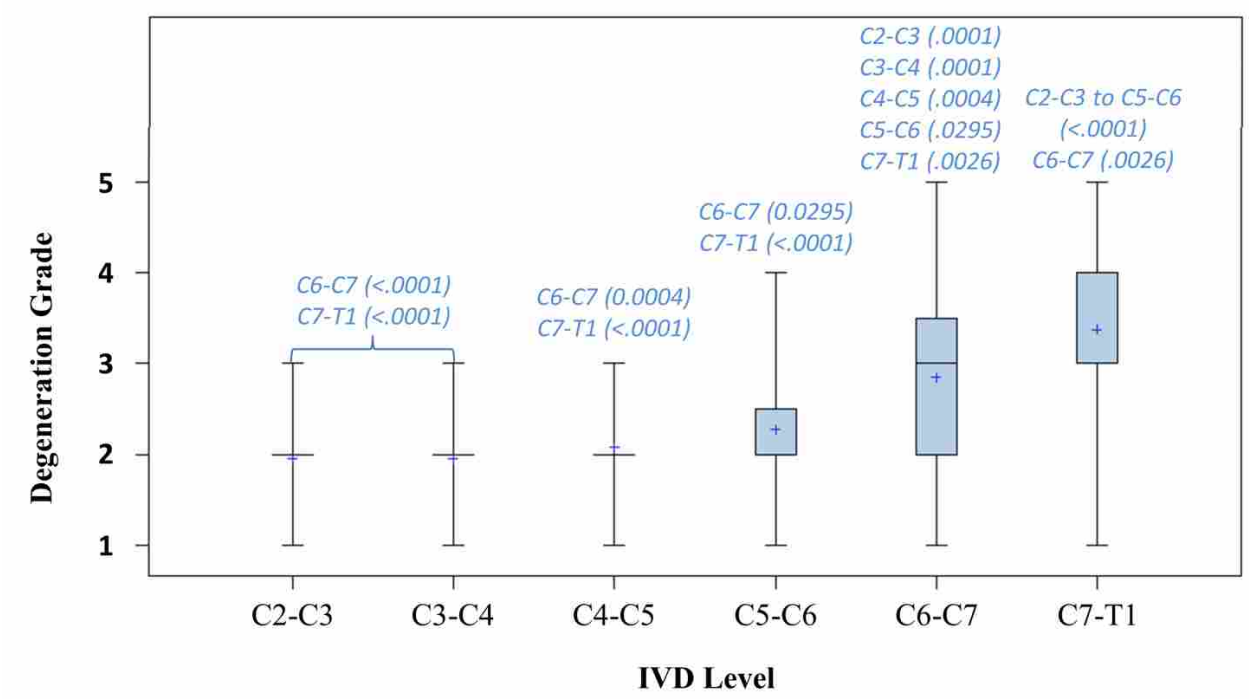

Figure 6-6: Boxplots of the Pfirrmann grades for all alpacas, grouped according to IVD level, show the positive correlation between DDD and IVD Level. Data mean is indicated by the "+" marker inside the box, which is bounded by the first and third quartiles, and the line inside the box represents the median. Where there is no box (e.g., C2-C3 to C4-C5), the median, and the first and third quartiles were identical. Whiskers indicate the maximum and minimum range of the dataset. P-values are shown above each whisker where the differences between the degeneration grade for the different IVD levels showed strong significance ($p<0.1$).

Analysis of the imaging results showed that DDD was more likely to occur in the older subgroup ($p = 0.0042$) (Figure 6-5). A strong positive correlation also was present between the location (IVD level) of the intervertebral disc in the cervical spine and the degree (or severity) of DDD ($p < 0.0001$), which was more likely to occur in the caudal cervical segments (e.g. C6-C7 and/or C7-T1) (Figure 6-6) with c7t1 being the most commonly affected disc.

In fact, there appears to be an interaction with both age and IVD level ($p = 0.0062$) as the differences between the two subgroups (young vs. old) increases with lower-level IVDs (Figure 6-7). Inspection of the data identified interesting similarities with the incidence rates of

degeneration in camelids according to the level of degeneration: advanced degeneration (Pfirrmann grade of at least 3) and severe degeneration (Pfirrmann grade of at least 4). In older alpacas, the incidence rate approaches 90% for advanced degeneration and upwards of 50% for severe degeneration, where degeneration was much more prevalent in the lower-level cervical IVDs and non-existent in the higher-level cervical IVDs In younger alpacas, the prevalence of severe degeneration was essentially zero for all cervical IVDs (Figure 6-8).

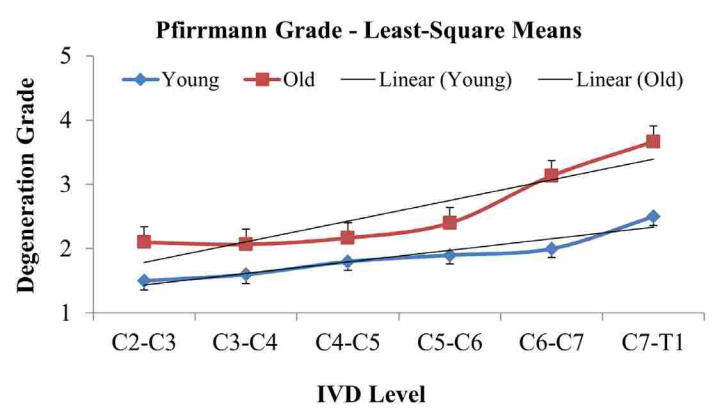

Figure 6-7: (a) Least-square means degeneration lines for the old and young age subgroup by disc segment. Note that the difference in disc degeneration between the old and young subgroups increases with the IVD level.

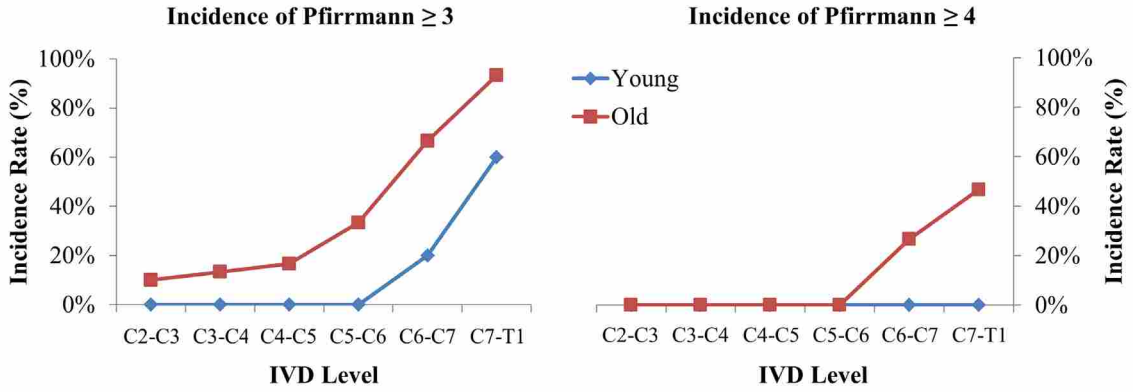

Figure 6-8: Incidence rate of advanced (left) and severe (right) intervertebral disc degeneration by disc segment for the old and young age subgroups.

6.3 Discussion

To the authors' knowledge, this study marks the first time the prevalence of naturally occurring disc degeneration has been evaluated for alpacas. The present work identified significant disc degeneration in the alpaca cervical spine at rates that indicate utility of the alpaca as a preclinical model for evaluating treatments for IVDD. Similar to humans, increasing age was correlated with a higher likelihood of IVDD. The progression of IVDD in aging camelids may be similar to the human condition in regards to prevalence, severity, and clinical signs. This, and other parallels of the alpaca and human pathology in regards to prevalence, severity, age, and location, strengthens the case to further investigate the camelid family to better understand the model's strengths and limitations in regards to types and mechanism of degeneration. An item that is particularly interesting is the observation that all the alpacas in this study were asymptomatic and did not exhibit clinical signs of pain or abnormality of gait, despite the common occurrence of degeneration.

Further research may investigate the prevalence of this condition across other species within the camelid family. There were several limitations of the present work that remain to be addressed in future work. This study only utilized female alpacas, which is ideal for production animals, but gender effects may introduce additional variation in disc degeneration status. Longitudinal evaluation of alpaca degeneration with age may also identify important similarities and differences with the human condition. Post-mortem inspection of the spine may also offer substantial histological and morphological details regarding the progression of disc degeneration in camelids. Finally, an increased sample size could allow improved accuracy in regards to investigation of all potential effects and their correlation between the severity of disc degeneration and animal age (e.g., increasing the number of age subgroups, or use age as a

continuous variable), breed, gender, genetics, weight, and more. These unique parallels may yield further understanding with the correlation between disc degeneration and other disc properties, such as disc size, biomechanics, nutrition, and posture.

From a biomechanics standpoint, there are significant differences between both the kinetics and the kinematics of quadrupeds and humans. Those animals that are currently used in spinal research have a horizontal spine orientation for the thoracic and lumbar spine while standing; however this is vertical in humans when standing.[49, 50] The passive compression provided by spinal musculature in the thoracic and lumbar spine is unlikely to capture the kinetic/kinematic effects of gravity and loading when the rostral and caudal ends are supported by the front and hind limbs.[50] However, in all animals, the cervical spine is loaded in an open-kinetic chain and more vertically oriented. In fact, the posture of the cervical spine directed over the front legs of a quadruped is markedly similar to the bipedal structure of the human.

In summary, the prevalence and severity of spontaneous intervertebral disc degeneration in the alpaca cervical spine makes the alpaca a unique candidate for large animal studies of IVD pathology and its treatment using therapeutics or surgical interventions.

7 INTERVERTEBRAL DISC BIOREACTOR

During my master's research, biomechanical studies were performed on cadaveric human intervertebral discs. Much effort was required in order to maintain the physical environment of the test specimen, such that it more closely resembled the natural (*in vivo*) environment that the test specimen encountered during the donor's life. Changes in temperature, humidity, and loading (follower load, load-type, and loading-rate) all affected the biomechanics of the test specimen. Understanding how different testing conditions could alter the physical results yielded increased understanding for all types of tests, particularly for biological systems. Similar to the identification of the strengths and weaknesses of a particular animal model, the degree of similarities of a test compared to the *in vivo* conditions was directly connected to the quality of a test. This principle was applied for identifying camelids as a good animal model, and this same principle can be applied to cellular studies of intervertebral disc biology.

Ideally, a bioreactor is meant to provide the nutrients sufficient to sustain the life of the tissue within the bioreactor, such that it has been proven to not significantly affect or change the cell density, viability, phenotype, or any type of disc biology, mechanics, biomechanics, and mechanobiology, even as if it had never been removed from the living body. This task is hard to accomplish and extremely difficult to verify. Only a select few researchers have been capable of creating bioreactors that have been able to sustain the life of the intervertebral disc for up to

several weeks for large animal intervertebral discs, or for up to several months for small animal intervertebral discs [25, 27, 194-196].

During my doctoral studies I had the opportunity to work with a collaborative multi-disciplinary research group that brought together mechanical engineering, molecular biology, and microbiology, on a project to create an intervertebral disc bioreactor and further understand the cellular biology of the disc. Our preliminary work was successful in recreating some current research with identifying the correct mixture procedure and recipe for intervertebral disc culture medium, performing live-dead cell staining and analysis using fluorescent microscopy, as well as developing the methods, procedures, and equipment for a static-culture intervertebral disc bioreactor, and genetic studies of the alpaca IVD.

My contribution to this work was specifically involved with the creation and validation of the static bioreactor and protocols (as described in Appendix D), fluorescent microscopy, and qualitative analysis of the IVDs; I also had the opportunity to partake in the preliminary steps and tests in the creation of a dynamic bioreactor. Any additional work of developing the IVD culture medium and proper cell culture techniques, and the genetic studies (included below) was directed by Dr. Bridgewater and her lab, and is included here for documentation purposes only.

7.1 Methodology

Intervertebral disc culture medium was mixed in a sterile environment and placed in the static bioreactor. The full neck from a mature alpaca was obtained immediately following slaughter. The neck was skinned, segmented, and dissected to remove several intact intervertebral discs within two hours from the time of death. Great care was taken to not damage the disc during removal and preparation. For preparation, the adjacent bone from the vertebral

body was removed in its entirety; even the more calcified bony endplate was removed so that only the cartilage endplate remained. Within two hours from time of death, two discs were placed in the live/dead cell-staining medium (LDCM), and two discs were placed in a custom-built static culture bioreactor, which continuously circulated the intervertebral disc culture medium (DCM).

The LDCM works by binding different dyes to the cell. Living cells are stained green as the *Cell-Tracker Green*® freely passes through the cell membrane, and becomes cell-impermeant; the cells will fluoresce green under green excitation/emission spectra (492-517 nm). When a cell dies, the cell membrane becomes compromised and the propidium-iodide, which is normally membrane impermeant, is able to access and bind to the nucleic acids (RNA and DNA) inside the cell. Once bound to a nucleic acid, propidium iodide will fluoresce over twenty times brighter when excited under the red excitation spectra (Figure 7-1).

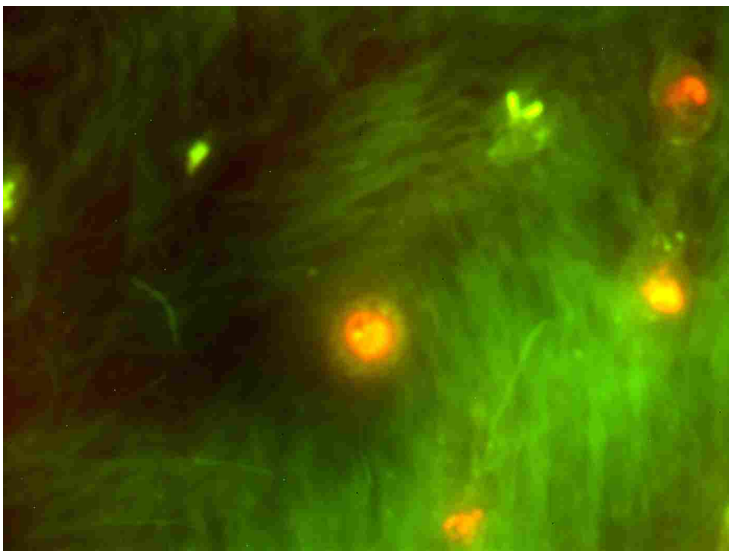

Figure 7-1: The propidium iodide identifies the dead cells by fluorescing bright red.

The two discs that were placed in the LDCM were placed on a cyclic translating platform inside an incubator and soaked for 45 – 60 minutes. These discs were then frozen in liquid nitrogen for several minutes, until the whole disc was frozen. These discs were sliced in the transverse plane using the cryostat into 8-micrometer (μm) thick sections from various heights (Figure 7-2) placed on glass slides for the fluorescent microscope. Each section included a complete transverse section of the intervertebral disc, with visible distinction of the NP and AF. Several images were taken at various levels, or depths, to qualitatively determine cell vitality of the intervertebral disc. This was used as the control test for the discs placed in the static-culture bioreactor.

Figure 7-2: The cryostat was used to slice 8 μm thick transverse sections of the intervertebral disc stained with live/dead cell-staining medium.

The two discs placed in the static culture bioreactor and followed the procedure outlined by Gawri et el. [25]: the discs were submerged in the DCM on elevated platforms within individual 100 milliliter polymethylpentene containers (Nalgene; Rochester, NY) and held inside an incubator at 37°C, 5%-CO_2. The DCM was circulated using a peristaltic pump at a rate of 3 microliters per minute, and the entire medium was changed every 3 days. One disc was removed after 4 days, and the second disc was removed after 7 days (Figure 7-3). Immediately after

removal from the bioreactor, the disc followed the procedure outlined above (and in Appendix D – Dynamic Bioreactor Protocols) for live/dead cell staining in order to determine cell vitality, compared to the control studies.

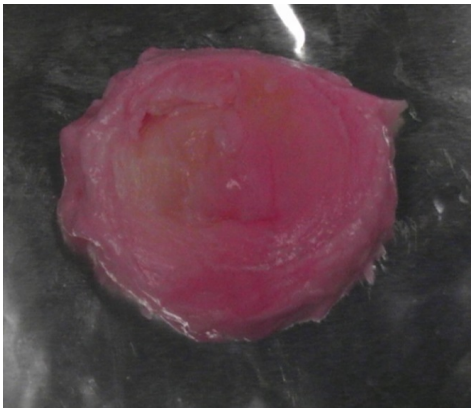

Figure 7-3: The intervertebral disc after 7 days in the static-culture bioreactor.

7.2 Results

Comparing the cell vitality between the intervertebral discs from control studies and the static culture bioreactor, the static-culture bioreactor was able to sustain whole viable alpaca discs for at least 7 days (Figure 7-3), as determined by live/dead cell staining. An interesting observation was how the cell vitality changed with the relative location within the disc, for both the control and bioreactor studies. Cell vitality increased with increasing depth; or, a cell was more likely to be alive the further it resided from the endplate, as shown in Figure 7-4. Without any follow-up research done concerning this matter, the assumption was that something happened during the preparation of the test specimen that killed those cells most near the surface. Several theories were presented with rough handling of the disc caused high stresses that triggered apoptosis, or (the most popular theory) that the heat created during the rapid cutting

process with the band saw would encourage cell-death. Removing the discs is an intense process that must be done as quickly as possible to preserve the life of the cells, and where this process was new to everyone involved, the excitement and anxiety of the process could have allowed multiple potential sources of error.

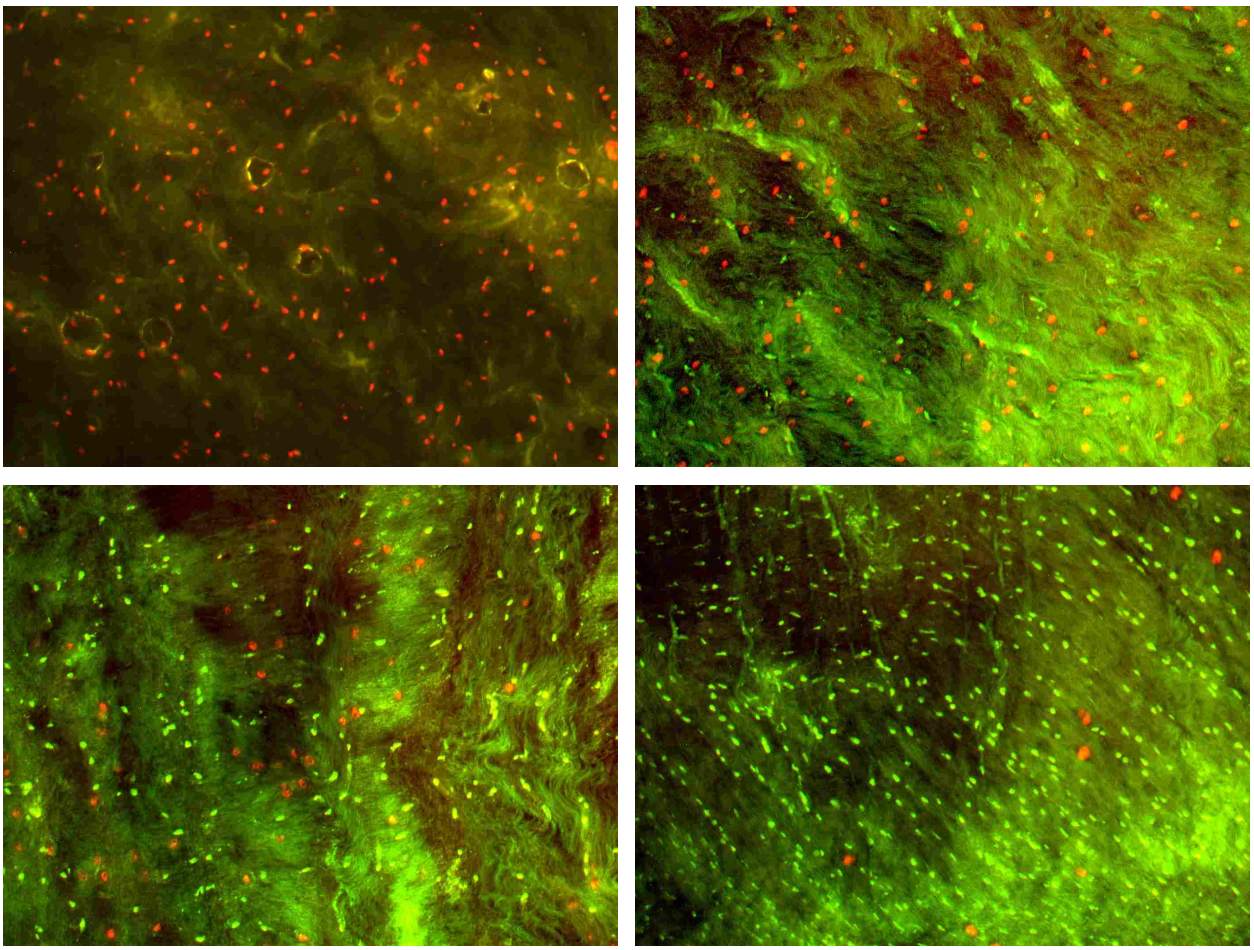

Figure 7-4: NP-cell vitality increased with deeper sections of the disc, as shown in the images at increasing depth from superficial, near the endplate, (upper left) to deep, mid-disc height, (lower right).

These efforts of creating an intervertebral disc bioreactor continue with the master's research of Amanda Beatty in the development of a dynamic in vitro culture system that utilizes

the same preparation protocols (Appendix D) and culture medium as the static-culture bioreactor, but the functions of the bioreactor itself are augmented to include pneumatic actuators that are programmed to cycle and physically move, load, and pump the alpaca intervertebral discs with a cyclic compressive load and other bending motions (e.g. flexion-extension and lateral-bending) that might be experienced throughout a person's normal activities of daily living.

7.3 Other Cellular Studies Done with the Alpaca Intervertebral Disc

In conjunction with the static culture system, specific work was done with genetic expression in regards to identifying disc degeneration. In order to do this, a specific primer is used for each individual gene of interest using a laboratory technique called qualitative, reverse transcription, polymeric chain reaction (qRT-PCR). The genes chosen for studying a possible correlation with disc degeneration included aggrecan, Col1a1, Col2a1, Sox9, MMP13, and ADAMTS5, which are specific for the particular animal's genome. As the alpaca or llama genome are not yet sequenced (which is an expensive process), and since there is a lot of similarities with mammalian biology, these experiments were done primarily to verify whether the qRT-PCR primers from the human genome would work for an alpaca.

RNA from alpaca annulus fibrosus was isolated, reverse transcribed, and amplified using several human-specific RT2-qPCR primers (Qiagen; Hilden, Germany). These tests were successful in amplifying the expression of Col2a1, Col1a1, Sox9, MMP13, and ADAMTS5 [27, 195] genes in alpaca intervertebral discs (Figure 7-5). While some instances of aggrecan amplified, it was not sufficient to be considered as a successful trial; however, this was an N=1 study, and future studies may perform better.

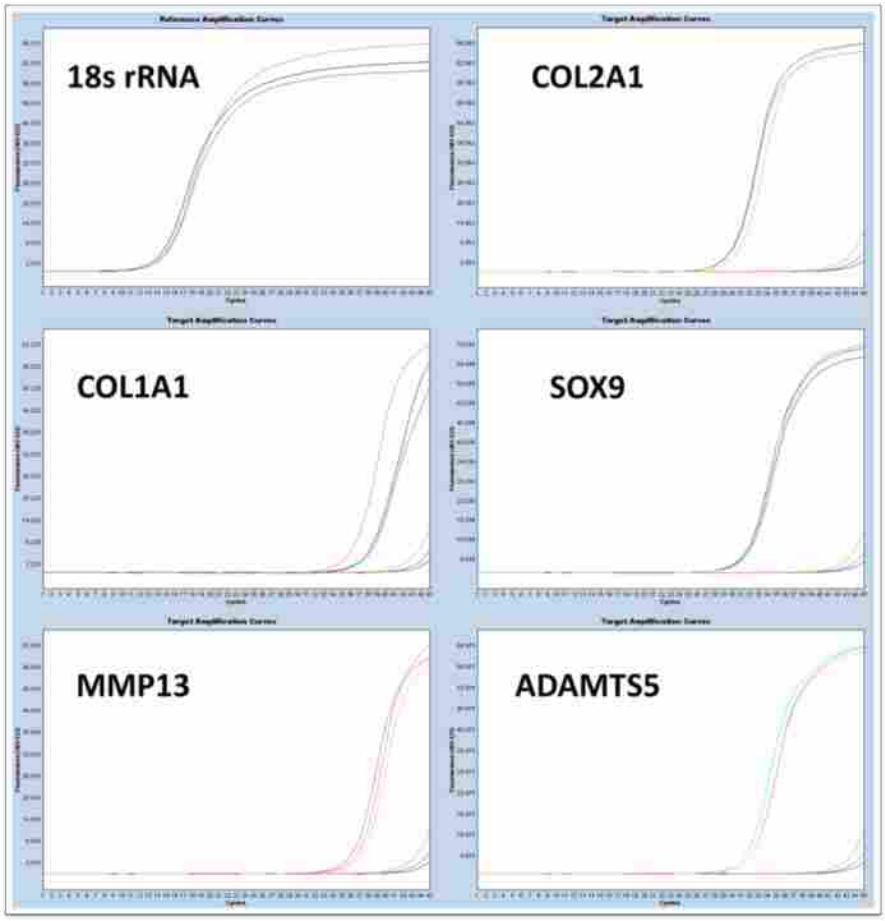

Figure 7-5: Human RT2-qPCR primers can be used to measure gene expression in alpaca intervertebral discs.

Using these regions of human-alpaca homology, a panel of alpaca-specific qRT-PCR primers may now be developed for these genes and other genes that are relevant to disc degeneration, with the ultimate goal of testing potential therapeutics, both *in vitro* (during bioreactor studies) and *in vivo*, by monitoring the genetic expression of the discs cells of a camelid model of intervertebral disc degeneration. Although the alpaca genome is not yet sequenced, gene expression studies can be performed on alpaca samples using human qRT2-PCR primers.

8 COLLABORATIVE CONTRIBUTIONS TO OTHER WORK

Throughout the course of my graduate research, I have had the opportunity to work with several collaborative research projects. This project in particular involves the application of a high-displacement nano-composite strain gauge for tracking in-vivo biomechanical motion, which units with the previous research through the common goal of understanding and tracking the development and treatment of DDD.

8.1 High-displacement Nano-composite Strain Gauge

Strain has long been used in engineering design and analysis using a previously-mounted strain gauge. In fact, the strain gauge "has been the single, most-powerful tool in the field of experimental stress analysis" [197]. However, traditional strain gauges are extremely limited as they can only report small (<5%) strains. An electrically conductive material is required, and the thin metal foil used in the strain gauge limits the usable strain range to be within the elastic region for the specific metal. If the strain passes the elastic region, the material may either break and is no longer conductive) or is permanently deformed (and would require recalibration). In order to overcome the small strain limitation of traditional strain gauges, the strain gauge material must be changed. This small-strain limitation of this otherwise robust technology instantly occludes several ground-breaking developments within medicine and biology.

The purpose of this research project was to exploit a novel nano-composite polymer, which has already proven to exhibit piezo-effects, to capture strain and motion in biological soft

tissue. By tracking the parameters of strain, which is directly correlated with motion, applications include:

- Improved characterization of biological soft tissue material properties to advance the design of orthopedic implants (e.g. shoulder, knee, hip, or spine arthroscopy);
- Simplified methods to characterize and identify mechanisms of injury; or
- Continuous, instantaneous monitoring of patient health to improve rehabilitation services.

My contributions to this project included a literature review of the materials, and compiling and submitting an application for the use of human subjects through the institutional review board (IRB), including creating recruiting material, and ensuring the safety of the potential volunteers. After IRB approval was given, my available time for this project was focused on supporting the project through my prior experience with the design of statistical experiments, and experimental setup and testing, which are given in more detail below.

8.1.1 Motivation

The nano-composite polymer of interest has proven effective at consistently measuring large (over 60%) strains, thereby overcoming the small-strain limitation and enabling a new class of sensors for biomedical applications. It is this reason, in particular, that I was interested in this technology. Attaching a network of gauges to the human lumbar spine (or the camelid cervical spine) could provide a non-invasive method to track motion throughout one's life, or following surgery, and the potential of correlating this physical motion with the development of DDD or healing after surgery was exciting.

The high strain is possible as the base/matrix material of this composite is an elastomer: a two-part silicone. The primary conductive filler is pure nickel, in the form of nickel nanostrands (NiNS). NiNS are high aspect-ratio, bifurcated nanostructures [198-204], which are made by Conductive Composities, LLC (Heber, UT), using a proprietary, low temperature, atmospheric pressure, chemical vapor deposition (LTAPCVD) process. The secondary conductive stabilizer is provided by carbon fibers, which are coated (20%, by weight) with pure nickel and cut to a length of approximately 1 – 2 mm. The nickel-coated carbon fiber (NCCF) is also provided by Conducitve Composites, LLC.

Combining these elements requires a fragile manufacturing process to ensure proper dispersion while protecting the structural integrity of the conductive fillers. The NiNs are screened through a 40-gauge mesh, and then gently mixed with one part of the silicone. The NCCF is mixed with the other part of the silicone, and then all combined with a cross-linking catalytic buffer for the solution viscosity. High shear stresses may damage the unique nanostructure of the NiNS, and a cross-linking catalyst allows proper mixing with decreased shear stresses. Mixing occurs using a planetary centrifugal mixer in order to achieve uniform dispersion of the conductive fillers, resulting in a macro-homogenous mixture, which is placed into an aluminum mold for curing.

The resulting nano-composite polymer maintains a majority of the elastic properties of the silicone, and some conductivity of the nickel additives is also present, which permits a piezoresistive response. The material may be characterized with a specific resistance ($10–10^6\Omega$, depending on the mix ratios) as a known electrical current passes through it and the voltage potential is measured across the connection; however, due to piezoresistivity, this characteristic resistance will change upon undergoing strain.

The piezoresistivity of this material is unique as it exhibits both negative and positive piezoresistivity. Specifically: the negative piezoresistance is observed as the material is stretched (positive strain) and the resistance consequently decreases; the positive piezoresistance is observed as the material is compressed (negative strain) and the resistance consequently decreases. The resistance decreases (i.e., conductance increases) with both tension and compression, with respect to the unstrained, "neutral" position. When the material is stretched, a change in resistance will follow a repeatable curve that will consistently measure strain without plastic deformation. During testing, the gauges have shown that accurate strains can be measured along this curve with less than 10% error [205] of optical marker tracking. This nano-composite strain gauge appears to be just as versatile (or more versatile) than any of the current high displacement measurement methods currently available. They are capable of real-time measurement, and are often more cost effective than other methods [205].

Previous studies performed by Fullwood, et al. [198-200, 204-206] indicate that Si/NiNS/NCCF nanocomposites in concentrations of 11% (by volume) NiNS + 2% (by volume) NCCF can be used as simple, inexpensive large displacement sensors that can accurately measure up to 40% strains [199]. However, further characterization of the material response was required in order to become productive gauges for *in situ* applications. We needed to identify a composite blend that would give a repeatable electrical signal for the functional strain range within the range of human physiological motion, while maintaining the most elasticity possible so as to not adversely affect the normal biomechanics.

8.1.2 Experimental Testing

Multiple statistical designs of experiments were created by former and current BYU graduate students Taylor Remington and Dan Baradoy to identify a base elastomer and the ideal concentrations of composite elements. The base elastomer must repeatedly stretch without yielding, and the ideal concentration of conductive elements is necessary for the piezo-effect. While the conductive elements were necessary for the piezo-effect, the stiffness of the nano-composite material would increase with increasing conductive elements. A balance was needed and in order to find the middle ground for the competing requirements of conductivity and stiffness. From these studies, the selected composition of silicone and conductive elements provided one of the largest pseudo-linear electrical responses within the range of physiological motion.

Once the gauge material was created, the material required "conditioning" before it was usable. Conditioning involved pre-straining or working the material to alleviate any residual stresses or binding that may have developed during the manufacturing process. A cold-rolling process was most effective for conditioning by applying a uniform pre-strain for the whole sensor material. Attaching the conditioned gauge material to a manufactured elastic/flexible material also helped to maintain a consistent signal, however the specific elastic material varied depending on the application and the stiffness of the elastic material. While these experiments are useful with the application of this technology, there is still much to learn about the technology of nano-composite strain gauges.

This technology maintains select advantages of using a strain gauge including: blind data collection, fast sampling rates; and, near real-time (RT) communication of results. The potential for this type of sensor remains largely unknown, yet I anticipate a large impact will occur with

medical applications—specifically orthopedics, rehabilitation, injury analysis, soft tissue biomechanics, and sport/exercise science. The advancement and further development of this exciting technology will be carried on with the research of Dan Baradoy and others. My contributions to this project were limited to a literature review of the materials, and gaining IRB approval, which were summarized in the background and motivation (above), in addition to supporting various experiments of others, which are also described above.

9 SUMMARY AND FUTURE WORK

The objective of this work was to examine the hypothesis that camelids (specifically llamas and alpacas) will naturally develop intervertebral disc degeneration in the cervical spine due to similarities in the cellular, morphological and biomechanical environment, and therefore would be a good animal model for intervertebral disc degeneration and the human lumbar spine. The present work identified degeneration in the alpaca cervical IVDs at rates that indicate utility of the alpaca as a preclinical model for evaluating treatments for DDD. Camelids show substantial characteristic similarities in regards to morphology and biomechanics, in addition to the prevalence of degenerative pathology, of the intervertebral disc. Similarities in size and biomechanics should make the camelid model more attractive than current models for preclinical trials of orthopaedic implants, specifically in regards to in vivo testing.

It is likely that the camelid model will have large applications with nutrition and degeneration studies of the IVD. There is still much to be learned concerning the development of DDD in camelids; however, that utilization of camelids for explorations of increasing age and the development of DDD would be extremely valuable. The progression of DDD in aging camelids was shown to be similar to the human condition in regards to prevalence, and severity. This, and other parallels of the alpaca and human pathology strengthens the case for further investigation of the camelid family to better understand the model's strengths and limitations in regards to types and mechanism of degeneration. An item that is particularly interesting is the

observation that all the alpacas in this study were asymptomatic and did not exhibit clinical signs of pain or abnormality of gait; however, clinical signs are not completely absent [8] from camelids.

To my knowledge, this research marks the first time the prevalence of naturally occurring disc degeneration has been evaluated for alpacas. The results of this research highlight key characteristics that suggest the alpaca and llama area a viable candidate for large animal studies of IVD degeneration. Both healthy and unhealthy spines can be studied using this animal model that substantially resembles the human lumbar IVD. It is likely that similar results would be found in llamas, other camelids, and any other animal according to the desired characteristics explained in Chapter 3. Furthermore, as alpaca and llama farms are located throughout the world, the results presented here encourage worldwide collaboration on a growing worldwide problem.

In summary, the camelid IVD model sufficiently mimics the human lumbar IVD in regards to spinal posture, size, shape, and biomechanics. The classification of spontaneous disc degeneration in the cervical spine is consistent with a lack of notochord cells, which is common with large animals. Future work may involve regeneration studies of a spontaneously degenerated IVD, which has been limited in the past by the availability of a viable large animal model, and further testing and validation is needed to better understand the application of this work in regards to the camelid's susceptibility to IVD degeneration and the potential for regeneration. Regardless, as alpaca or llama farms are located throughout the world the results presented here indicate exciting potential for using camelids as a model of human lumbar disc degeneration all over the world

9.1 Recommendations for Continuing Work

While the use of a camelid (alpaca or llama) model of intervertebral disc degeneration may help bridge the gap for an improved understanding of DDD, all models have their limitations. Understanding those limitations is equally important as the model itself, as this understanding further strengthens the application and utilization of that particular model. Specific limitations of this model are not fully understood yet, but our understanding will continue to increase with future independent utilization, testing, and verification, of the camelid model of lumbar disc degeneration.

There were several limitations of the present work that remain to be addressed in future work. Further research may investigate the prevalence of this condition across other species within the camelid family. Also, these studies only utilized female alpacas, which are ideal for production animals, but gender effects may introduce additional variation in disc degeneration susceptibility. The camelid cervical segments appeared to be more flexible than the human lumbar segments in flexion-extension and lateral-bending; however, this increased flexibility may be attributed to the lack of the bilateral nuchae ligaments during the flexibility studies, which are assumed to provide a substantial increase in stiffness and resistance to flexion and lateral-bending. Future ex-vivo or in-vivo testing that incorporates these ligaments during flexibility testing may confirm the average ROM of the cervical spine.

Future research may help to further understand the effect of age and its correlation with DDD; tracking the development of degeneration throughout the lifetime of a camelid would allow a longitudinal statistical evaluation of alpaca degeneration with age, which may identify important similarities and differences with the human condition. Post-mortem inspection of the spine may also offer substantial histological and morphological details regarding the progression

of disc degeneration in camelids, particularly if a Pfirrmann-grade analysis is completed prior to death.

As always, an increased sample size could allow improved accuracy in regards to the above studies and their correlation between the severity of disc degeneration and animal age (e.g., increasing the number of age subgroups, or use age as a continuous variable), breed, gender, genetics, weight, and more. These unique parallels may yield further understanding of potential correlations between DDD and other intervertebral disc properties, such as disc size and nutrition, spine biomechanics and posture, or cell density and type. These are just a few of the limitations. Ultimately, by investigating a new animal, there is still much to learn. The investigation of the applicability of the camelid cervical spine as a model for the human lumbar spine and disc degeneration is ongoing.

REFERENCES

1. Lotz, J. C., Hsieh, A. H., Walsh, A. L., Palmer, E. I., and Chin, J. R. "Mechanobiology of the intervertebral disc." *Biochem Soc Trans* 30, no. Pt 6 (Nov 2002): 853-8.

2. Setton, L. A., and Chen, J. "Cell mechanics and mechanobiology in the intervertebral disc." *Spine (Phila Pa 1976)* 29, no. 23 (Dec 1 2004): 2710-23.

3. Adams, M. A., and Roughley, P. J. "What is intervertebral disc degeneration, and what causes it?". *Spine (Phila Pa 1976)* 31, no. 18 (Aug 15 2006): 2151-61.

4. Andersson, G. B. "Epidemiological features of chronic low-back pain." *Lancet* 354, no. 9178 (Aug 14 1999): 581-5.

5. Coppes, M. H., Marani, E., Thomeer, R. T., and Groen, G. J. "Innervation of "painful" lumbar discs." *Spine* 22, no. 20 (Oct 15 1997): 2342-9; discussion 49-50.

6. Inoue, N., and Espinoza Orias, A. A. "Biomechanics of intervertebral disk degeneration." *Orthop Clin North Am* 42, no. 4 (Oct 2011): 487-99, vii.

7. Hsieh, A. H., and Twomey, J. D. "Cellular mechanobiology of the intervertebral disc: new directions and approaches." *J Biomech* 43, no. 1 (Jan 5 2010): 137-45.

8. Valentine, B. A., Saulez, M. N., Cebra, C. K., and Fischer, K. A. "Compressive myelopathy due to intervertebral disk extrusion in a llama (Lama glama)." *J Vet Diagn Invest* 18, no. 1 (Jan 2006): 126-9.

9. Hughes, S. P., Freemont, A. J., Hukins, D. W., Mcgregor, A. H., and Roberts, S. "The pathogenesis of degeneration of the intervertebral disc and emerging therapies in the management of back pain." *J Bone Joint Surg Br* 94, no. 10 (Oct 2012): 1298-304.

10. Adams, M. A., and Dolan, P. "Spine biomechanics." *J Biomech* 38, no. 10 (Oct 2005): 1972-83.

11. Clouet, J., Vinatier, C., Merceron, C., Pot-Vaucel, M., Hamel, O., Weiss, P., Grimandi, G., and Guicheux, J. "The intervertebral disc: from pathophysiology to tissue engineering." *Joint Bone Spine* 76, no. 6 (Dec 2009): 614-8.

12. Frank, J. W., Brooker, A. S., Demaio, S. E., Kerr, M. S., Maetzel, A., Shannon, H. S., Sullivan, T. J., Norman, R. W., and Wells, R. P. "Disability resulting from occupational low back pain. Part II: What do we know about secondary prevention? A review of the scientific evidence on prevention after disability begins." *Spine (Phila Pa 1976)* 21, no. 24 (Dec 15 1996): 2918-29.

13. Frank, J. W., Kerr, M. S., Brooker, A. S., Demaio, S. E., Maetzel, A., Shannon, H. S., Sullivan, T. J., Norman, R. W., and Wells, R. P. "Disability resulting from occupational low back pain. Part I: What do we know about primary prevention? A review of the scientific evidence on prevention before disability begins." *Spine (Phila Pa 1976)* 21, no. 24 (Dec 15 1996): 2908-17.

14. Dagenais, S., Caro, J., and Haldeman, S. "A systematic review of low back pain cost of illness studies in the United States and internationally." *Spine J* 8, no. 1 (Jan-Feb 2008): 8-20.

15. Gore, M., Sadosky, A., Stacey, B. R., Tai, K. S., and Leslie, D. "The burden of chronic low back pain: clinical comorbidities, treatment patterns, and health care costs in usual care settings." *Spine (Phila Pa 1976)* 37, no. 11 (May 15 2012): E668-77.

16. Lehmann, T. R., Spratt, K. F., Tozzi, J. E., Weinstein, J. N., Reinarz, S. J., El-Khoury, G. Y., and Colby, H. "Long-term follow-up of lower lumbar fusion patients." *Spine (Phila Pa 1976)* 12, no. 2 (Mar 1987): 97-104.

17. Kuslich, S. D., Ulstrom, C. L., Griffith, S. L., Ahern, J. W., and Dowdle, J. D. "The Bagby and Kuslich method of lumbar interbody fusion. History, techniques, and 2-year follow-up results of a United States prospective, multicenter trial." *Spine (Phila Pa 1976)* 23, no. 11 (Jun 1 1998): 1267-78; discussion 79.

18. Katz, J. N. "Lumbar disc disorders and low-back pain: socioeconomic factors and consequences." *J Bone Joint Surg Am* 88 Suppl 2 (Apr 2006): 21-4.

19. Katz, R. T. "Impairment and disability rating in low back pain." *Clin Occup Environ Med* 5, no. 3 (2006): 719-40, viii.

20. Alini, M., Eisenstein, S. M., Ito, K., Little, C., Kettler, A. A., Masuda, K., Melrose, J., Ralphs, J., Stokes, I., and Wilke, H. J. "Are animal models useful for studying human disc disorders/degeneration?". *Eur Spine J* 17, no. 1 (Jan 2008): 2-19.

21. Kikkawa, J., Cunningham, B. W., Shirado, O., Hu, N., Mcafee, P. C., and Oda, H. "Biomechanical evaluation of a posterolateral lumbar disc arthroplasty device: an in vitro human cadaveric model." *Spine (Phila Pa 1976)* 35, no. 19 (Sep 1 2010): 1760-8.

22. Panjabi, M. M., Goel, V., Oxland, T., Takata, K., Duranceau, J., Krag, M., and Price, M. "Human lumbar vertebrae. Quantitative three-dimensional anatomy." *Spine (Phila Pa 1976)* 17, no. 3 (Mar 1992): 299-306.

23. Stolworthy, D. K., Zirbel, S. A., Howell, L. L., Samuels, M., and Bowden, A. E. "Characterization and prediction of rate-dependent flexibility in lumbar spine biomechanics at room and body temperature." *Spine J* 14, no. 5 (May 1 2014): 789-98.

24. Zirbel, S. A., Stolworthy, D. K., Howell, L. L., and Bowden, A. E. "Intervertebral disc degeneration alters lumbar spine segmental stiffness in all modes of loading under a compressive follower load." *The Spine Journal* (Mar 15 2013).

25. Gawri, R., Mwale, F., Ouellet, J., Roughley, P. J., Steffen, T., Antoniou, J., and Haglund, L. "Development of an organ culture system for long-term survival of the intact human intervertebral disc." *Spine (Phila Pa 1976)* 36, no. 22 (Oct 15 2011): 1835-42.

26. Jim, B., Steffen, T., Moir, J., Roughley, P., and Haglund, L. "Development of an intact intervertebral disc organ culture system in which degeneration can be induced as a prelude to studying repair potential." *Eur Spine J* 20, no. 8 (Aug 2011): 1244-54.

27. Risbud, M. V., Izzo, M. W., Adams, C. S., Arnold, W. W., Hillibrand, A. S., Vresilovic, E. J., Vaccaro, A. R., Albert, T. J., and Shapiro, I. M. "An organ culture system for the study of the nucleus pulposus: description of the system and evaluation of the cells." *Spine (Phila Pa 1976)* 28, no. 24 (Dec 15 2003): 2652-8; discussion 58-9.

28. An, H. S., and Masuda, K. "Relevance of in vitro and in vivo models for intervertebral disc degeneration." *J Bone Joint Surg Am* 88 Suppl 2 (Apr 2006): 88-94.

29. Lotz, J. C. "Animal models of intervertebral disc degeneration: lessons learned." *Spine (Phila Pa 1976)* 29, no. 23 (Dec 1 2004): 2742-50.

30. Vo, N., Niedernhofer, L. J., Nasto, L. A., Jacobs, L., Robbins, P. D., Kang, J., and Evans, C. H. "An overview of underlying causes and animal models for the study of age-related degenerative disorders of the spine and synovial joints." *J Orthop Res* (Mar 11 2013).

31. Stolworthy, D. K. "Characterization and Biomechanical Analysis of the Human Lumbar Spine with In Vitro Testing Conditions." Thesis, Brigham Young University, 2012.

32. Stolworthy, D. K., Fullwood, R. A., Merrell, T. M., Bridgewater, L. C., and Bowden, A. E. "Biomechanical Analysis of the Camelid Cervical Intervertebral Disc." *Journal of Orthopaedic Translation* (2014).

33. Remington, T.D, Merrell, A. J., Stolworthy, D. K., Mcarthur, D. R., Fullwood, D. T., Bowden, A. E., Hansen, N. D., "Biomechanical Applications of Quantum Nano-composite Strain Gauges," in *Society for the Advancement of Material and Process Engineering*. Long Beach, CA, 2013.

34. Bertram, J. E., and Gutmann, A. "Motions of the running horse and cheetah revisited: fundamental mechanics of the transverse and rotary gallop." *J R Soc Interface* 6, no. 35 (Jun 6 2009): 549-59.

35. Pfau, T., Hinton, E., Whitehead, C., Wiktorowicz-Conroy, A., and Hutchinson, J. R. "Temporal gait parameters in the alpaca and the evolution of pacing and trotting locomotion in the Camelidae." *Journal of Zoology* 283, no. 3 (Mar 2011): 193-202.

36. Smith, L. J., Nerurkar, N. L., Choi, K. S., Harfe, B. D., and Elliott, D. M. "Degeneration and regeneration of the intervertebral disc: lessons from development." *Dis Model Mech* 4, no. 1 (Jan 2011): 31-41.

37. Guerin, H. L., and Elliott, D. M. "Quantifying the contributions of structure to annulus fibrosus mechanical function using a nonlinear, anisotropic, hyperelastic model." *J Orthop Res* 25, no. 4 (Apr 2007): 508-16.

38. Heuer, F., Schmidt, H., and Wilke, H. J. "The relation between intervertebral disc bulging and annular fiber associated strains for simple and complex loading." *J Biomech* 41, no. 5 (2008): 1086-94.

39. Adams, M. A., Mcmillan, D. W., Green, T. P., and Dolan, P. "Sustained loading generates stress concentrations in lumbar intervertebral discs." *Spine (Phila Pa 1976)* 21, no. 4 (Feb 15 1996): 434-8.

40. Hwang, D., Gabai, A. S., Yu, M., Yew, A. G., and Hsieh, A. H. "Role of load history in intervertebral disc mechanics and intradiscal pressure generation." *Biomech Model Mechanobiol* 11, no. 1-2 (Jan 2012): 95-106.

41. Kettler, A., Liakos, L., Haegele, B., and Wilke, H. J. "Are the spines of calf, pig and sheep suitable models for pre-clinical implant tests?". *Eur Spine J* 16, no. 12 (Dec 2007): 2186-92.

42. Panjabi, M., Brown, M., Lindahl, S., Irstam, L., and Hermens, M. "Intrinsic disc pressure as a measure of integrity of the lumbar spine." *Spine (Phila Pa 1976)* 13, no. 8 (Aug 1988): 913-7.

43. Schnake, K. J., Putzier, M., Haas, N. P., and Kandziora, F. "Mechanical concepts for disc regeneration." *Eur Spine J* 15 Suppl 3 (Aug 2006): S354-60.

44. Feng, H., Danfelter, M., Stromqvist, B., and Heinegard, D. "Extracellular matrix in disc degeneration." *J Bone Joint Surg Am* 88 Suppl 2 (Apr 2006): 25-9.

45. Humzah, M. D., and Soames, R. W. "Human intervertebral disc: structure and function." *Anat Rec* 220, no. 4 (Apr 1988): 337-56.

46. Raj, P. P. "Intervertebral disc: anatomy-physiology-pathophysiology-treatment." *Pain Pract* 8, no. 1 (Jan-Feb 2008): 18-44.

47. Chan, W. C., Sze, K. L., Samartzis, D., Leung, V. Y., and Chan, D. "Structure and biology of the intervertebral disk in health and disease." *Orthop Clin North Am* 42, no. 4 (Oct 2011): 447-64, vii.

48. Kitano, T., Zerwekh, J. E., Usui, Y., Edwards, M. L., Flicker, P. L., and Mooney, V. "Biochemical changes associated with the symptomatic human intervertebral disk." *Clin Orthop Relat Res*, no. 293 (Aug 1993): 372-7.

49. Urban, J. P., and Roberts, S. "Degeneration of the intervertebral disc." *Arthritis Res Ther* 5, no. 3 (2003): 120-30.

50. Freemont, A. J., Peacock, T. E., Goupille, P., Hoyland, J. A., O'brien, J., and Jayson, M. I. "Nerve ingrowth into diseased intervertebral disc in chronic back pain." *Lancet* 350, no. 9072 (Jul 19 1997): 178-81.

51. Urban, J. P., Smith, S., and Fairbank, J. C. "Nutrition of the intervertebral disc." *Spine (Phila Pa 1976)* 29, no. 23 (Dec 1 2004): 2700-9.

52. Grunhagen, T., Wilde, G., Soukane, D. M., Shirazi-Adl, S. A., and Urban, J. P. "Nutrient supply and intervertebral disc metabolism." *J Bone Joint Surg Am* 88 Suppl 2 (Apr 2006): 30-5.

53. Adams, M. A., Pollintine, P., Tobias, J. H., Wakley, G. K., and Dolan, P. "Intervertebral disc degeneration can predispose to anterior vertebral fractures in the thoracolumbar spine." *J Bone Miner Res* 21, no. 9 (Sep 2006): 1409-16.

54. Buckwalter, J. A. "Aging and degeneration of the human intervertebral disc." *Spine* 20, no. 11 (Jun 1 1995): 1307-14.

55. Horner, H. A., and Urban, J. P. "2001 Volvo Award Winner in Basic Science Studies: Effect of nutrient supply on the viability of cells from the nucleus pulposus of the intervertebral disc." *Spine (Phila Pa 1976)* 26, no. 23 (Dec 1 2001): 2543-9.

56. Urban, J. P., Holm, S., Maroudas, A., and Nachemson, A. "Nutrition of the intervertebral disk. An in vivo study of solute transport." *Clin Orthop Relat Res*, no. 129 (Nov-Dec 1977): 101-14.

57. Yoganandan, N., Nahum, A. M., and Melvin, J. *Accidental injury : biomechanics and prevention*. Third edition. ed. New York: Springer, 2015.

58. White, A. A., and Panjabi, M. M. *Clinical biomechanics of the spine*. Vol. 2: Lippincott Philadelphia, 1990.

59. Ghosh, P. *The Biology of the intervertebral disc*. 2 vols. Boca Raton, Fla.: CRC Press, 1988.

60. Walter, B. A., Korecki, C. L., Purmessur, D., Roughley, P. J., Michalek, A. J., and Iatridis, J. C. "Complex loading affects intervertebral disc mechanics and biology." *Osteoarthritis Cartilage* 19, no. 8 (Aug 2011): 1011-8.

61. Guehring, T., Wilde, G., Sumner, M., Grunhagen, T., Karney, G. B., Tirlapur, U. K., and Urban, J. P. "Notochordal intervertebral disc cells: sensitivity to nutrient deprivation." *Arthritis Rheum* 60, no. 4 (Apr 2009): 1026-34.

62. Hunter, C. J., Matyas, J. R., and Duncan, N. A. "The notochordal cell in the nucleus pulposus: a review in the context of tissue engineering." *Tissue Eng* 9, no. 4 (Aug 2003): 667-77.

63. Kim, K. W., Lim, T. H., Kim, J. G., Jeong, S. T., Masuda, K., and An, H. S. "The origin of chondrocytes in the nucleus pulposus and histologic findings associated with the transition of a notochordal nucleus pulposus to a fibrocartilaginous nucleus pulposus in intact rabbit intervertebral discs." *Spine (Phila Pa 1976)* 28, no. 10 (May 15 2003): 982-90.

64. Risbud, M. V., Schaer, T. P., and Shapiro, I. M. "Toward an understanding of the role of notochordal cells in the adult intervertebral disc: from discord to accord." *Dev Dyn* 239, no. 8 (Aug 2010): 2141-8.

65. Risbud, M. V., and Shapiro, I. M. "Notochordal cells in the adult intervertebral disc: new perspective on an old question." *Crit Rev Eukaryot Gene Expr* 21, no. 1 (2011): 29-41.

66. Yang, F., Leung, V. Y., Luk, K. D., Chan, D., and Cheung, K. M. "Injury-induced sequential transformation of notochordal nucleus pulposus to chondrogenic and fibrocartilaginous phenotype in the mouse." *J Pathol* 218, no. 1 (May 2009): 113-21.

67. Zhao, C. Q., Wang, L. M., Jiang, L. S., and Dai, L. Y. "The cell biology of intervertebral disc aging and degeneration." *Ageing Res Rev* 6, no. 3 (Oct 2007): 247-61.

68. Adams, M. A., Freeman, B. J., Morrison, H. P., Nelson, I. W., and Dolan, P. "Mechanical initiation of intervertebral disc degeneration." *Spine (Phila Pa 1976)* 25, no. 13 (Jul 1 2000): 1625-36.

69. Singh, K., Masuda, K., and An, H. S. "Animal models for human disc degeneration." *Spine J* 5, no. 6 Suppl (Nov-Dec 2005): 267S-79S.

70. Buckwalter, J. A. "Aging and degeneration of the human intervertebral disc." *Spine (Phila Pa 1976)* 20, no. 11 (Jun 1 1995): 1307-14.

71. Podichetty, V. K. "The aging spine: the role of inflammatory mediators in intervertebral disc degeneration." *Cell Mol Biol (Noisy-le-grand)* 53, no. 5 (2007): 4-18.

72. Roberts, S., Evans, H., Trivedi, J., and Menage, J. "Histology and pathology of the human intervertebral disc." *J Bone Joint Surg Am* 88 Suppl 2 (Apr 2006): 10-4.

73. An, H. S., Anderson, P. A., Haughton, V. M., Iatridis, J. C., Kang, J. D., Lotz, J. C., Natarajan, R. N., Oegema, T. R., Jr., Roughley, P., Setton, L. A., Urban, J. P., Videman, T., Andersson, G. B., and Weinstein, J. N. "Introduction: disc degeneration: summary." *Spine (Phila Pa 1976)* 29, no. 23 (Dec 1 2004): 2677-8.

74. Battie, M. C., Videman, T., and Parent, E. "Lumbar disc degeneration: epidemiology and genetic influences." *Spine (Phila Pa 1976)* 29, no. 23 (Dec 1 2004): 2679-90.

75. Shimer, A. L., Chadderdon, R. C., Gilbertson, L. G., and Kang, J. D. "Gene therapy approaches for intervertebral disc degeneration." *Spine (Phila Pa 1976)* 29, no. 23 (Dec 1 2004): 2770-8.

76. Diamant, B., Karlsson, J., and Nachemson, A. "Correlation between lactate levels and pH in discs of patients with lumbar rhizopathies." *Experientia* 24, no. 12 (Dec 15 1968): 1195-6.

77. Roughley, P. J. "Biology of intervertebral disc aging and degeneration: involvement of the extracellular matrix." *Spine (Phila Pa 1976)* 29, no. 23 (Dec 1 2004): 2691-9.

78. Berry, R. J. "Genetical studies on the skeleton of the mouse XXVI Pintail." *Genetical Research* 1, no. 3 (1960): 439-51.

79. Furuya, S., Ohtsuki, T., Yabe, Y., and Hosoda, Y. "Ultrastructural study on calcification of cartilage: comparing ICR and twy mice." *J Bone Miner Metab* 18, no. 3 (2000): 140-7.

80. Hamrick, M. W., Pennington, C., and Byron, C. D. "Bone architecture and disc degeneration in the lumbar spine of mice lacking GDF-8 (myostatin)." *J Orthop Res* 21, no. 6 (Nov 2003): 1025-32.

81. Kimura, T., Nakata, K., Tsumaki, N., Miyamoto, S., Matsui, Y., Ebara, S., and Ochi, T. "Progressive degeneration of articular cartilage and intervertebral discs. An experimental study in transgenic mice bearing a type IX collagen mutation." *Int Orthop* 20, no. 3 (1996): 177-81.

82. Mason, R. M., and Palfrey, A. J. "Intervertebral disc degeneration in adult mice with hereditary kyphoscoliosis." *J Orthop Res* 2, no. 4 (1984): 333-8.

83. Sahlman, J., Inkinen, R., Hirvonen, T., Lammi, M. J., Lammi, P. E., Nieminen, J., Lapvetelainen, T., Prockop, D. J., Arita, M., Li, S. W., Hyttinen, M. M., Helminen, H. J., and Puustjarvi, K. "Premature vertebral endplate ossification and mild disc degeneration

in mice after inactivation of one allele belonging to the Col2a1 gene for Type II collagen." *Spine (Phila Pa 1976)* 26, no. 23 (Dec 1 2001): 2558-65.

84. Sweet, H. O., and Green, M. C. "Progressive ankylosis, a new skeletal mutation in the mouse." *J Hered* 72, no. 2 (Mar-Apr 1981): 87-93.

85. Watanabe, H., Nakata, K., Kimata, K., Nakanishi, I., and Yamada, Y. "Dwarfism and age-associated spinal degeneration of heterozygote cmd mice defective in aggrecan." *Proc Natl Acad Sci U S A* 94, no. 13 (Jun 24 1997): 6943-7.

86. Watanabe, H., and Yamada, Y. "Chondrodysplasia of gene knockout mice for aggrecan and link protein." *Glycoconj J* 19, no. 4-5 (May-Jun 2002): 269-73.

87. Weinreich, S., Hoebe, B., and Ivanyi, P. "Maternal age influences risk for HLA-B27 associated ankylosing enthesopathy in transgenic mice." *Ann Rheum Dis* 54, no. 9 (Sep 1995): 754-6.

88. Hammer, R. E., Maika, S. D., Richardson, J. A., Tang, J. P., and Taurog, J. D. "Spontaneous inflammatory disease in transgenic rats expressing HLA-B27 and human beta 2m: an animal model of HLA-B27-associated human disorders." *Cell* 63, no. 5 (Nov 30 1990): 1099-112.

89. Moskowitz, R. W., Ziv, I., Denko, C. W., Boja, B., Jones, P. K., and Adler, J. H. "Spondylosis in sand rats: a model of intervertebral disc degeneration and hyperostosis." *J Orthop Res* 8, no. 3 (May 1990): 401-11.

90. Taurog, J. D., Maika, S. D., Satumtira, N., Dorris, M. L., Mclean, I. L., Yanagisawa, H., Sayad, A., Stagg, A. J., Fox, G. M., Le O'brien, A., Rehman, M., Zhou, M., Weiner, A. L., Splawski, J. B., Richardson, J. A., and Hammer, R. E. "Inflammatory disease in HLA-B27 transgenic rats." *Immunol Rev* 169 (Jun 1999): 209-23.

91. Bergknut, N., Rutges, J. P., Kranenburg, H. J., Smolders, L. A., Hagman, R., Smidt, H. J., Lagerstedt, A. S., Penning, L. C., Voorhout, G., Hazewinkel, H. A., Grinwis, G. C., Creemers, L. B., Meij, B. P., and Dhert, W. J. "The dog as an animal model for intervertebral disc degeneration?". *Spine (Phila Pa 1976)* 37, no. 5 (Mar 1 2012): 351-8.

92. Kramer, P. A., Newell-Morris, L. L., and Simkin, P. A. "Spinal degenerative disk disease (DDD) in female macaque monkeys: epidemiology and comparison with women." *J Orthop Res* 20, no. 3 (May 2002): 399-408.

93. Lauerman, W. C., Platenberg, R. C., Cain, J. E., and Deeney, V. F. "Age-related disk degeneration: preliminary report of a naturally occurring baboon model." *J Spinal Disord* 5, no. 2 (Jun 1992): 170-4.

94. Nuckley, D. J., Kramer, P. A., Del Rosario, A., Fabro, N., Baran, S., and Ching, R. P. "Intervertebral disc degeneration in a naturally occurring primate model: radiographic and biomechanical evidence." *J Orthop Res* 26, no. 9 (Sep 2008): 1283-8.

95. Seiler, G., Hani, H., Scheidegger, J., Busato, A., and Lang, J. "Staging of lumbar intervertebral disc degeneration in nonchondrodystrophic dogs using low-field magnetic resonance imaging." *Vet Radiol Ultrasound* 44, no. 2 (Mar-Apr 2003): 179-84.

96. Sether, L. A., Nguyen, C., Yu, S. N., Haughton, V. M., Ho, K. C., Biller, D. S., Strandt, J. A., and Eurell, J. C. "Canine intervertebral disks: correlation of anatomy and MR imaging." *Radiology* 175, no. 1 (Apr 1990): 207-11.

97. Coppes, M. H., Marani, E., Thomeer, R. T. W. M., and Groen, G. J. "Innervation of "Painful" Lumbar Discs." *Spine (Phila Pa 1976)* 22, no. 20 (1997): 2342-49.

98. Peng, B., Hao, J., Hou, S., Wu, W., Jiang, D., Fu, X., and Yang, Y. "Possible pathogenesis of painful intervertebral disc degeneration." *Spine (Phila Pa 1976)* 31, no. 5 (Mar 1 2006): 560-6.

99. Karppinen, J., Shen, F. H., Luk, K. D., Andersson, G. B., Cheung, K. M., and Samartzis, D. "Management of degenerative disk disease and chronic low back pain." *Orthop Clin North Am* 42, no. 4 (Oct 2011): 513-28, viii.

100. Samartzis, D., and Cheung, K. M. "Lumbar intervertebral disk degeneration." *Orthop Clin North Am* 42, no. 4 (Oct 2011): xi-xii.

101. Samartzis, D., Karppinen, J., Chan, D., Luk, K. D., and Cheung, K. M. "The association of lumbar intervertebral disc degeneration on MRI in overweight and obese adults: A population-based study." *Arthritis Rheum* (Jan 27 2012).

102. An, Y. H., and Friedman, R. J. *Animal models in orthopaedic research*. Boca Raton: CRC Press, 1999.

103. Cheung, A. K. "Animal models to study the cardiopulmonary effects of artificial kidney membranes." *Blood Purif* 5, no. 2-3 (1987): 155-61.

104. Pearce, A. I., Richards, R. G., Milz, S., Schneider, E., and Pearce, S. G. "Animal models for implant biomaterial research in bone: a review." *Eur Cell Mater* 13 (2007): 1-10.

105. Muschler, G. F., Raut, V. P., Patterson, T. E., Wenke, J. C., and Hollinger, J. O. "The design and use of animal models for translational research in bone tissue engineering and regenerative medicine." *Tissue Eng Part B Rev* 16, no. 1 (Feb 2010): 123-45.

106. Sandhu, H. S., and Khan, S. N. "Animal models for preclinical assessment of bone morphogenetic proteins in the spine." *Spine (Phila Pa 1976)* 27, no. 16 Suppl 1 (Aug 15 2002): S32-8.

107. An, H. S., Masuda, K., and Inoue, N. "Intervertebral disc degeneration: biological and biomechanical factors." *J Orthop Sci* 11, no. 5 (Oct 2006): 541-52.

108. Wetzel, F. T., Panjabi, M. M., and Pelker, R. R. "Biomechanics of the rabbit cervical spine as a function of component transection." *J Orthop Res* 7, no. 5 (1989): 723-7.

109. Wilke, H. J., Kettler, A., and Claes, L. E. "Are sheep spines a valid biomechanical model for human spines?". *Spine (Phila Pa 1976)* 22, no. 20 (Oct 15 1997): 2365-74.

110. Winkelstein, B. A., and Myers, B. S. "The biomechanics of cervical spine injury and implications for injury prevention." *Med Sci Sports Exerc* 29, no. 7 Suppl (Jul 1997): S246-55.

111. Zhang, Y., Drapeau, S., An, H. S., Markova, D., Lenart, B. A., and Anderson, D. G. "Histological features of the degenerating intervertebral disc in a goat disc-injury model." *Spine (Phila Pa 1976)* 36, no. 19 (Sep 1 2011): 1519-27.

112. Kroeber, M. W., Unglaub, F., Wang, H., Schmid, C., Thomsen, M., Nerlich, A., and Richter, W. "New in vivo animal model to create intervertebral disc degeneration and to investigate the effects of therapeutic strategies to stimulate disc regeneration." *Spine (Phila Pa 1976)* 27, no. 23 (Dec 1 2002): 2684-90.

113. Korecki, C. L., Kuo, C. K., Tuan, R. S., and Iatridis, J. C. "Intervertebral disc cell response to dynamic compression is age and frequency dependent." *J Orthop Res* 27, no. 6 (Jun 2009): 800-6.

114. Schimandle, J. H., and Boden, S. D. "Spine update. The use of animal models to study spinal fusion." *Spine (Phila Pa 1976)* 19, no. 17 (Sep 1 1994): 1998-2006.

115. Michalek, A. J., and Iatridis, J. C. "Height and torsional stiffness are most sensitive to annular injury in large animal intervertebral discs." *Spine J* 12, no. 5 (May 2012): 425-32.

116. Barthelemy, C. R., Johansen, J., Carrera, G. F., and Haughton, V. M. "Animal model for studying the chronic effects of herniated disks and spinal surgery." *AJNR Am J Neuroradiol* 5, no. 1 (Jan-Feb 1984): 67-9.

117. Showalter, B. L., Beckstein, J. C., Martin, J. T., Beattie, E. E., Espinoza Orias, A. A., Schaer, T. P., Vresilovic, E. J., and Elliott, D. M. "Comparison of animal discs used in disc research to human lumbar disc: torsion mechanics and collagen content." *Spine (Phila Pa 1976)* 37, no. 15 (Jul 1 2012): E900-7.

118. Drespe, I. H., Polzhofer, G. K., Turner, A. S., and Grauer, J. N. "Animal models for spinal fusion." *Spine J* 5, no. 6 Suppl (Nov-Dec 2005): 209S-16S.

119. Seifert, J. L., Bell, J. E., Elmer, B. B., Sucato, D. J., and Romero, M. I. "Characterization of a novel bidirectional distraction spinal cord injury animal model." *J Neurosci Methods* 197, no. 1 (Apr 15 2011): 97-103.

120. Kim, J. S., Kroin, J. S., Buvanendran, A., Li, X., Van Wijnen, A. J., Tuman, K. J., and Im, H. J. "Characterization of a new animal model for evaluation and treatment of back pain due to lumbar facet joint osteoarthritis." *Arthritis Rheum* 63, no. 10 (Oct 2011): 2966-73.

121. Gullung, G. B., Woodall, J. W., Tucci, M. A., James, J., Black, D. A., and Mcguire, R. A. "Platelet-rich plasma effects on degenerative disc disease: analysis of histology and imaging in an animal model." *Evid Based Spine Care J* 2, no. 4 (Nov 2011): 13-8.

122. Jacobs, L., Vo, N., Coehlo, J. P., Dong, Q., Bechara, B., Woods, B., Hempen, E., Hartman, R., Preuss, H., Balk, J., Kang, J., and Sowa, G. "Glucosamine Supplementation Demonstrates a Negative Effect On Intervertebral Disc Matrix in an Animal Model of Disc Degeneration." *Spine (Phila Pa 1976)* (Jan 15 2013).

123. Klironomos, G., Karadimas, S., Mavrakis, A., Mirilas, P., Savvas, I., Papadaki, E., Papachristou, D. J., and Gatzounis, G. "New experimental rabbit animal model for cervical spondylotic myelopathy." *Spinal Cord* 49, no. 11 (Nov 2011): 1097-102.

124. Pleticha, J., Maus, T. P., Jeng-Singh, C., Marsh, M. P., Al-Saiegh, F., Christner, J. A., Lee, K. H., and Beutler, A. S. "Pig lumbar spine anatomy and imaging-guided lateral lumbar puncture: A new large animal model for intrathecal drug delivery." *J Neurosci Methods* 216, no. 1 (May 30 2013): 10-5.

125. Kasch, R., Mensel, B., Schmidt, F., Ruetten, S., Barz, T., Froehlich, S., Seipel, R., Merk, H. R., and Kayser, R. "Disc volume reduction with percutaneous nucleoplasty in an animal model." *PLoS One* 7, no. 11 (2012): e50211.

126. Jones, C. F., Cripton, P. A., and Kwon, B. K. "Gross morphological changes of the spinal cord immediately after surgical decompression in a large animal model of traumatic spinal cord injury." *Spine (Phila Pa 1976)* 37, no. 15 (Jul 1 2012): E890-9.

127. Galovich, L. A., Perez-Higueras, A., Altonaga, J. R., Orden, J. M., Barba, M. L., and Morillo, M. T. "Biomechanical, histological and histomorphometric analyses of calcium phosphate cement compared to PMMA for vertebral augmentation in a validated animal model." *Eur Spine J* 20 Suppl 3 (Aug 2011): 376-82.

128. Hasler, C., Sprecher, C. M., and Milz, S. "Comparison of the immature sheep spine and the growing human spine: a spondylometric database for growth modulating research." *Spine (Phila Pa 1976)* 35, no. 23 (Nov 1 2010): E1262-72.

129. Michalek, A. J., Buckley, M. R., Bonassar, L. J., Cohen, I., and Iatridis, J. C. "The effects of needle puncture injury on microscale shear strain in the intervertebral disc annulus fibrosus." *Spine J* 10, no. 12 (Dec 2010): 1098-105.

130. Hoell, T., Huschak, G., Beier, A., Holzhausen, H. J., Meisel, H. J., and Emmrich, F. "Vertebral osteoporosis: perfused animal cadaver model for testing new vertebroplastic agents." *Spine (Phila Pa 1976)* 35, no. 25 (Dec 1 2010): E1449-54.

131. Chen, X., Milne, N., and O'higgins, P. "Morphological variation of the thoracolumbar vertebrae in Macropodidae and its functional relevance." *J Morphol* 266, no. 2 (Nov 2005): 167-81.

132. Jinkins, J. R. "Acquired degenerative changes of the intervertebral segments at and suprajacent to the lumbosacral junction. A radioanatomic analysis of the nondiskal structures of the spinal column and perispinal soft tissues." *Radiol Clin North Am* 39, no. 1 (Jan 2001): 73-99.

133. Detiger, S. E., Hoogendoorn, R. J., Van Der Veen, A. J., Van Royen, B. J., Helder, M. N., Koenderink, G. H., and Smit, T. H. "Biomechanical and rheological characterization of mild intervertebral disc degeneration in a large animal model." *J Orthop Res* 31, no. 5 (May 2013): 703-9.

134. Benneker, L. M., Gisep, A., Krebs, J., Boger, A., Heini, P. F., and Boner, V. "Development of an in vivo experimental model for percutaneous vertebroplasty in sheep." *Vet Comp Orthop Traumatol* 25, no. 3 (May 15 2012): 173-7.

135. Qin, J., He, X., Wang, D., Qi, P., Guo, L., Huang, S., Cai, X., Li, H., and Wang, R. "Artificial cervical vertebra and intervertebral complex replacement through the anterior approach in animal model: a biomechanical and in vivo evaluation of a successful goat model." *PLoS One* 7, no. 12 (2012): e52910.

136. Pacheco Torres, V. C. R., Altamirano Enciso, A. J., and Guerra Porras, E. S. *The osteology of South American camelids*. Archaeological research tools of *3*. Los Angeles: Institute of Archaeology, University of California, 1986.

137. Shapiro, I. M., and Risbud, M. V. "Transcriptional profiling of the nucleus pulposus: say yes to notochord." *Arthritis Res Ther* 12, no. 3 (2010): 117.

138. "Camelid." Wikipedia, http://en.wikipedia.org/wiki/Camelid (accessed 8 March 2015 2015).

139. Mow, V. C., and Huiskes, R. *Basic orthopaedic biomechanics & mechano-biology*. 3rd ed. Philadelphia: Lippincott Williams & Wilkins, 2005.

140. Grunhagen, T., Shirazi-Adl, A., Fairbank, J. C., and Urban, J. P. "Intervertebral disk nutrition: a review of factors influencing concentrations of nutrients and metabolites." *Orthop Clin North Am* 42, no. 4 (Oct 2011): 465-77, vii.

141. Patwardhan, A. G., Havey, R. M., Carandang, G., Simonds, J., Voronov, L. I., Ghanayem, A. J., Meade, K. P., Gavin, T. M., and Paxinos, O. "Effect of compressive follower preload on the flexion-extension response of the human lumbar spine." *J Orthop Res* 21, no. 3 (May 2003): 540-6.

142. Renner, S. M., Natarajan, R. N., Patwardhan, A. G., Havey, R. M., Voronov, L. I., Guo, B. Y., Andersson, G. B., and An, H. S. "Novel model to analyze the effect of a large compressive follower pre-load on range of motions in a lumbar spine." *J Biomech* Online First (Jul 13 2006).

143. Kroeze, R. J., Van Der Veen, A. J., Van Royen, B. J., Bank, R. A., Helder, M. N., and Smit, T. H. "Relation between radiological assessment and biomechanical stability of lumbar interbody fusion in a large animal model." *Eur Spine J* (Sep 17 2013).

144. Nakao, S., Minamide, A., Kawakami, M., Boden, S. D., and Yoshida, M. "The influence of alendronate on spine fusion in an osteoporotic animal model." *Spine (Phila Pa 1976)* 36, no. 18 (Aug 15 2011): 1446-52.

145. Ding, M., Cheng, L., Bollen, P., Schwarz, P., and Overgaard, S. "Glucocorticoid induced osteopenia in cancellous bone of sheep: validation of large animal model for spine fusion and biomaterial research." *Spine (Phila Pa 1976)* 35, no. 4 (Feb 15 2010): 363-70.

146. Wojtkiewicz, J., Kowalski, I. M., Kmiec, Z., Crayton, R., Babinska, I., Bladowski, M., Szarek, J., Kiebzak, W., Majewski, M., Barczewska, M., Grzegorzewski, W., and Kloc, W. "The effect of lateral electrical surface stimulation (LESS) on motor end-plates in an animal model of experimental scoliosis." *J Physiol Pharmacol* 63, no. 3 (Jun 2012): 285-91.

147. Odent, T., Cachon, T., Peultier, B., Gournay, J., Jolivet, E., Elie, C., Abdoul, H., and Viguier, E. "Porcine model of early onset scoliosis based on animal growth created with posterior mini-invasive spinal offset tethering: a preliminary report." *Eur Spine J* 20, no. 11 (Nov 2011): 1869-76.

148. Zhang, Y. G., Zheng, G. Q., Zhang, X. S., and Wang, Y. "Scoliosis model created by pedicle screw tethering in immature goats: the feasibility, reliability, and complications." *Spine (Phila Pa 1976)* 34, no. 21 (Oct 1 2009): 2305-10.

149. Braun, J. T., Ogilvie, J. W., Akyuz, E., Brodke, D. S., Bachus, K. N., and Stefko, R. M. "Experimental scoliosis in an immature goat model: a method that creates idiopathic-type deformity with minimal violation of the spinal elements along the curve." *Spine* 28, no. 19 (Oct 1 2003): 2198-203.

150. Gebhard, H., Bowles, R., Dyke, J., Saleh, T., Doty, S., Bonassar, L., and Hartl, R. "Total disc replacement using a tissue-engineered intervertebral disc in vivo: new animal model and initial results." *Evid Based Spine Care J* 1, no. 2 (Aug 2010): 62-6.

151. So, K., Takemoto, M., Fujibayashi, S., Neo, M., Kyomoto, M., Hayami, T., Hyon, S. H., and Nakamura, T. "Antidegenerative effects of partial disc replacement in an animal surgery model." *Spine (Phila Pa 1976)* 32, no. 15 (Jul 1 2007): 1586-91.

152. Hu, N., Cunningham, B. W., Mcafee, P. C., Kim, S. W., Sefter, J. C., Cappuccino, A., and Pimenta, L. "Porous coated motion cervical disc replacement: a biomechanical, histomorphometric, and biologic wear analysis in a caprine model." *Spine (Phila Pa 1976)* 31, no. 15 (Jul 1 2006): 1666-73.

153. Mcafee, P. C., Cunningham, B., Dmitriev, A., Hu, N., Woo Kim, S., Cappuccino, A., and Pimenta, L. "Cervical disc replacement-porous coated motion prosthesis: a comparative biomechanical analysis showing the key role of the posterior longitudinal ligament." *Spine (Phila Pa 1976)* 28, no. 20 (Oct 15 2003): S176-85.

154. Cunningham, B. W., Dmitriev, A. E., Hu, N., and Mcafee, P. C. "General principles of total disc replacement arthroplasty: seventeen cases in a nonhuman primate model." *Spine* 28, no. 20 (Oct 15 2003): S118-24.

155. Kostuik, J. P. "Intervertebral disc replacement. Experimental study." *Clin Orthop Relat Res*, no. 337 (Apr 1997): 27-41.

156. Cotterill, P. C., Kostuik, J. P., D'angelo, G., Fernie, G. R., and Maki, B. E. "An anatomical comparison of the human and bovine thoracolumbar spine." *J Orthop Res* 4, no. 3 (1986): 298-303.

157. Easley, N. E., Wang, M., Mcgrady, L. M., and Toth, J. M. "Biomechanical and radiographic evaluation of an ovine model for the human lumbar spine." *Proc Inst Mech Eng H* 222, no. 6 (Aug 2008): 915-22.

158. Kumar, N., Kukreti, S., Ishaque, M., and Mulholland, R. "Anatomy of deer spine and its comparison to the human spine." *Anat Rec* 260, no. 2 (Oct 1 2000): 189-203.

159. O'connell, G. D., Vresilovic, E. J., and Elliott, D. M. "Comparison of animals used in disc research to human lumbar disc geometry." *Spine (Phila Pa 1976)* 32, no. 3 (Feb 1 2007): 328-33.

160. Schmidt, H., and Reitmaier, S. "Is the ovine intervertebral disc a small human one? A finite element model study." *J Mech Behav Biomed Mater* 17 (Jan 2013): 229-41.

161. Sheng, S. R., Wang, X. Y., Xu, H. Z., Zhu, G. Q., and Zhou, Y. F. "Anatomy of large animal spines and its comparison to the human spine: a systematic review." *Eur Spine J* 19, no. 1 (Jan 2010): 46-56.

162. Yingling, V. R., Callaghan, J. P., and Mcgill, S. M. "The porcine cervical spine as a model of the human lumbar spine: an anatomical, geometric, and functional comparison." *J Spinal Disord* 12, no. 5 (Oct 1999): 415-23.

163. Shirazi-Adl, A., Taheri, M., and Urban, J. P. "Analysis of cell viability in intervertebral disc: Effect of endplate permeability on cell population." *J Biomech* 43, no. 7 (May 7 2010): 1330-6.

164. Das, D. B., Welling, A., Urban, J. P., and Boubriak, O. A. "Solute transport in intervertebral disc: experiments and finite element modeling." *Ann N Y Acad Sci* 1161 (Apr 2009): 44-61.

165. Bibby, S. R., Jones, D. A., Lee, R. B., Yu, J., and Urban, J. P. G. "The pathophysiology of the intervertebral disc." *Joint Bone Spine* 68, no. 6 (2001): 537-42.

166. Busscher, I., Ploegmakers, J. J., Verkerke, G. J., and Veldhuizen, A. G. "Comparative anatomical dimensions of the complete human and porcine spine." *Eur Spine J* 19, no. 7 (Jul 2010): 1104-14.

167. Beckstein, J. C., Sen, S., Schaer, T. P., Vresilovic, E. J., and Elliott, D. M. "Comparison of animal discs used in disc research to human lumbar disc: axial compression mechanics and glycosaminoglycan content." *Spine (Phila Pa 1976)* 33, no. 6 (Mar 15 2008): E166-73.

168. Cannella, M., Arthur, A., Allen, S., Keane, M., Joshi, A., Vresilovic, E., and Marcolongo, M. "The role of the nucleus pulposus in neutral zone human lumbar intervertebral disc mechanics." *J Biomech* 41, no. 10 (Jul 19 2008): 2104-11.

169. Wilke, H. J., Kettler, A., Wenger, K. H., and Claes, L. E. "Anatomy of the sheep spine and its comparison to the human spine." *Anat Rec* 247, no. 4 (Apr 1997): 542-55.

170. Hamilton, L., Franklin, R. J., and Jeffery, N. D. "Development of a universal measure of quadrupedal forelimb-hindlimb coordination using digital motion capture and computerised analysis." *BMC Neurosci* 8 (2007): 77.

171. Konz, R. J., Fatone, S., Stine, R. L., Ganju, A., Gard, S. A., and Ondra, S. L. "A kinematic model to assess spinal motion during walking." *Spine (Phila Pa 1976)* 31, no. 24 (Nov 15 2006): E898-906.

172. Panjabi, M. M., Krag, M. H., White, A. A., 3rd, and Southwick, W. O. "Effects of preload on load displacement curves of the lumbar spine." *Orthop Clin North Am* 8, no. 1 (Jan 1977): 181-92.

173. Ardigo, L. P., Saibene, F., and Minetti, A. E. "The optimal locomotion on gradients: walking, running or cycling?". *Eur J Appl Physiol* 90, no. 3-4 (Oct 2003): 365-71.

174. Saibene, F., and Minetti, A. E. "Biomechanical and physiological aspects of legged locomotion in humans." *Eur J Appl Physiol* 88, no. 4-5 (Jan 2003): 297-316.

175. Panjabi, M., Malcolmson, G., Teng, E., Tominaga, Y., Henderson, G., and Serhan, H. "Hybrid testing of lumbar CHARITE discs versus fusions." *Spine (Phila Pa 1976)* 32, no. 9 (Apr 20 2007): 959-66; discussion 67.

176. Panjabi, M. M., Crisco, J. J., Vasavada, A., Oda, T., Cholewicki, J., Nibu, K., and Shin, E. "Mechanical properties of the human cervical spine as shown by three-dimensional load-displacement curves." *Spine (Phila Pa 1976)* 26, no. 24 (Dec 15 2001): 2692-700.

177. Panjabi, M. M., Summers, D. J., Pelker, R. R., Videman, T., Friedlaender, G. E., and Southwick, W. O. "Three-dimensional load-displacement curves due to forces on the cervical spine." *J Orthop Res* 4, no. 2 (1986): 152-61.

178. Panjabi, M. M., and White, A. A., 3rd. "Basic biomechanics of the spine." *Neurosurgery* 7, no. 1 (Jul 1980): 76-93.

179. Yamamoto, I., Panjabi, M. M., Crisco, T., and Oxland, T. "Three-dimensional movements of the whole lumbar spine and lumbosacral joint." *Spine (Phila Pa 1976)* 14, no. 11 (Nov 1989): 1256-60.

180. Busscher, I., Van Der Veen, A. J., Van Dieen, J. H., Kingma, I., Verkerke, G. J., and Veldhuizen, A. G. "In vitro biomechanical characteristics of the spine: a comparison between human and porcine spinal segments." *Spine (Phila Pa 1976)* 35, no. 2 (Jan 15 2010): E35-42.

181. Atlas, O. K., Dodds, S. D., and Panjabi, M. M. "Single and incremental trauma models: a biomechanical assessment of spinal instability." *Eur Spine J* 12, no. 2 (Apr 2003): 205-10.

182. Cripton, P. A., Jain, G. M., Wittenberg, R. H., and Nolte, L. P. "Load-sharing characteristics of stabilized lumbar spine segments." *Spine (Phila Pa 1976)* 25, no. 2 (Jan 15 2000): 170-9.

183. Panjabi, M. M., Oxland, T. R., Yamamoto, I., and Crisco, J. J. "Mechanical behavior of the human lumbar and lumbosacral spine as shown by three-dimensional load-displacement curves." *J Bone Joint Surg Am* 76, no. 3 (Mar 1994): 413-24.

184. Acosta, F. L., Buckley, J. M., Xu, Z., Lotz, J. C., and Ames, C. P. "Biomechanical comparison of three fixation techniques for unstable thoracolumbar burst fractures." *Journal of Neurosurgery: Spine* 8, no. 4 (2008): 341-46.

185. Wilke, H. J., Geppert, J., and Kienle, A. "Biomechanical in vitro evaluation of the complete porcine spine in comparison with data of the human spine." *Eur Spine J* 20, no. 11 (Nov 2011): 1859-68.

186. Zirbel, S. A., Stolworthy, D. K., Howell, L. L., and Bowden, A. E. "A standardized representation of spinal quality of motion." *Proc Inst Mech Eng H* 228, no. 11 (Nov 2014): 1168-75.

187. Wen, N., Lavaste, F., Santin, J. J., and Lassau, J. P. "Three-dimensional biomechanical properties of the human cervical spine in vitro. I. Analysis of normal motion." *Eur Spine J* 2, no. 1 (Jun 1993): 2-11.

188. Neyt, J. G., Buckwalter, J. A., and Carroll, N. C. "Use of animal models in musculoskeletal research." *Iowa Orthop J* 18 (1998): 118-23.

189. Abrahamsen, E. J. "Chemical restraint, anesthesia, and analgesia for camelids." *Vet Clin North Am Food Anim Pract* 25, no. 2 (Jul 2009): 455-94.

190. Abrahamsen, E. J. *Llama and alpaca care: medicine, surgery, reproduction, nutrition, and herd health; Chapter 46: Injectable Anesthesia of Camelids*. Edited by Cebra, C., Anderson, D. E., Tibary, A., Saun, R. J. V. and Johnson, L. W., 2014.

191. Anderson, D. E. "Camelid: Handling, Chemical Restraint, and Anesthesia in Field Settings " https://www.arilist.com/resources/dyn/files/232831z48fd9c49/_fn/Notes-Handling-Restraint-and-Field-Anesthesia-of-Camelids.pdf (2014).

192. Garcia Pereira, F. L., Greene, S. A., Mcewen, M. M., and Keegan, R. "Analgesia and anesthesia in camelids." *Small Ruminant Research* 61, no. 2ΓÇô3 (2// 2006): 227-33.

193. Pfirrmann, C. W., Metzdorf, A., Zanetti, M., Hodler, J., and Boos, N. "Magnetic resonance classification of lumbar intervertebral disc degeneration." *Spine (Phila Pa 1976)* 26, no. 17 (Sep 1 2001): 1873-8.

194. Paul, C. P., Zuiderbaan, H. A., Zandieh Doulabi, B., Van Der Veen, A. J., Van De Ven, P. M., Smit, T. H., Helder, M. N., Van Royen, B. J., and Mullender, M. G. "Simulated-physiological loading conditions preserve biological and mechanical properties of caprine lumbar intervertebral discs in ex vivo culture." *PLoS One* 7, no. 3 (2012): e33147.

195. Ponnappan, R. K., Markova, D. Z., Antonio, P. J., Murray, H. B., Vaccaro, A. R., Shapiro, I. M., Anderson, D. G., Albert, T. J., and Risbud, M. V. "An organ culture system to model early degenerative changes of the intervertebral disc." *Arthritis Res Ther* 13, no. 5 (2011): R171.

196. Ramakrishnan, P. S., Hong, J., Martin, J. A., Kurriger, G. L., Buckwalter, J. A., and Lim, T. H. "Biomechanical disc culture system: feasibility study using rat intervertebral discs." *Proc Inst Mech Eng H* 225, no. 6 (Jun 2011): 611-20.

197. Window, A. L., and Holister, G. S. *Strain gauge technology*. 1st ed. London ; New York: Applied Science Publishers, 1982.

198. Johnson, O., Gardner, C., Seegmiller, D., Mara, N., Dattelbaum, A., Rae, P., Kaschner, G., Mason, T., Fullwood, D., and Hansen, G. "Multiscale Model for the Extreme Piezoresistivity in Silicone/Nickel Nanostrand Nanocomposites." *Metallurgical and Materials Transactions A* 42, no. 13 (2011/12/01 2011): 3898-906.

199. Johnson, O. K., Kaschner, G. C., Mason, T. A., Fullwood, D. T., and Hansen, G. C. "Optimization of nickel nanocomposite for large strain sensing applications." *Sensors and Actuators A: Physical* 166, no. 1 (3// 2011): 40-47.

200. Johnson, T. M., Fullwood, D. T., and Hansen, G. C. "Strain monitoring of carbon fiber composite via embedded nickel nano-particles." *Composites Part B: Engineering* 43, no. 3 (4// 2012): 1155-63.

201. Johnson, O. K., Gardner, C. J., Fullwood, D. T., Adams, B. L., and Hansen, G. C. in *Society for the Advancement of Material and Process Engineering*. Baltimore, MD, 2009.

202. Johnson, O. K., Gardner, C. J., Fullwood, D. T., Adams, B. L., Hansen, N. D., and Hansen, G. C. *Comput. Mater. Continua* 15 (2010): 87–112.

203. Hansen, A., and Kertesz, J. "Tunnelling percolation: universality and application to the integer quantum Hall effect." *Philosophical Magazine B-Physics of Condensed Matter Statistical Mechanics Electronic Optical and Magnetic Properties* 77, no. 5 (May 1998): 1301-11.

204. Hansen, N., Adams, D. O., and Fullwood, D. T. "Quantitative methods for correlating dispersion and electrical conductivity in conductor–polymer nanostrand composites." *Composites Part A: Applied Science and Manufacturing* 43, no. 11 (11// 2012): 1939-46.

205. Hyatt, T., Fullwood, D., Bradshaw, R., Bowden, A., and Johnson, O. "Nano-composite Sensors for Wide Range Measurement of Ligament Strain." Chap. 59 In *Experimental and Applied Mechanics, Volume 6*, edited by Proulx, T. Volume 17 of *Conference Proceedings of the Society for Experimental Mechanics Series*, 359-64: Springer New York, 2011.

206. Calkins, T. B., Fullwood, D. T., Ghosh, S., Hyatt, T. B., Johnson, O. K., Hansen, N., and Hansen, G. "Applications For A Nano-composite High Displacement Strain Gauge." *42nd ISTC* (2010).

APPENDIX A – STATISTICAL CODE FOR DATA ANALYSIS

A.1 Geometry and Flexibility Data Analysis

```
goptions reset=all; /*Clear format settings*/
ods listing;                /*turn on output delivery system (ODS)*/
option mprint;
*ods listing close;       /*turn off ODS*/

%let data1 = Biomech;
%let data2 = Geometry;
%let Path =
C:\Users\Dean\Dropbox\1_PhD\2_AnimalModel\Paper1_CamelidBiomechanics\Data;
%let Tmax = 4.0; /*Nm*/
%let Tmin = -4.0; /*Nm*/
%let Tstep = 0.004;
%let SS = 0.05; /*Statistical Significance p-value, alpha<0.05*/
%let NZpercent = 0.85; /*range of NZ to use when calculating H and K*/

title1 "&data SAS Analysis";

/*============Import Data============*/
/* Import DIP Boltzmann parameters from datafile */
proc import out = WORK.Dean
        datafile
='C:\Users\Dean\Dropbox\1_PhD\2_AnimalModel\Paper1_CamelidBiomechanics\
Data\Alpaca_v3.xlsx'
        dbms = EXCEL replace;
        range = "DIPboltzman$";
        getnames = YES;
        mixed = NO;
        scantext = YES;
        usedate = YES;
        scantime = YES;
run;

data &data1;
        set Dean (drop=F20 F21 F22);
        if ROM = . then delete;
```

```
        if ROM = 0 then delete;
        if Species = 'Llama' then Temp='ROOM';
        if Species = 'Alpaca' then Temp='ROOM';
        if Load = 'nL';
        UA = -ROM/2;
        UB = ROM/2;
        LA = UA;
        LB = UB;
        *ROM = mean(abs(UB-UA),abs(LB-LA));
        UAREA = UA*(&Tmax-&Tmin) - UA/Ua1*log((1+exp(Ua1*(&Tmax-
Um1)))/(1+exp(Ua1*(&Tmin-Um1)))) + UB/Ua2*log((1+exp(Ua2*(&Tmax-
Um2)))/(1+exp(Ua2*(&Tmin-Um2))));
        LAREA = LA*(&Tmax-&Tmin) - LA/La1*log((1+exp(La1*(&Tmax-
Lm1)))/(1+exp(La1*(&Tmin-Lm1)))) + LB/La2*log((1+exp(La2*(&Tmax-
Lm2)))/(1+exp(La2*(&Tmin-Lm2))));
        AREA = UAREA - LAREA;
        HA = AREA/ROM;    /*HysteresisArea calculates the average spread per degree of the
ROM*/
run;

proc sort data=&Data1;
        by Species Dir Load Segment ROM;
run;

data DataNZkh;
        set &Data1;
        do m = &Tmin to &Tmax by &Tstep;
                /*thetaUP*/
                Utheta = UA/(1+exp(Ua1*(m-Um1))) - UB/(1+exp(Ua2*(m-Um2))) + UB;
                /*thetaLOW*/
                Ltheta = LA/(1+exp(La1*(m-Lm1))) - LB/(1+exp(La2*(m-Lm2))) + LB;
                Dtheta = Utheta - Ltheta;
                output;
        end;
run;

/*Determine NZ as the maximum rotation difference between upper and lower curves*/
proc means data=DataNZkh (keep=Dir Load Species Segment ROM Dtheta) max noprint;
        var Dtheta;
        by Species Dir Load Segment ROM;
        output out=DataNZ(drop=_TYPE_ _FREQ_)
                max=NZ;
run;

/*Attach NZ to NZkh dataset */
/*Set limit for calculating K and H, based on NZ*/
```

```
/*Calculate derivative of upper and lower curves within a% of NZ*/
data DataNZkh (keep=Dir Load Species Segment ROM NZ mUP mLOW UK LK);
	merge DataNZkh DataNZ;
	by Species Dir Load Segment ROM;
	/*To get NZ flexibility coefficient, determine the slope of the torque-rotation curve at
	rotation=0*/
	if Utheta>-&NZpercent*NZ/2 and Utheta<&NZpercent*NZ/2 then Uf = -
	UA*Ua1*exp(Ua1*(m-Um1))/(1+exp(Ua1*(m-Um1)))**2 + UB*Ua2*exp(Ua2*(m-
	Um2))/(1+exp(Ua2*(m-Um2)))**2;
	UK=1/Uf;	/* [Stiffness] = 1/[Flexibility] */
	if Ltheta>-&NZpercent*NZ/2 and Ltheta<&NZpercent*NZ/2 then Lf = -
	LA*La1*exp(La1*(m-Lm1))/(1+exp(La1*(m-Lm1)))**2 + LB*La2*exp(La2*(m-
	Lm2))/(1+exp(La2*(m-Lm2)))**2;
	LK=1/Lf;	/* [Stiffness] = 1/[Flexibility] */
	if Utheta>-&NZpercent*NZ/2 and Utheta<&NZpercent*NZ/2 then mUP = m;
	if Ltheta>-&NZpercent*NZ/2 and Ltheta<&NZpercent*NZ/2 then mLOW = m;
run;

/*Select UK, LK, mUP, and mLOW for each test subject (FSU+TEMP+DIR)*/
proc means data=DataNZkh mean noprint;
	var UK LK mUP mLOW;
	by Species Dir Load Segment ROM NZ; /*want UK, LK for each obs*/
	output out=DataNZkh(drop=_TYPE_ _FREQ_)
		mean=UK LK mUP mLOW;
run;

/*Attach NZ UK LK to raw dataset*/
data &data1(drop=mLOW mUP UA LA UB LB);
	merge &data1 DataNZkh;
	by Species Dir Load Segment ROM;
	if mUP=. or mLOW=. or UK=. or LK=. then delete;
	K=mean(UK,LK); /*average stiffness coefficient of subject*/
	H=mLOW-mUP;	/*hysteresis: focuses on the mid-portion of the torque-rotation
curve*/
	NZROMr=NZ/ROM; /*NZ-to-ROM ratio*/
run;

proc sort data=&data1;
	by Species Dir;
run;

/*
ods rtf file="C:/Users/Dean/sasDATA.rtf";
proc means data=&data1 mean std min max maxdec=1;
	class Species Dir;
	var ROM AREA NZ NZROMr HA H UK LK K;
```

```
        output out=DataSumm_(drop=_TYPE_ _FREQ_ _Label_);
run;
ods rtf close;
*/
/*=================Report Analysis Datasets, raw and normalized=============*/
ods listing off; /*turn off ODS*/
options orientation=portrait; /*page formatting*/ /*page formatting*/ /*options 1s=78 pageno=1
*/
*ods pdf file="&Path\DATA.pdf";
*ods rtf file="&Path\DATA.rtf";

/* Report DIP-Boltzmann Data */
proc report data=&data1 nowd headline headskip;
        column Species Dir Load Segment Ua1 Um1 Ua2 Um2 La1 Lm1 La2 Lm2 ROM;
        define Species / display center;
        define Dir / display center;
        define Load / display center;
        define Segment / display center width=7;
        define Ua1 / center format=BEST6.;
        define Um1 / center format=BEST6.;
        define Ua2 / center format=BEST6.;
        define Um2 / center format=BEST6.;
        define La1 / center format=BEST6.;
        define Lm1 / center format=BEST6.;
        define La2 / center format=BEST6.;
        define Lm2 / center format=BEST6.;
        define ROM / center format=BEST6.;
        title2 "&Data DIP-Boltzmann Data";
run;

/*Report Calculated Flexibility Data*/
        proc report data=&data1 nowd headline headskip;
        column Species Dir Load Segment ROM AREA NZ NZROMr HA H UK LK K;
        define Species / display center;
        define Dir / display center;
        define Load/ display center;
        define Segment / display center width=7;
        define ROM / center format=BEST6.;
        define AREA / center format=BEST6.;
        define HA / center format=BEST6.;
        define H / center format=BEST6.;
        define NZ / center format=BEST6.;
        define NZROMr / center 'NZ\ROM' format=BEST6.;
        define UK / center format=BEST6.;
        define LK / center format=BEST6.;
        define K / center format=BEST6.;
```

```
        title2 "&Data Flexibility Raw Data";
run;

goptions reset=footnote symbol;
options orientation=landscape; /*page formatting*/ /*page formatting*/ /*options ls=78
pageno=1 */

proc sort data=&data1;
        by Dir Load Species;
run;
data Camelid; set &data1;
        if Species = 'H. Lumbar' then delete;
run;

data DataAR; set Camelid;
        if Dir = 'AR';
run;

data DataFE; set Camelid;
        if Dir = 'FE';
run;

data DataLB; set Camelid;
        if Dir = 'LB';
run;

/*Import Geometry Data*/
proc import out = Dean
        datafile ='C:\Users\Dean\Dropbox\1_PhD\
        2_AnimalModel\Paper1_CamelidBiomechanics\Data\Alpaca_v3.xlsx'
        dbms = EXCEL replace;
        range = "GeoDATA$";
        getnames = YES;
        mixed = NO;
        scantext = YES;
        usedate = YES;
        scantime = YES;
run;

data &data2; set Dean;
run;

proc sort data = Dean;
        by species segment nspecie;
run;
```

```
proc means data=&data2 mean std min max maxdec=1;
	class Species;
	var Depth_Total Width_Total Depth_NP Width_NP Depth_AF Width_AF Height;
	output out=DataGeo(drop=_TYPE_);
run;

/*Create Boxplots and export to .rtf file*/
goptions reset=all;
symbol1 v=none i=none cv=red ci=red co=red;
ods listing;  /*turn on ODS*/
ods rtf file="&Path\boxplots.rtf";

	%macro boxFlexPar1(dat1=, var=, t2=, t3=, ref1=, ref2=,);
	*title2 "&t2";
	title3 "&t3";

	proc boxplot data=&dat1;
		plot &var*Species /
			cvref=red /*specifies color of vertical reference lines*/
			lvref=2 /*specifies line-type of vertical reference lines*/
			vref=&ref1 &ref2/*specifies vertical position of vertical reference lines*/
			/*vreflabels ='H.Lumbar' 'H.Cervical'/* specifies labels for vertical
reference lines*/
			vreflabpos=2 /*specifies position of labels for vertical reference lines*/
			height=7.5;
			label    &var = "&t2";
	run;
	%mend;
	%boxFlexPar1(dat1=DataAR, var=ROM, t2=Range of Motion (deg), t3=Axial Rotation,
ref1=4, ref2=10);
	%boxFlexPar1(dat1=DataFE, var=ROM, t2=Range of Motion (deg), t3=Flexion
Extension, ref1=15, ref2=16);
	%boxFlexPar1(dat1=DataLB, var=ROM, t2=Range of Motion (deg), t3=Lateral Bending,
ref1=12, ref2=17);
	%boxFlexPar1(dat1=DataAR, var=NZ, t2=Neutral Zone (deg), t3=Axial Rotation,
ref1=0.6, ref2=12);
	%boxFlexPar1(dat1=DataFE, var=NZ, t2=Neutral Zone (deg), t3=Flexion Extension,
ref1=0.9, ref2=14);
	%boxFlexPar1(dat1=DataLB, var=NZ, t2=Neutral Zone (deg), t3=Lateral Bending,
ref1=4.2, ref2=19);

%macro boxFlexPar2(dat1=, var=, t2=, t3=, ref1=, ref2=,);
	*title2 "&t2";
	title3 "&t3";

proc boxplot data=&dat1;
```

```
        plot &var*Species /
        cvref=red /*specifies color of vertical reference lines*/
                lvref=2 /*specifies line-type of vertical reference lines*/
                vref=&ref1/*specifies vertical position of vertical reference lines*/
                /*vreflabels ='H.Lumbar'/* specifies labels for vertical reference lines*/
                vreflabpos=2 /*specifies position of labels for vertical reference lines*/
                height=7.5;
                label    &var = "&t2";
run;
%mend;
%boxFlexPar2(dat1=DataAR, var=K, t2=Stiffness (N-m/deg), t3=Axial Rotation, ref1=2.1);
%boxFlexPar2(dat1=DataFE, var=K, t2=Stiffness (N-m/deg), t3=Flexion Extension, ref1=0.7);
%boxFlexPar2(dat1=DataLB, var=K, t2=Stiffness (N-m/deg), t3=Lateral Bending, ref1=0.3);
%boxFlexPar2(dat1=DataAR, var=H, t2=Hysteresis (N-m), t3=Axial Rotation, ref1=1);
%boxFlexPar2(dat1=DataFE, var=H, t2=Hysteresis (N-m), t3=Flexion Extension, ref1=0.4);
%boxFlexPar2(dat1=DataLB, var=H, t2=Hysteresis (N-m), t3=Lateral Bending, ref1=0.6);

/*Geometry*/
%macro boxMACRO(var=, t2=, ref=);
title2 "&t2";

proc boxplot data=&data2;
        plot &var*Species /
        cvref=red /*specifies color of vertical reference lines*/
        lvref=2 /*specifies line-type of vertical reference lines*/
        vref=&ref/*specifies vertical position of vertical reference lines*/
        /*vreflabels ='H.Lumbar'/* specifies labels for vertical reference lines*/
        vreflabpos=2 /*specifies position of labels for vertical reference lines*/
        height=7.5;
        label    &var = "&t2";
run;
%mend;
%boxMACRO(var=Depth_Total__mm_, t2=Total Depth, ref=34);
%boxMACRO(var=Width_Total__mm_, t2=Total Width, ref=50);
%boxMACRO(var=Depth_NP__mm_, t2=NP Depth, ref=17);
%boxMACRO(var=Width_NP__mm_, t2=NP Width, ref=36);
%boxMACRO(var=Depth_AF__mm_, t2=AF Depth, ref=15);
%boxMACRO(var=Width_AF__mm_, t2=AF Width, ref=15);
%boxMACRO(var=Height__mm_, t2=Height, ref=10);
ods rtf close;

%macro MixAn(dvar=, dlp3=);
/* Perform Mixed-Models ANOVA for (model=&dvar) variables of the selected datasets*/
/* Mixed-Models ANOVA of Specie */
proc mixed data=&data1 maxiter=100;
        class Segment Species Dir NSpecie;
```

```
        model &dvar = Species Dir Species*Dir /*Species(Segment)*/;
        random Nspecie/subject=NSpecie;
        title "Mixed-Models ANOVA for &dvar ";
        lsmeans Species*Dir/pdiff adjust=tukey;
        ods output Tests3 = &dlp3.P(keep=ProbF);
        ods output diffs=&dlp3.diff;
run;

data &dlp3.diff; set dlp3.diff;
        if Species=_Species or          Dir=_Dir;
run;

proc sort data=&dlp3.diff;
        by AdjP;
run;

proc print data=&dlp3.diff;
        run;
%mend MixAn;
%MixAn(dvar=ROM, dlp3=ROMdlp3);
%MixAn(dvar=NZ, dlp3=NZdlp3);
%MixAn(dvar=H, dlp3=Hdlp3);
%MixAn(dvar=K, dlp3=Kdlp3);
%MixAn(dvar=Area, dlp3=Areadlp3);
%MixAn(dvar=HA, dlp3=HAdlp3);
%MixAn(dvar=NZromR, dlp3=NZromRdlp3);
%MixAn(dvar=UK, dlp3=UKdlp3);
%MixAn(dvar=LK, dlp3=LKdlp3);
%MixAn(dvar=Ua1, dlp3=Ua1dlp3);
%MixAn(dvar=Um1, dlp3=Um1dlp3);
%MixAn(dvar=Ua2, dlp3=Ua2dlp3);
%MixAn(dvar=Um2, dlp3=Um2dlp3);
%MixAn(dvar=La1, dlp3=La1dlp3);
%MixAn(dvar=Lm1, dlp3=Lm1dlp3);
%MixAn(dvar=La2, dlp3=La2dlp3);
%MixAn(dvar=Lm2, dlp3=Lm2dlp3);

/*Organize p-value tables*/
        %macro          Ptable(TAB=, Eff=, Ua1=, Um1=, Ua2=, Um2=, La1=, Lm1=, La2=,
Lm2=, ROM=, NZ=, NZromR=, AREA=, HA=, H=, UK=, LK=, K=);

data &TAB;
        merge &Eff
        &Ua1(rename=(ProbF=Ua1)) &Um1(rename=(ProbF=Um1))
&Ua2(rename=(ProbF=Ua2)) &Um2(rename=(ProbF=Um2))
```

```
        &La1(rename=(ProbF=La1)) &Lm1(rename=(ProbF=Lm1))
&La2(rename=(ProbF=La2)) &Lm2(rename=(ProbF=Lm2))
        &ROM(rename=(ProbF=ROM)) &AREA(rename=(ProbF=Area))
&NZ(rename=(ProbF=NZ)) &NZromR(rename=(ProbF=NZromR))
        &HA(rename=(ProbF=HA)) &H(rename=(ProbF=H))
        &UK(rename=(ProbF=UK)) &LK(rename=(ProbF=LK)) &K(rename=(ProbF=K));
        label ROM='ROM' Area='Area' NZ='NZ' NZromR='NZromR' HA='HA' H='H' UK='UK'
LK ='LK' K='K'
        Ua1='Ua1' Um1='Um1' Ua2='Ua2' Um2='Um2' La1='La1' Lm1='Lm1' La2='La2'
Lm2='Lm2';
        *format Ua1 Um1 Ua2 Um2 La1 Lm1 La2 Lm2 ROM AREA H NZ UK LK K pFMT.;
/*apply format*/
run;

*       proc datasets library=work;
*               delete &Ua1 &Um1 &Ua2 &Um2 &La1 &Lm1 &La2 &Lm2 &ROM &AREA
&NZ &NZromR &HA &H &UK &LK &K;
        *       run;
%mend Ptable;
        %Ptable(TAB=Pdlp3, Eff=Effects, Ua1=Ua1dlp3, Um1=Um1dlp3, Ua2=Ua2dlp3,
Um2=Um2dlp3, La1=La1dlp3, Lm1=Lm1dlp3, La2=La2dlp3, Lm2=Lm2dlp3,
ROM=ROMdlp3, NZ=NZdlp3, NZromR=NZromRdlp3, AREA=AREAdlp3, HA=HAdlp3,
H=Hdlp3, UK=UKdlp3, LK=LKdlp3, K=Kdlp3); /*DLP p-value*/


%macro MixAn(dvar=, dlp3=);
/* Perform Mixed-Models ANOVA for (model=&dvar) variables of the selected datasets*/
/* Mixed-Models ANOVA of Specie */
proc mixed data=Dean maxiter=100;
        class Segment Species Nspecie;
        model &dvar = Species Segment /*Nspecie Species(Segment)*/;
        random Nspecie/subject=Nspecie;
        title "Mixed-Models ANOVA for &dvar ";
        ods output Tests3 = &dlp3(keep=ProbF);
run;
%mend MixAn;
%MixAn(dvar=Depth_Total, dlp3=DT);
%MixAn(dvar=Width_Total, dlp3=WT);
%MixAn(dvar=Depth_NP, dlp3=dNP);
%MixAn(dvar=Width_NP, dlp3=wNP);
%MixAn(dvar=Height, dlp3=H);

/*
%MixAn(dvar=Area, dlp3=Areadlp3);
%MixAn(dvar=HA, dlp3=HAdlp3);
%MixAn(dvar=NZromR, dlp3=NZromRdlp3);
```

```
%MixAn(dvar=UK, dlp3=UKdlp3);
%MixAn(dvar=LK, dlp3=LKdlp3);
%MixAn(dvar=Ua1, dlp3=Ua1dlp3);
%MixAn(dvar=Um1, dlp3=Um1dlp3);
%MixAn(dvar=Ua2, dlp3=Ua2dlp3);
%MixAn(dvar=Um2, dlp3=Um2dlp3);
%MixAn(dvar=La1, dlp3=La1dlp3);
%MixAn(dvar=Lm1, dlp3=Lm1dlp3);
%MixAn(dvar=La2, dlp3=La2dlp3);
%MixAn(dvar=Lm2, dlp3=Lm2dlp3);
```

A.2 MRI Data Analysis

```
%let Path = C:\Users\Dean\Dropbox\1_PhD\Alpaca Disc;
%let data1 = MAN1;
option mprint;
/*============Import Data============*/
proc import out = &data1
        datafile = 'C:\Users\Dean\Dropbox\1_PhD\Alpaca  Disc\Data\ AlpacaMRI_Dean2.xlsx'
        dbms = EXCEL replace;
        range = "SAS$";
        getnames = YES;
        mixed = NO;
        scantext = YES;
        usedate = YES;
        scantime = YES;
run;

data &Data1;
        set &DATA1;
        if Pfirrmann < 3 then PfirrBIN="Healthy";
                else PfirrBIN="Degen";
        if Pfirrmann < 3 then PfirrMULT=1;
                else if Pfirrmann = 3 then PfirrMULT=2;
                else PfirrMULT=3;
        if Age <= 6 then AGE2="Young";
                else AGE2="Old";
        if Reviewer="SStV" then Rad="VR";
                else if Reviewer="W" then Rad="HR";
        run;

proc sort data=&Data1;
        by AGE2 Segment Rad;
run;

proc means data=&Data1 mean std min max maxdec=2;
```

```
	class AGE2;
	var Age Weight Pfirrmann;
	output out=DataSumm(drop=_TYPE_);
run;

/* Perform Mixed-Models ANOVA for (model=&dvar) variables of the selected datasets*/
/* Mixed-Models ANOVA of Pfirrmann */
proc mixed data=&DATA1 maxiter=100;
	class AGE2 Segment Alpaca/*Disc (no repeats-->infinite likelihood*/;
	model Pfirrmann = Segment AGE2 Segment*AGE2/*each Alpaca tested at one Age*/
	/*Alpaca*Segment/*Each segment of each alpaca tested*/;
	random Alpaca(AGE2)/subject=Alpaca;
	title "Mixed-Model ANOVA for Alpaca MRI Pfirrmann ";
	lsmeans /*AGE2*/ Segment /*Segment*AGE2 */ / pdiff adjust=tukey;
	ods output diffs = PFdiff;
run;

/*Pfirrmann Degeneration boxplots*/
%macro boxPfirrmann(var1=, var2=, t1=, t2=);
	proc sort data=&Data1;
		by &var2;
	run;

	proc boxplot data=&Data1;
		plot &var1*&var2 /
		cvref=red /*specifies color of vertical reference lines*/
		lvref=2 /*specifies line-type of vertical reference lines*/
		height=7.5;
		label	&var1 = "&t1 vs &t2";
	run;
%mend;
%boxPfirrmann(var1=Pfirrmann, var2=AGE2 , t1=Pfirrmann Grade, t2=Age Subgroup);
%boxPfirrmann(var1=Pfirrmann, var2=Segment , t1=Pfirrmann Grade, t2=IVD Level);
```

APPENDIX B – DATA TABLES

B.1 Alpaca and Llama DIP-Boltzman Parameters

Table B-1: Alpaca and Llama DIP-Boltzmann Parameters

Species	DIR	Load	Segment	Ua1	Um1	Ua2	Um2	La1	Lm1	La2	Lm2	ROM
Alpaca	AR	nL	c3c4	0.6852	-0.389	0.6852	-0.389	0.7078	0.4987	0.7078	0.4987	4.2063
Alpaca	AR	nL	c3c4	0.8653	-0.46	0.8653	-0.46	0.8874	0.3857	0.8874	0.3857	6.9827
Alpaca	AR	nL	c4c5	0.5962	-0.964	0.5962	-0.964	0.5678	0.872	0.5678	0.872	2.6158
Alpaca	AR	nL	c4c5	0.7055	-0.42	0.7055	-0.42	0.7037	0.631	0.7037	0.631	4.4821
Alpaca	AR	nL	c4c5	0.8294	-0.323	0.8294	-0.323	0.8823	0.3018	0.8823	0.3018	6.3775
Alpaca	AR	nL	c4c5	0.9205	-0.377	0.9205	-0.377	0.9122	0.4516	0.9122	0.4516	8.741
Alpaca	AR	nL	c5c6	0.6871	-1.122	0.6871	-1.122	0.6677	0.5237	0.6677	0.5237	2.9396
Alpaca	AR	nL	c5c6	0.5505	-0.502	0.5505	-0.502	0.5965	0.7987	0.5965	0.7987	3.7238
Alpaca	AR	nL	c6c7	0.7093	-1.181	0.7093	-1.181	0.5938	0.1209	0.5938	0.1209	2.2056
Alpaca	AR	nL	c7t1	0.8255	-0.352	0.8255	-0.352	0.7536	0.7993	0.7536	0.7993	4.1685
Alpaca	FE	nL	c3c4	0.9252	-0.962	0.9252	-0.962	1.0612	-0.474	1.0612	-0.474	24.904
Alpaca	FE	nL	c3c4	0.8682	-0.466	0.8682	-0.466	0.8821	-0.084	0.8821	-0.084	27.233
Alpaca	FE	nL	c4c5	0.8704	0.5446	0.8704	0.5446	0.8441	1.143	0.8441	1.143	22.416
Alpaca	FE	nL	c4c5	0.8421	-0.523	0.8421	-0.523	0.8769	-0.024	0.8769	-0.024	26.699
Alpaca	FE	nL	c5c6	0.8697	-1.13	0.8697	-1.13	0.9526	-0.678	0.9526	-0.678	25.204
Alpaca	FE	nL	c5c6	0.9185	-0.656	0.9185	-0.656	0.9493	-0.198	0.9493	-0.198	26.883
Alpaca	FE	nL	c7t1	1.4499	1.2242	1.4499	1.2242	1.3054	1.6628	1.3054	1.6628	21.413
Alpaca	LB	nL	c3c4	0.9218	-0.556	0.9218	-0.556	0.8429	0.3333	0.8429	0.3333	29.484
Alpaca	LB	nL	c4c5	0.8476	0.0815	0.8476	0.0815	0.8101	0.6167	0.8101	0.6167	27.327
Alpaca	LB	nL	c4c5	1.0435	-0.112	1.0435	-0.112	0.9783	0.3246	0.9783	0.3246	34.522
Alpaca	LB	nL	c4c5	1.1843	-0.165	1.1843	-0.165	1.1412	0.6083	1.1412	0.6083	36.247
Alpaca	LB	nL	c4c5	0.8725	-0.549	0.8725	-0.549	0.9806	0.1055	0.9806	0.1055	36.353
Alpaca	LB	nL	c5c6	0.8976	-0.095	0.8976	-0.095	0.8677	0.3254	0.8677	0.3254	25.967
Alpaca	LB	nL	c5c6	0.8211	-0.343	0.8211	-0.343	0.8404	0.1263	0.8404	0.1263	29.798
Alpaca	LB	nL	c6c7	0.7957	-0.18	0.7957	-0.18	0.712	0.4214	0.712	0.4214	22.339

Species	DIR	Load	Segment	Ua1	Um1	Ua2	Um2	La1	Lm1	La2	Lm2	ROM
Alpaca	LB	nL	c7t1	0.9919	0.0299	0.9919	0.0299	1.136	0.5125	1.136	0.5125	13.277
Llama	AR	nL	c2c3	0.7713	-0.445	0.7713	-0.445	0.7688	0.4232	0.7688	0.4232	7.0519
Llama	AR	nL	c3c4	0.7724	-0.668	0.7724	-0.668	0.7563	0.2111	0.7563	0.2111	6.566
Llama	AR	nL	c5c6	0.7153	-0.28	0.7153	-0.28	0.7195	0.7365	0.7195	0.7365	4.5145
Llama	FE	nL	c2c3	0.8402	-0.258	0.8402	-0.258	0.9232	0.2806	0.9232	0.2806	29.643
Llama	FE	nL	c3c4	0.9323	-0.778	0.9323	-0.778	1.0059	-0.348	1.0059	-0.348	28.812
Llama	FE	nL	c5c6	0.785	-0.895	0.785	-0.895	0.8366	-0.317	0.8366	-0.317	23.556
Llama	LB	nL	c2c3	1.0239	-0.561	1.0239	-0.561	1.0791	-0.025	1.0791	-0.025	33.764
Llama	LB	nL	c3c4	0.876	-0.559	0.876	-0.559	0.9058	0.4173	0.9058	0.4173	35.046
Llama	LB	nL	c5c6	0.8664	-0.492	0.8664	-0.492	0.8954	0.098	0.8954	0.098	29.691

B.2 Alpaca and Llama Flexibility Parameters

Table B-2: Alpaca and Llama Flexibility Parameters

Species	DIR	Load	Segment	ROM	AREA	NZ	NZ\ROM	HA	H	UK	LK	K
Alpaca	AR	nL	c3c4	4.2063	3.2957	0.6466	0.1537	0.7835	0.888	1.3959	1.3513	1.3736
Alpaca	AR	nL	c3c4	6.9827	5.5505	1.2801	0.1833	0.7949	0.844	0.6675	0.6509	0.6592
Alpaca	AR	nL	c4c5	2.6158	3.9192	0.6835	0.2613	1.4983	1.836	2.6089	2.7393	2.6741
Alpaca	AR	nL	c4c5	4.4821	4.1693	0.8207	0.1831	0.9302	1.052	1.2754	1.2788	1.2771
Alpaca	AR	nL	c4c5	6.3775	3.7262	0.8574	0.1344	0.5843	0.624	0.7596	0.714	0.7368
Alpaca	AR	nL	c4c5	8.741	6.8725	1.6398	0.1876	0.7862	0.828	0.5015	0.5061	0.5038
Alpaca	AR	nL	c5c6	2.9396	4.2058	0.7991	0.2719	1.4307	1.646	2.0171	2.076	2.0466
Alpaca	AR	nL	c5c6	3.7238	3.9523	0.6932	0.1861	1.0613	1.3	1.968	1.8162	1.8921
Alpaca	AR	nL	c6c7	2.2056	2.5094	0.4763	0.216	1.1377	1.302	2.5866	3.0897	2.8382
Alpaca	AR	nL	c7t1	4.1685	4.3639	0.9382	0.2251	1.0469	1.152	1.1771	1.2893	1.2332
Alpaca	FE	nL	c3c4	24.904	11.202	3.2081	0.1288	0.4498	0.488	0.1743	0.152	0.1631
Alpaca	FE	nL	c3c4	27.233	9.7504	2.2757	0.0836	0.358	0.382	0.1695	0.1668	0.1681
Alpaca	FE	nL	c4c5	22.416	12.23	2.8685	0.128	0.5456	0.6	0.2058	0.2122	0.209
Alpaca	FE	nL	c4c5	26.699	12.406	2.8766	0.1077	0.4647	0.5	0.1784	0.1713	0.1749
Alpaca	FE	nL	c5c6	25.204	10.217	2.6987	0.1071	0.4054	0.454	0.183	0.1671	0.175
Alpaca	FE	nL	c5c6	26.883	11.626	2.88	0.1071	0.4325	0.458	0.1624	0.1572	0.1598
Alpaca	FE	nL	c7t1	21.413	8.8982	3.2945	0.1539	0.4156	0.44	0.1296	0.1439	0.1368
Alpaca	LB	nL	c3c4	29.484	24.731	5.7728	0.1958	0.8388	0.888	0.1486	0.1625	0.1555

Species	DIR	Load	Segment	ROM	AREA	NZ	NZ\ROM	HA	H	UK	LK	K
Alpaca	LB	nL	c4c5	27.327	13.454	3.0475	0.1115	0.4923	0.534	0.1732	0.1812	0.1772
Alpaca	LB	nL	c4c5	34.522	14.526	3.8727	0.1122	0.4208	0.438	0.1114	0.1188	0.1151
Alpaca	LB	nL	c4c5	36.247	27.423	8.0208	0.2213	0.7565	0.772	0.0943	0.0979	0.0961
Alpaca	LB	nL	c4c5	36.353	22.426	5.6447	0.1553	0.6169	0.656	0.1268	0.1129	0.1199
Alpaca	LB	nL	c5c6	25.967	10.27	2.4216	0.0933	0.3955	0.422	0.172	0.1779	0.1749
Alpaca	LB	nL	c5c6	29.798	12.987	2.9053	0.0975	0.4358	0.472	0.1639	0.1601	0.162
Alpaca	LB	nL	c6c7	22.339	12.07	2.654	0.1188	0.5403	0.602	0.2258	0.2523	0.2391
Alpaca	LB	nL	c7t1	13.277	6.2704	1.7958	0.1353	0.4723	0.482	0.3051	0.2664	0.2857
Llama	AR	nL	c2c3	7.0519	5.5772	1.1681	0.1656	0.7909	0.868	0.7403	0.7427	0.7415
Llama	AR	nL	c3c4	6.566	5.2463	1.0937	0.1666	0.799	0.88	0.794	0.811	0.8025
Llama	AR	nL	c5c6	4.5145	4.0826	0.814	0.1803	0.9043	1.014	1.2486	1.2412	1.2449
Llama	FE	nL	c2c3	29.643	15.037	3.625	0.1223	0.5073	0.538	0.1612	0.1467	0.1539
Llama	FE	nL	c3c4	28.812	11.594	3.0774	0.1068	0.4024	0.43	0.1493	0.1384	0.1439
Llama	FE	nL	c5c6	23.556	12.264	2.7964	0.1187	0.5206	0.58	0.2171	0.2037	0.2104
Llama	LB	nL	c2c3	33.764	17.468	4.7634	0.1411	0.5174	0.536	0.1163	0.1103	0.1133
Llama	LB	nL	c3c4	35.046	32.264	7.5141	0.2144	0.9206	0.978	0.1318	0.1275	0.1296
Llama	LB	nL	c5c6	29.691	16.445	3.8494	0.1296	0.5539	0.59	0.1561	0.1511	0.1536

B.3 Boxplot comparisons of Alpaca and Llama Flexibility Data

The following boxplots were used for comparison of the alpaca and llama data, which included the biomechanical flexibility parameters noted above (Range of Motion, ROM; Neutral Zone, NZ; Neutral-Zone Stiffness, K; and Hysteresis, H), in addition to other flexibility parameters not described above, including: Area, NZ-ROM Ratio, Hysteresis-Area, Upper Stiffness, and Lower Stiffness. Further details and explanation concerning these flexibility parameters may be obtained from my masters work [31]. Boxplots are also included for comparison of the parameters that make up the DIP-Boltzmann curve. Further details and explanation concerning these parameters may also be obtained from my masters work [31].

Animal SAS Analysis

Range of Motion

DIR=AR Load=nL

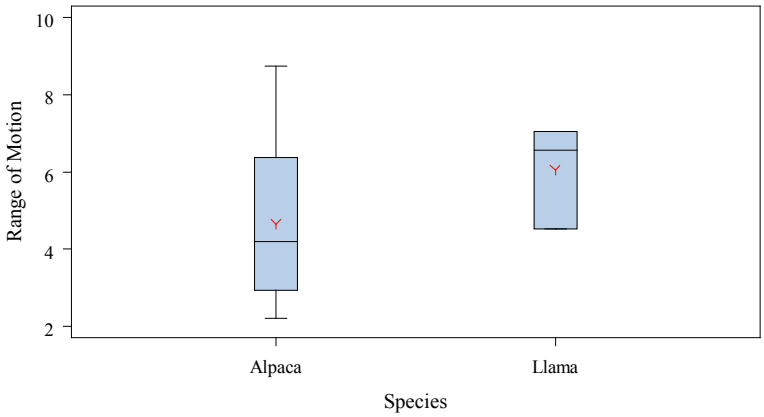

Animal SAS Analysis

Range of Motion

DIR=FE Load=nL

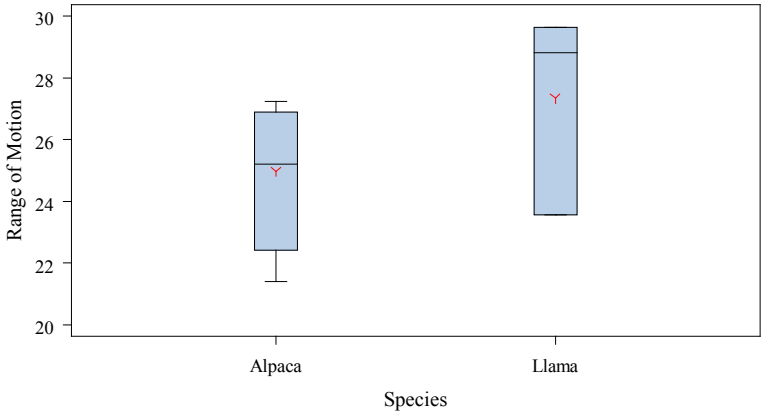

Animal SAS Analysis

Range of Motion

DIR=LB Load=nL

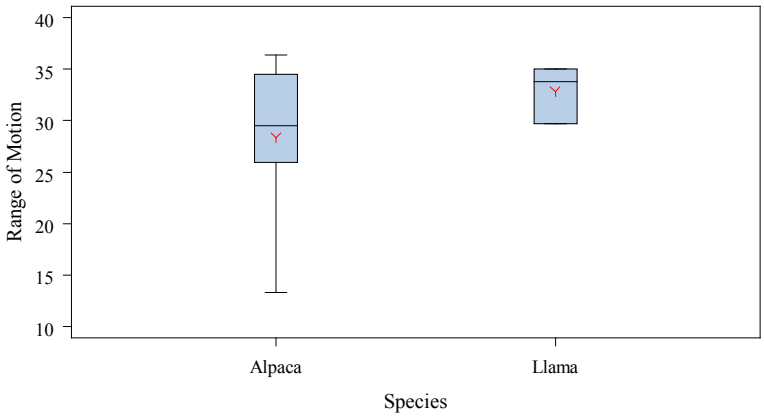

Animal SAS Analysis

Area

DIR=AR Load=nL

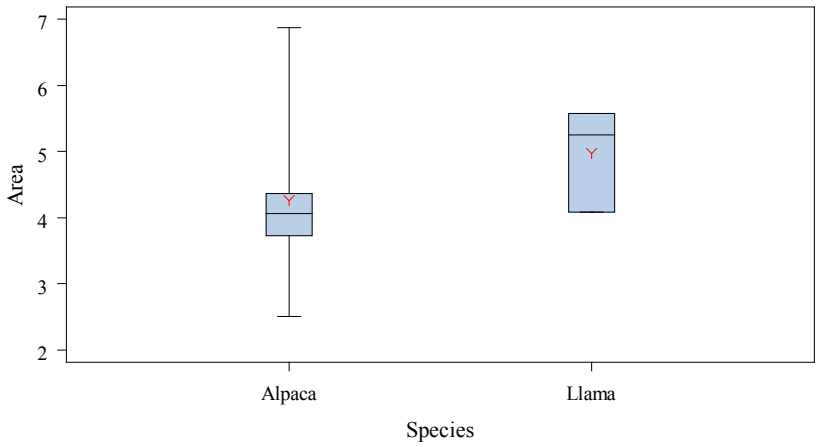

Animal SAS Analysis

Area

DIR=FE Load=nL

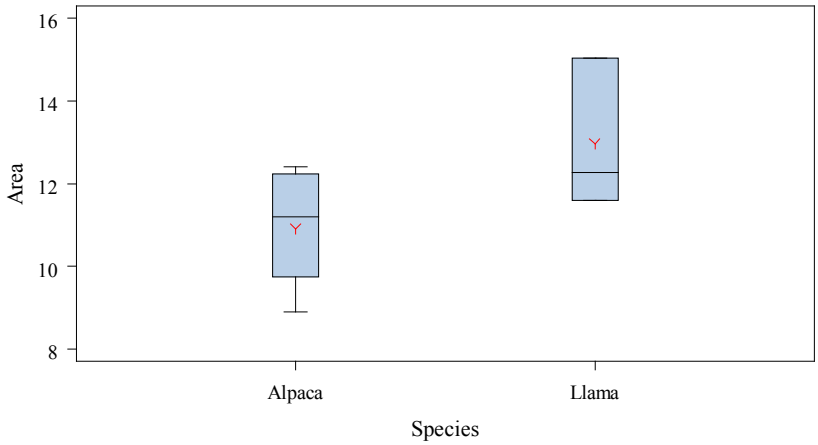

Animal SAS Analysis

Area

DIR=LB Load=nL

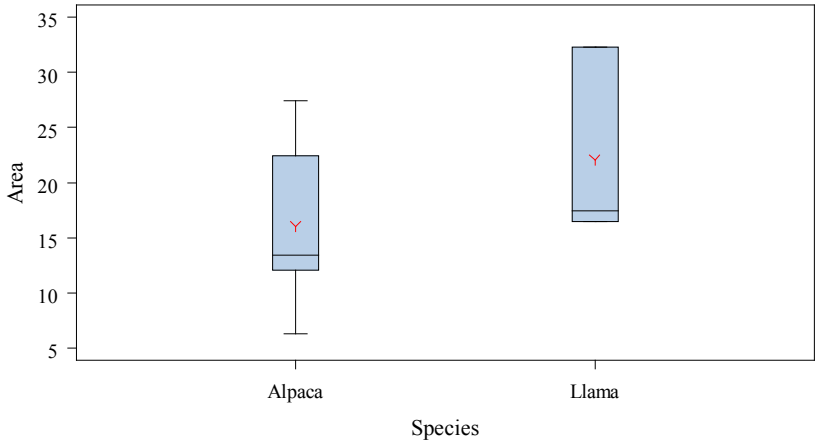

Animal SAS Analysis

Neutral Zone

DIR=AR Load=nL

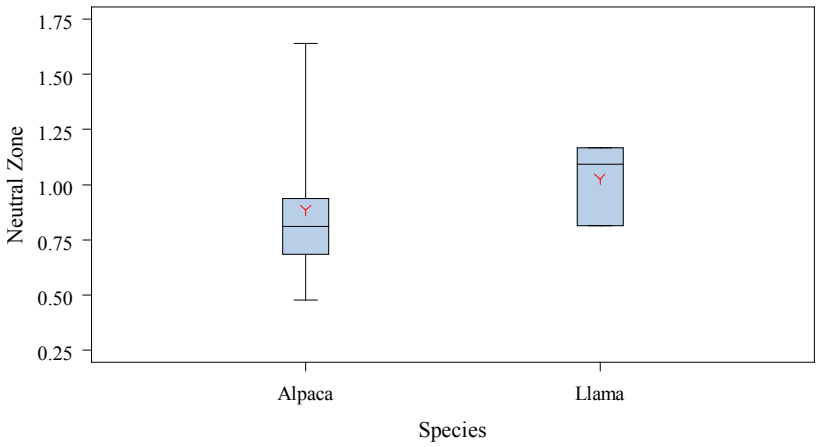

Animal SAS Analysis

Neutral Zone

DIR=FE Load=nL

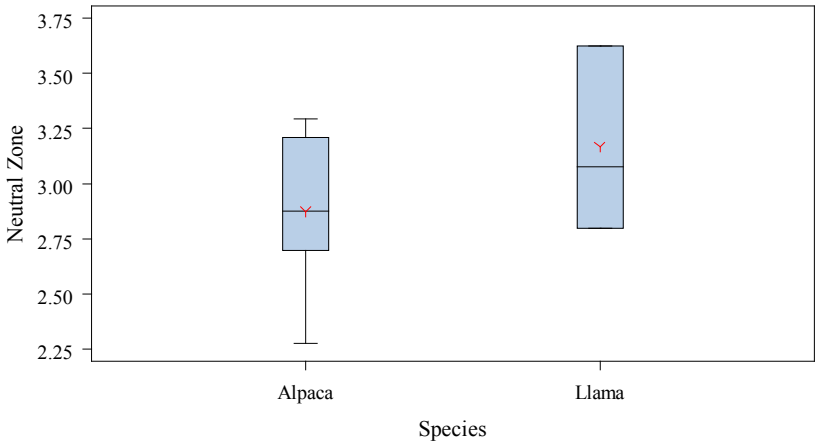

Animal SAS Analysis

Neutral Zone

DIR=LB Load=nL

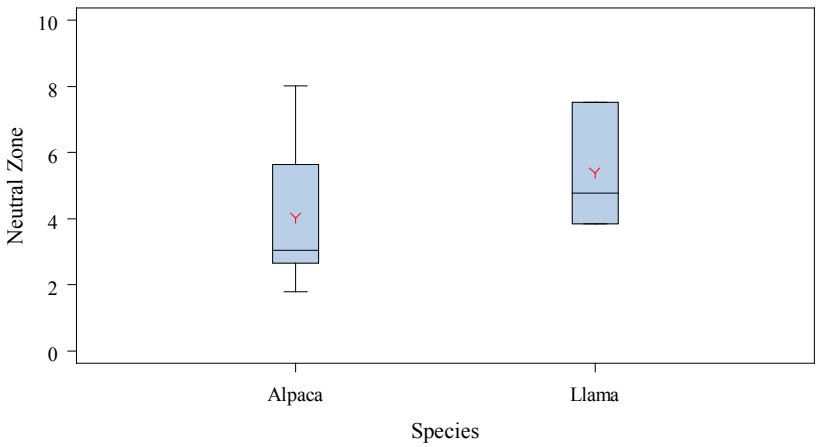

Animal SAS Analysis

NZ-ROM-ratio

DIR=AR Load=nL

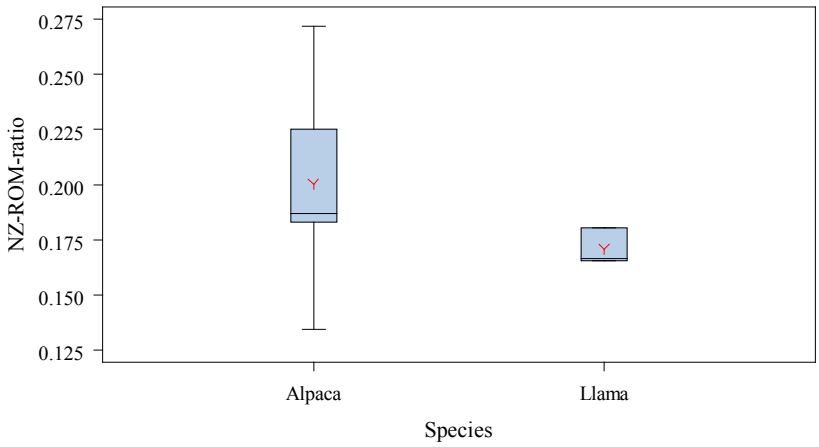

Animal SAS Analysis

NZ-ROM-ratio

DIR=FE Load=nL

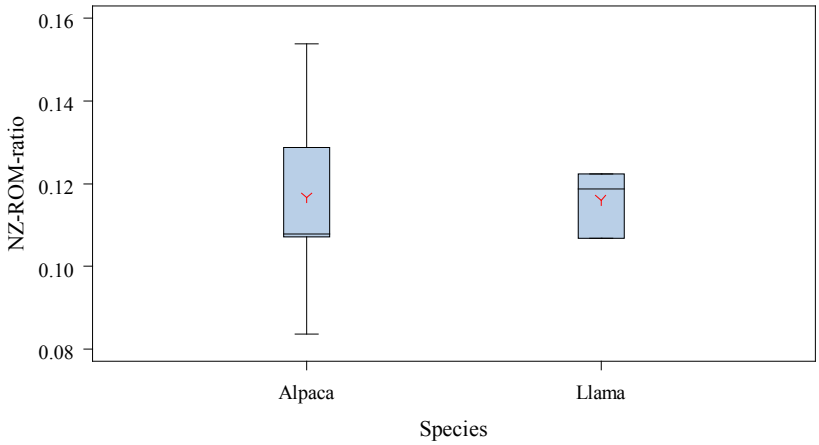

Animal SAS Analysis

NZ-ROM-ratio

DIR=LB Load=nL

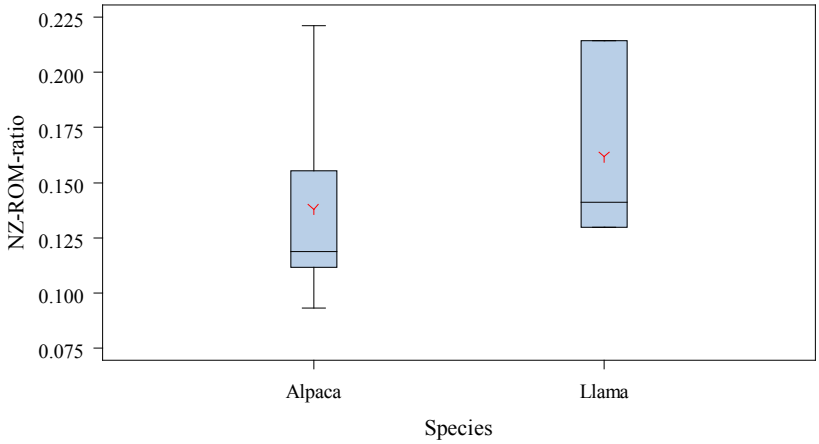

Animal SAS Analysis

Hysteresis Area

DIR=AR Load=nL

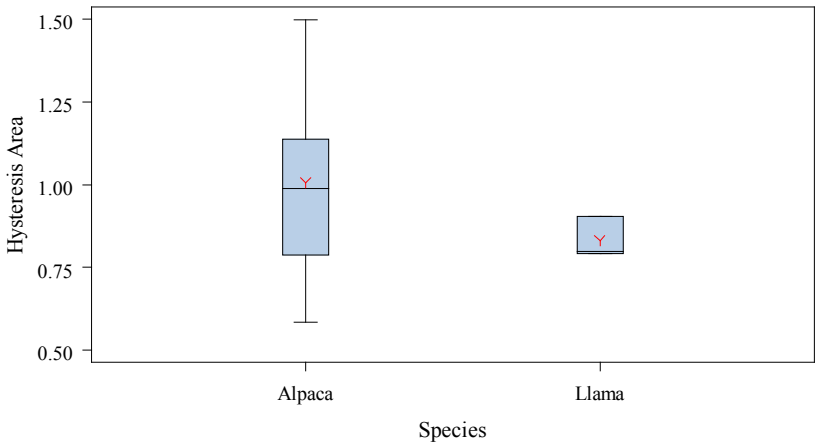

Animal SAS Analysis

Hysteresis Area

DIR=FE Load=nL

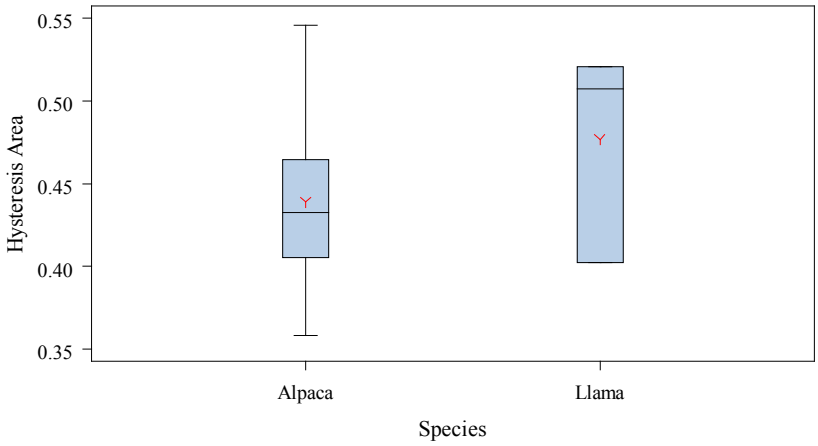

Animal SAS Analysis

Hysteresis Area

DIR=LB Load=nL

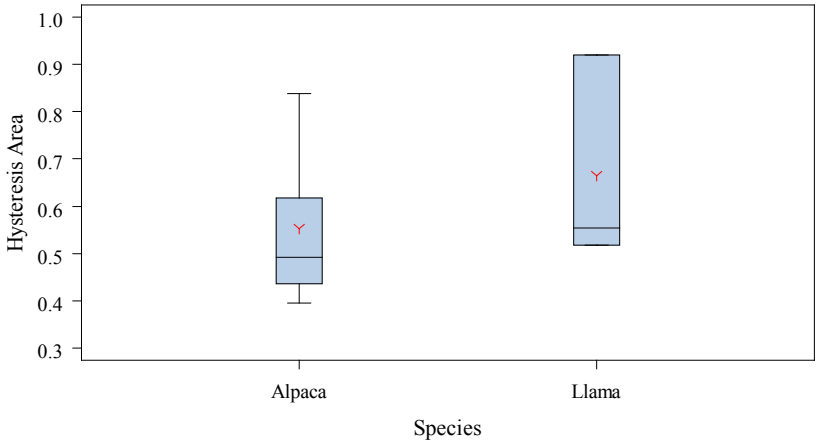

Animal SAS Analysis

Hysteresis

DIR=AR Load=nL

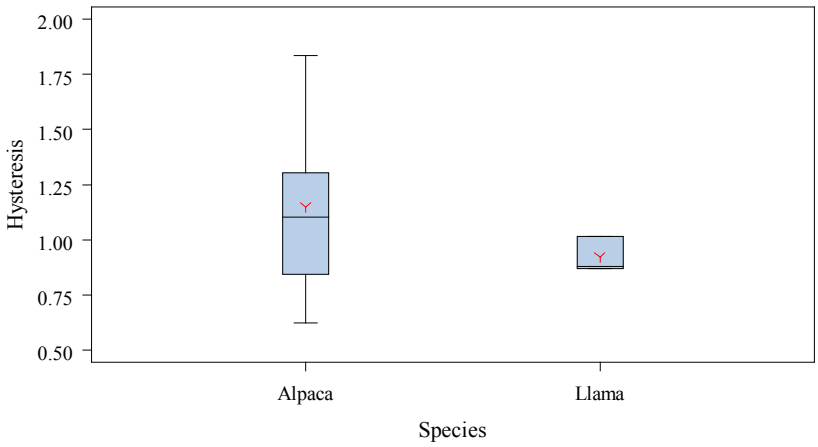

Animal SAS Analysis

Hysteresis

DIR=FE Load=nL

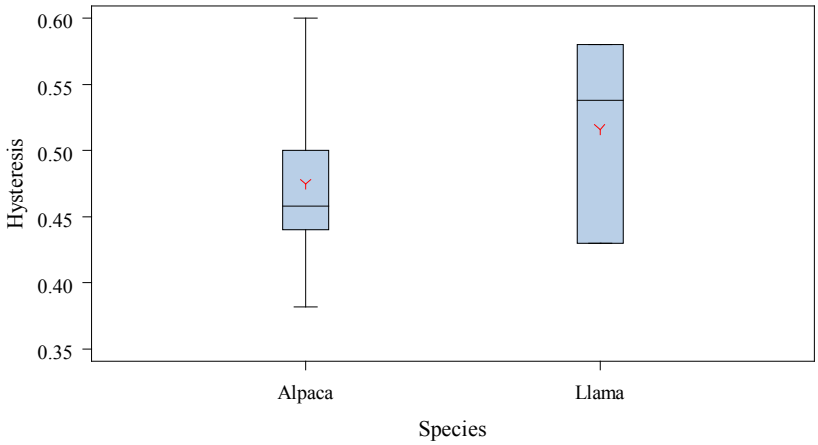

Animal SAS Analysis

Hysteresis

DIR=LB Load=nL

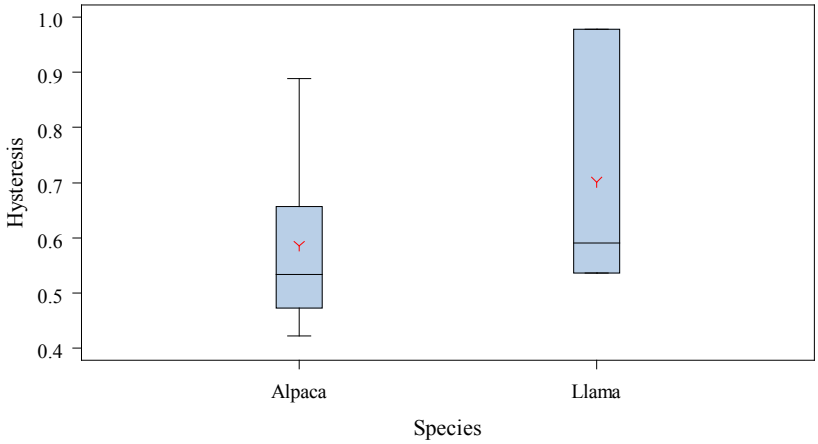

Animal SAS Analysis

Upper Stiffness

DIR=AR Load=nL

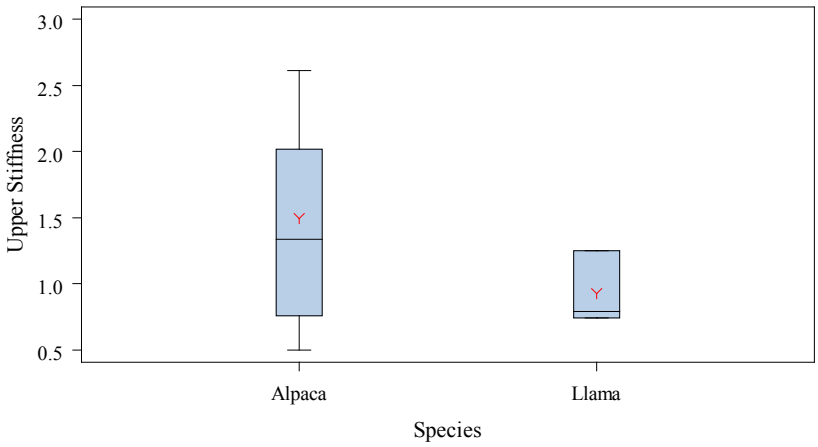

Animal SAS Analysis

Upper Stiffness

DIR=FE Load=nL

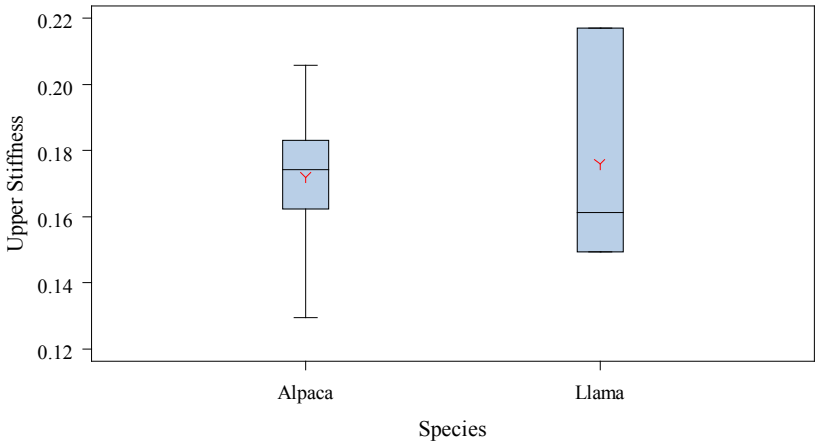

Animal SAS Analysis

Upper Stiffness

DIR=LB Load=nL

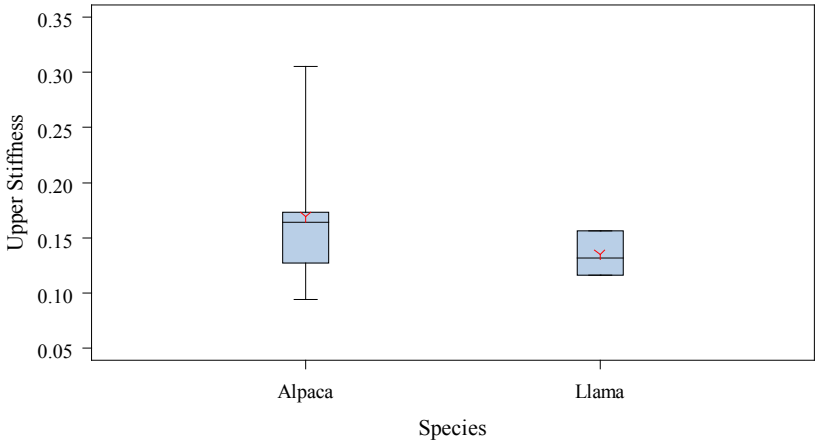

Animal SAS Analysis

Lower Stiffness

DIR=AR Load=nL

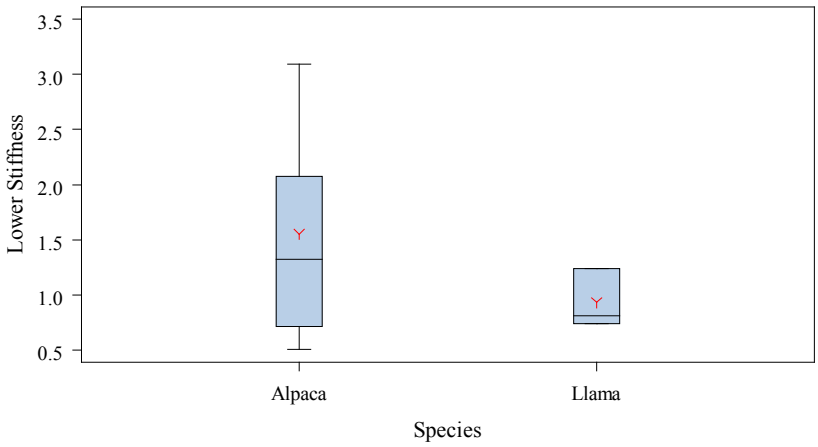

Animal SAS Analysis

Lower Stiffness

DIR=FE Load=nL

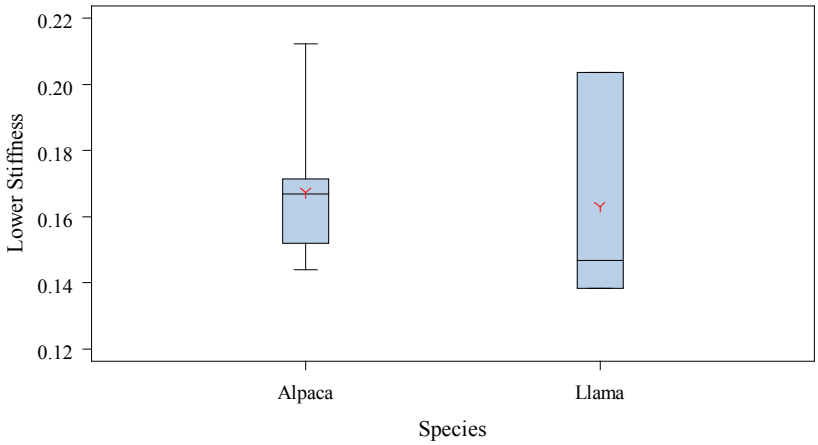

Animal SAS Analysis

Lower Stiffness

DIR=LB Load=nL

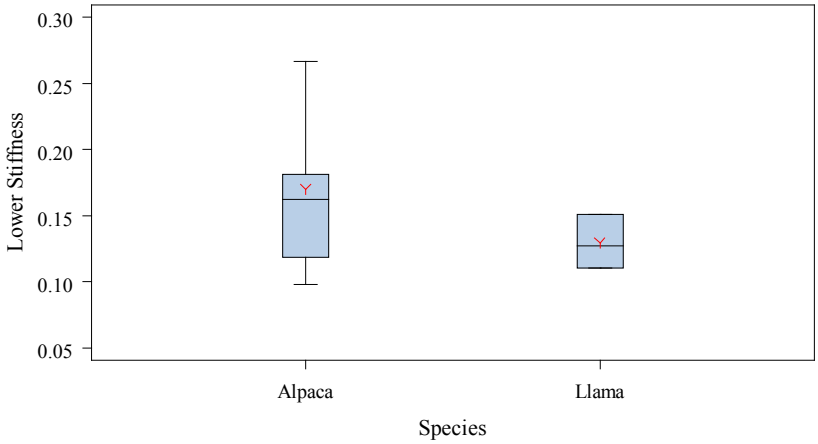

Animal SAS Analysis

Stiffness

DIR=AR Load=nL

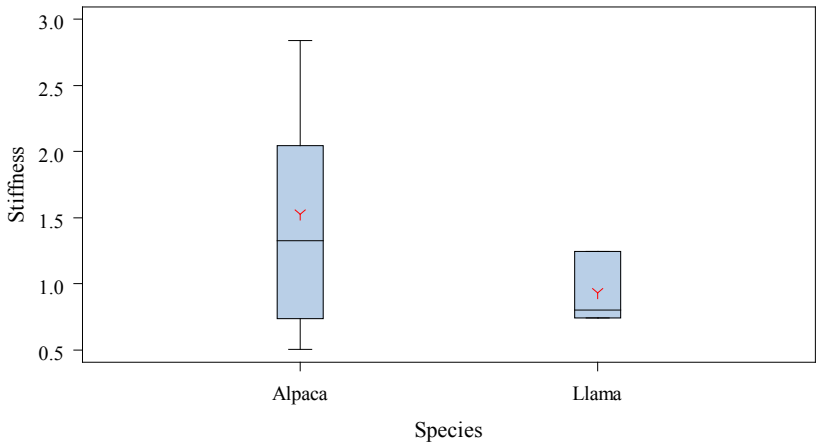

Animal SAS Analysis

Stiffness

DIR=FE Load=nL

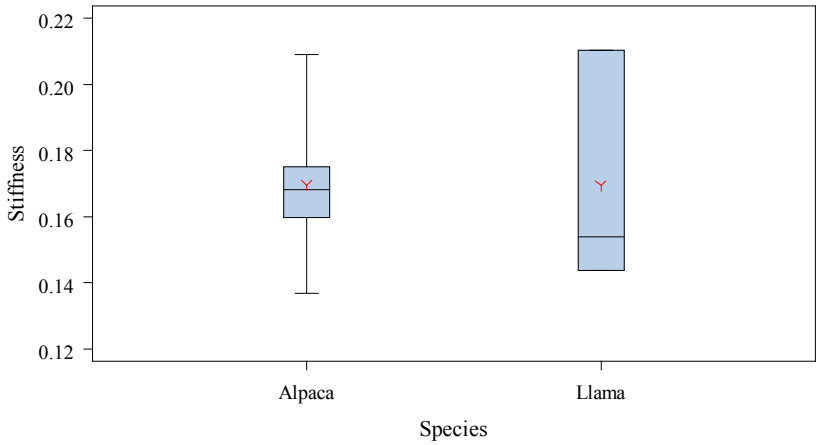

Animal SAS Analysis

Stiffness

DIR=LB Load=nL

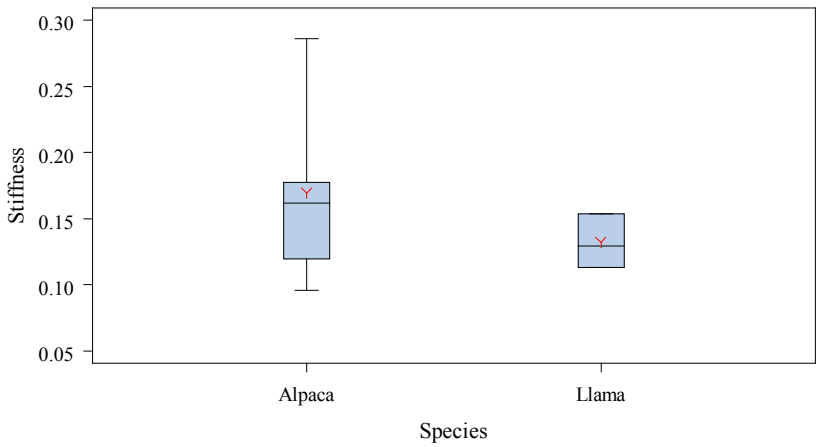

Animal SAS Analysis

alpha1UPPER

DIR=AR Load=nL

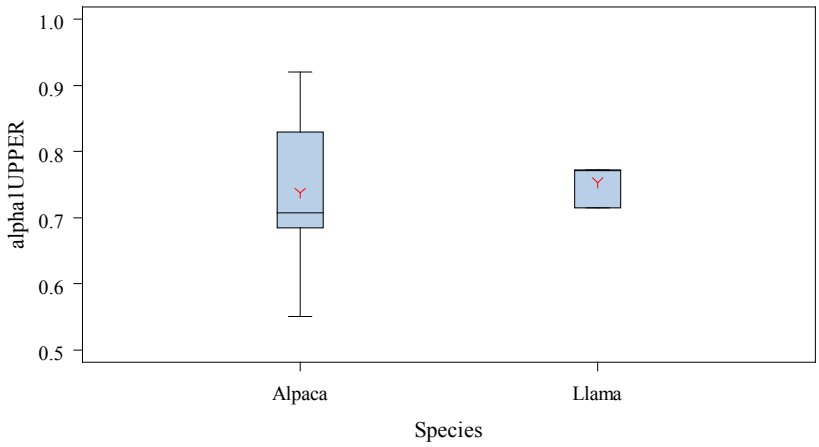

Animal SAS Analysis

alpha1UPPER

DIR=FE Load=nL

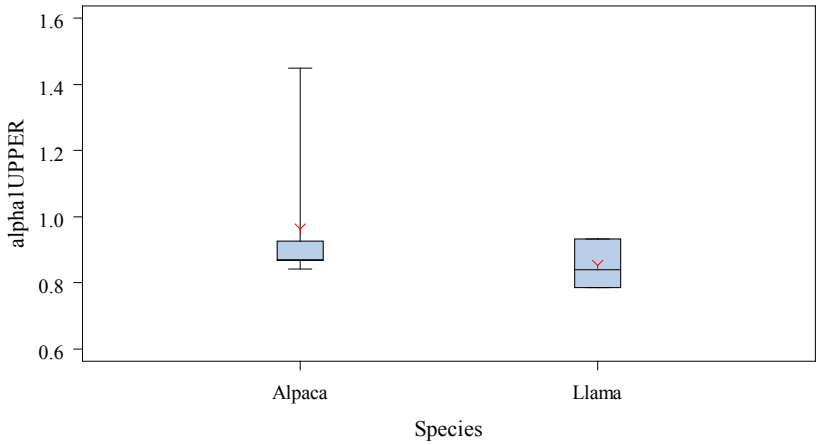

Animal SAS Analysis

alpha1UPPER

DIR=LB Load=nL

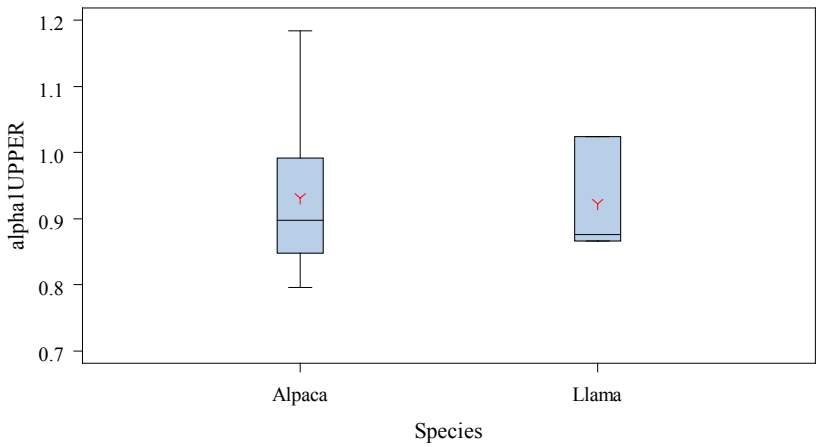

Animal SAS Analysis

m1UPPER

DIR=AR Load=nL

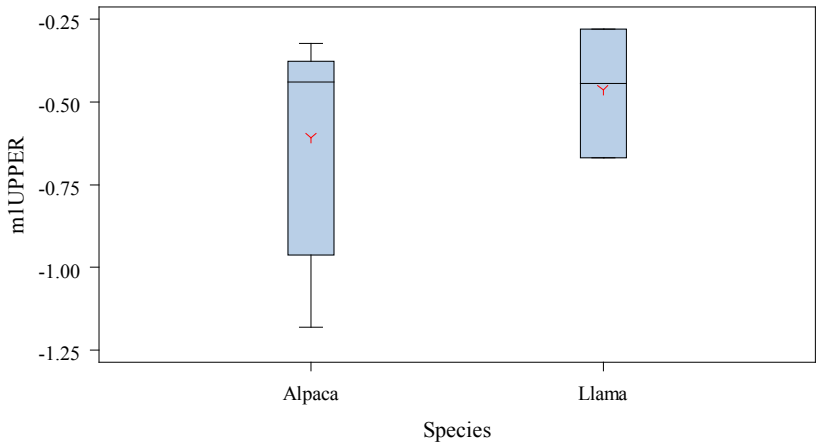

Animal SAS Analysis

m1UPPER

DIR=FE Load=nL

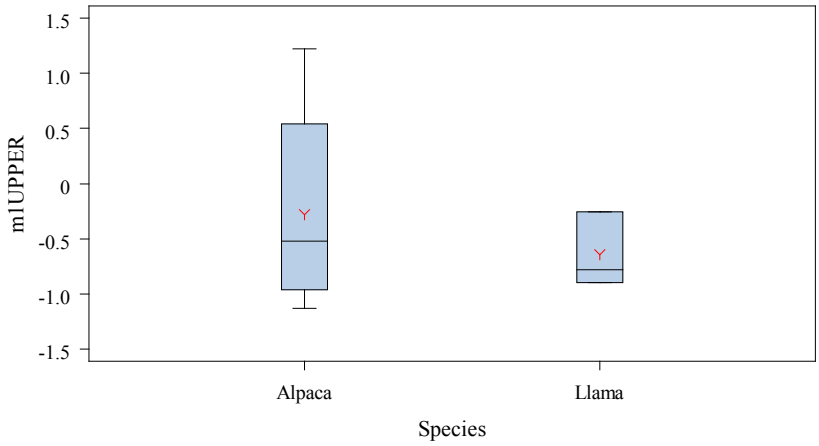

Animal SAS Analysis

m1UPPER

DIR=LB Load=nL

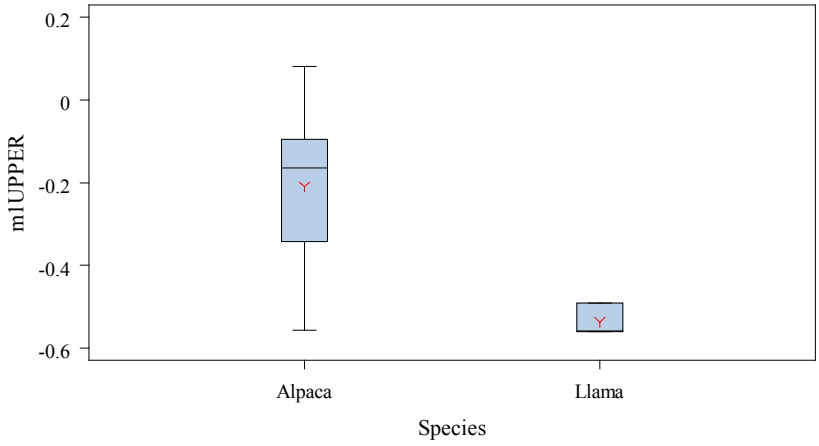

Animal SAS Analysis

alpha2UPPER

DIR=AR Load=nL

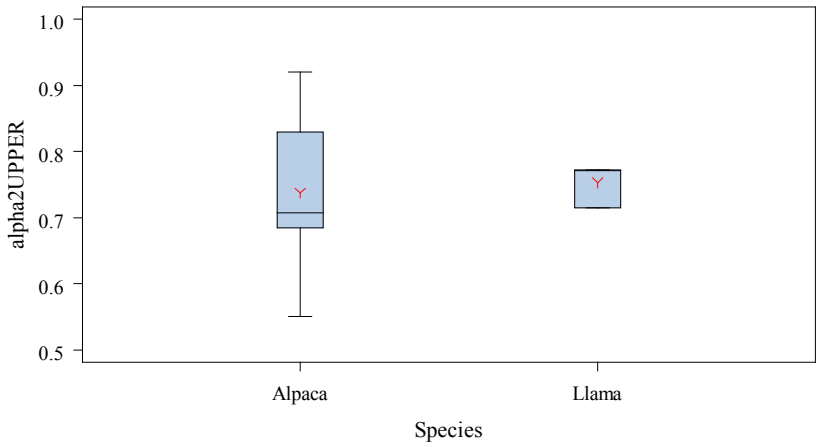

Animal SAS Analysis

alpha2UPPER

DIR=FE Load=nL

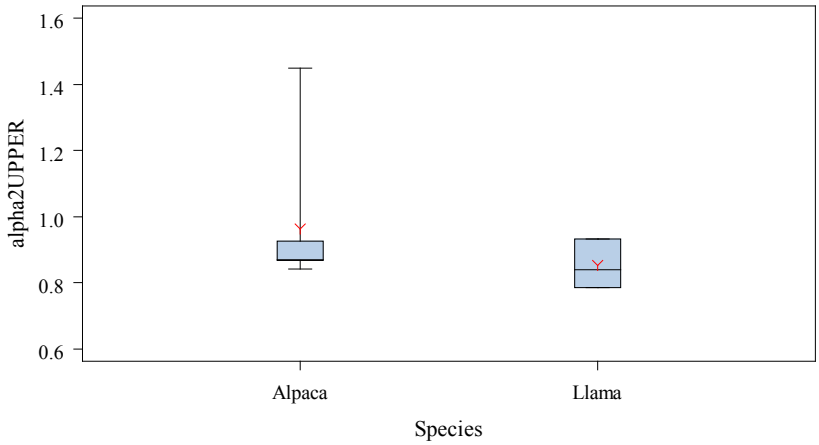

Animal SAS Analysis

alpha2UPPER

DIR=LB Load=nL

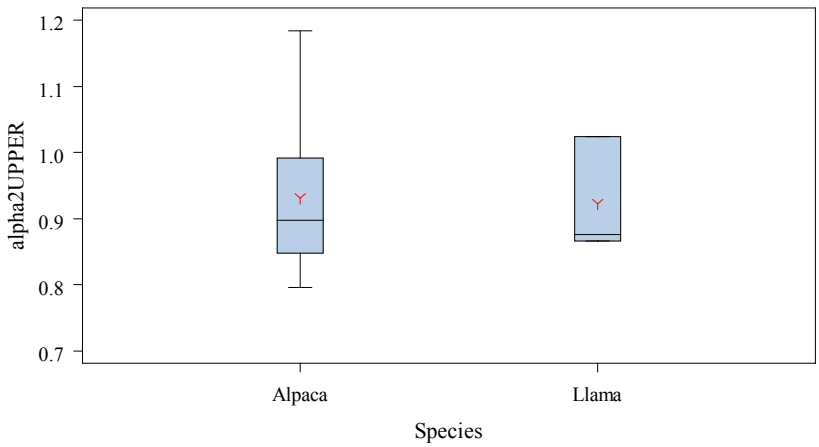

Animal SAS Analysis

m2UPPER

DIR=AR Load=nL

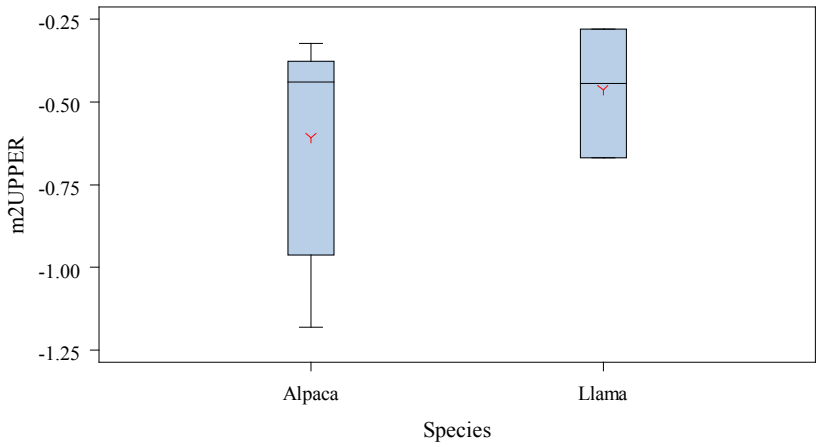

Animal SAS Analysis

m2UPPER

DIR=FE Load=nL

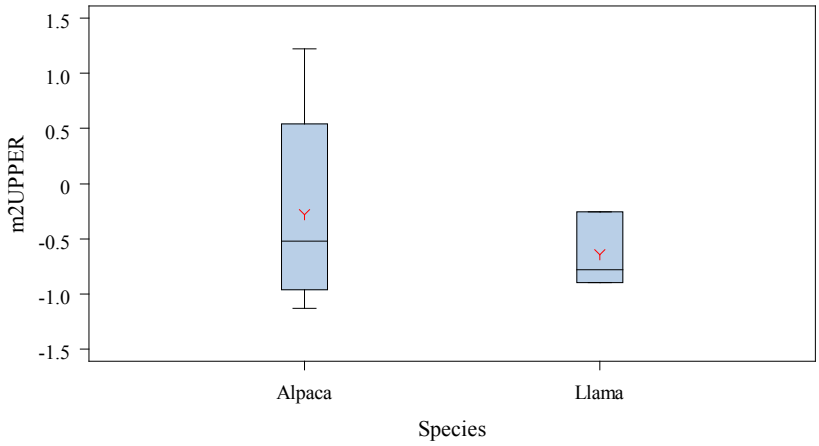

Animal SAS Analysis

m2UPPER

DIR=LB Load=nL

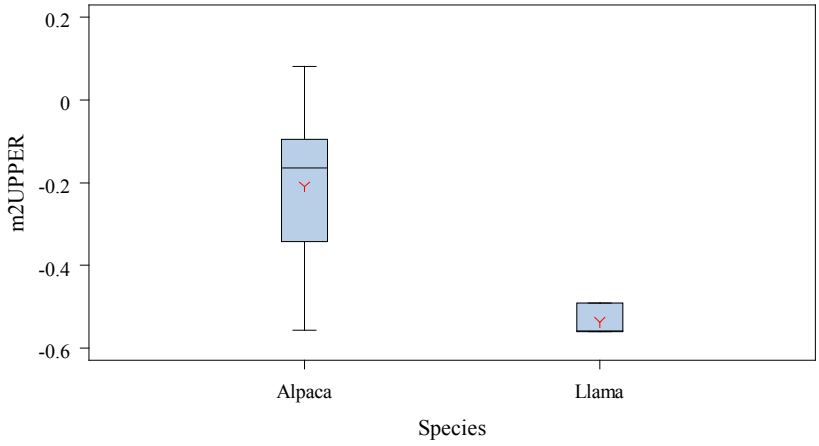

Animal SAS Analysis

alpha1LOWER

DIR=AR Load=nL

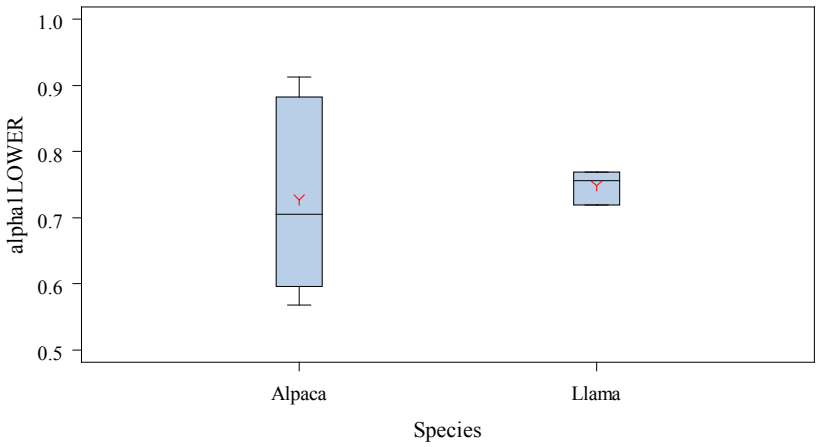

Animal SAS Analysis

alpha1LOWER

DIR=FE Load=nL

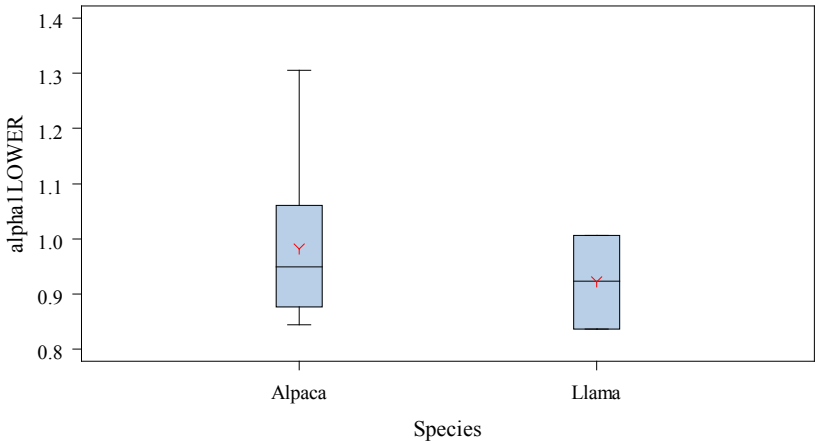

Animal SAS Analysis

alpha1LOWER

DIR=LB Load=nL

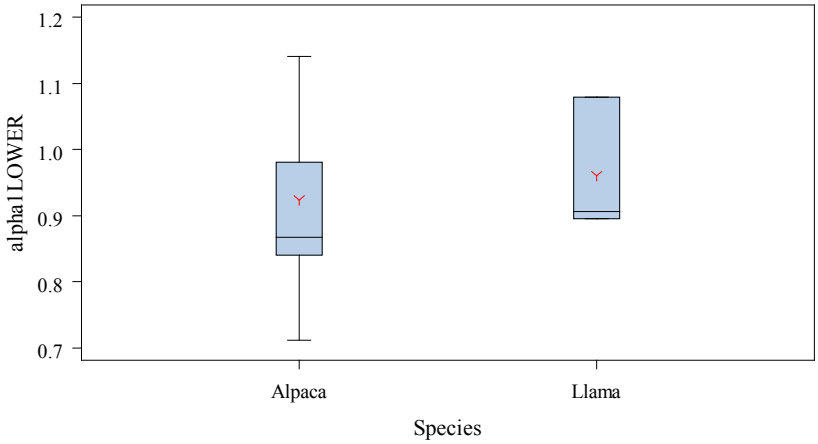

Animal SAS Analysis

M1LOWER

DIR=AR Load=nL

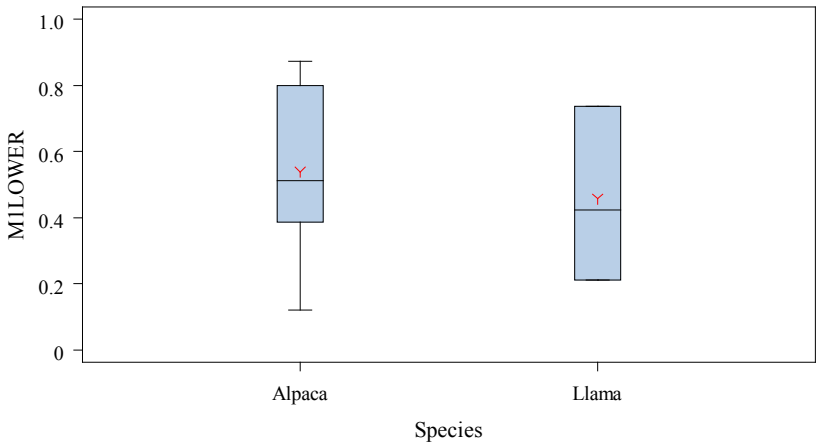

Animal SAS Analysis

M1LOWER

DIR=FE Load=nL

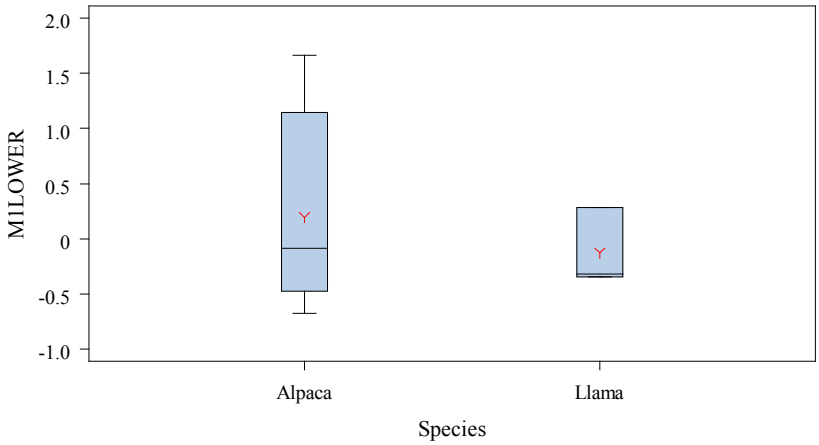

Animal SAS Analysis

M1LOWER

DIR=LB Load=nL

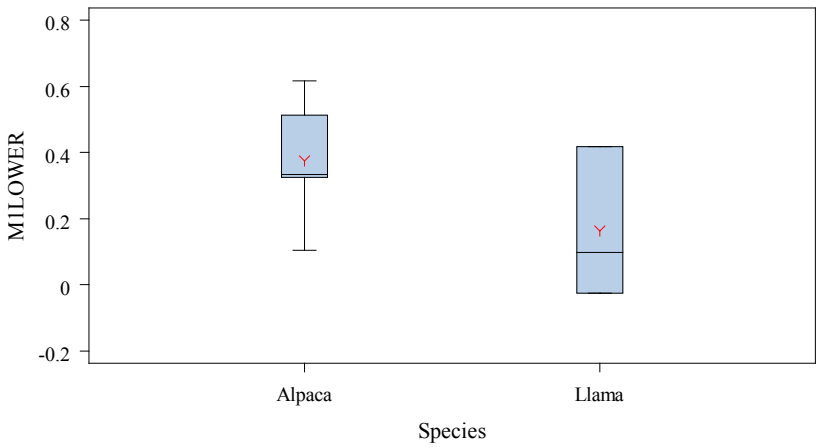

Animal SAS Analysis

alpha2LOWER

DIR=AR Load=nL

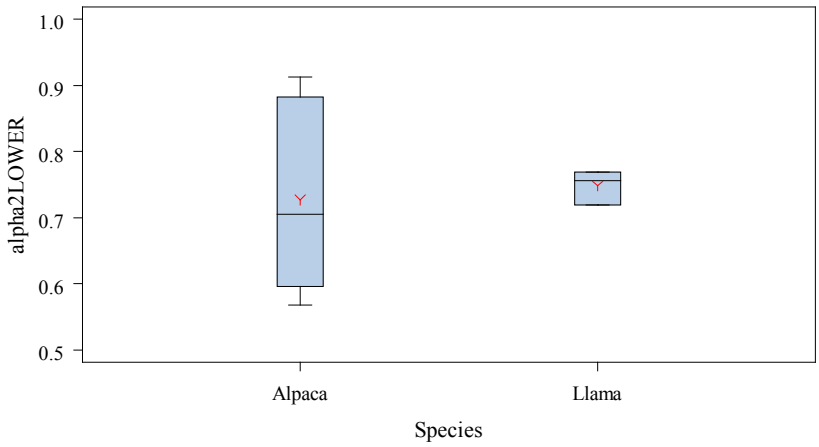

Animal SAS Analysis

alpha2LOWER

DIR=FE Load=nL

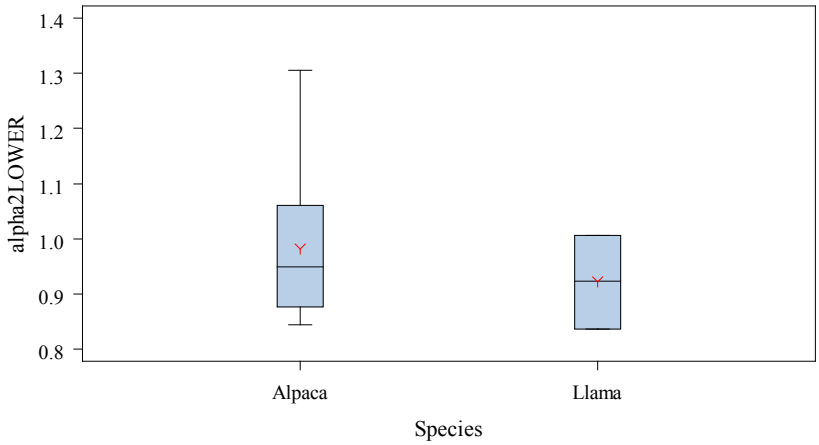

Animal SAS Analysis

alpha2LOWER

DIR=LB Load=nL

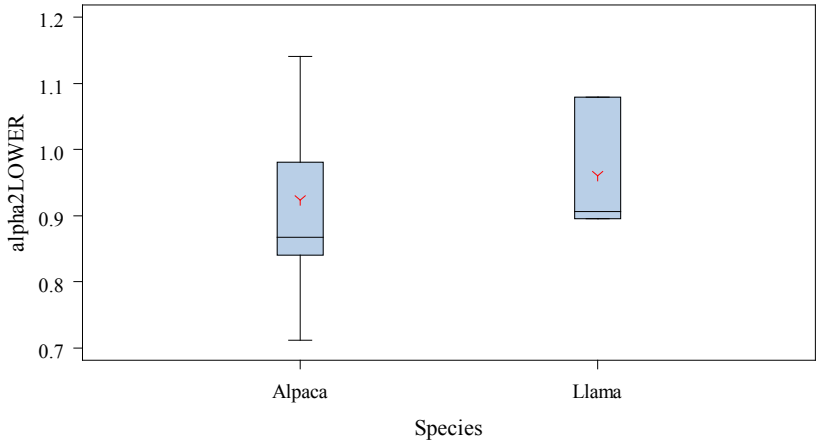

Animal SAS Analysis

m2LOWER

DIR=AR Load=nL

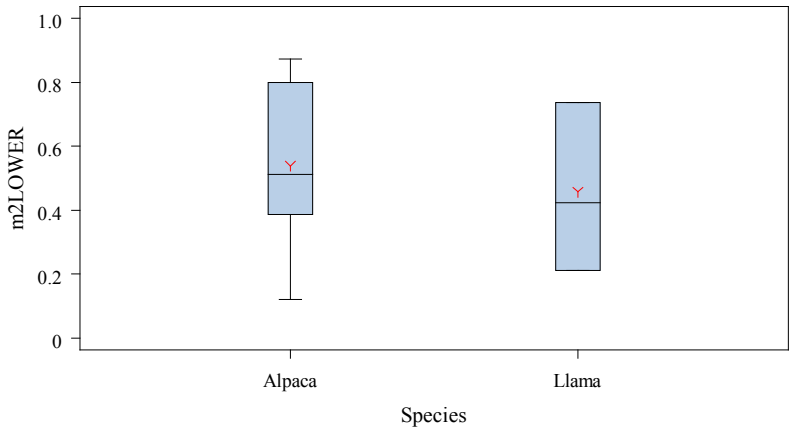

Animal SAS Analysis

m2LOWER

DIR=FE Load=nL

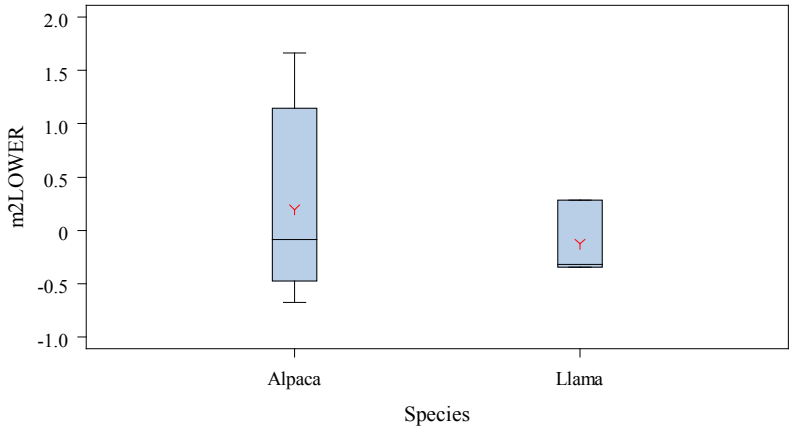

Animal SAS Analysis

m2LOWER

DIR=LB Load=nL

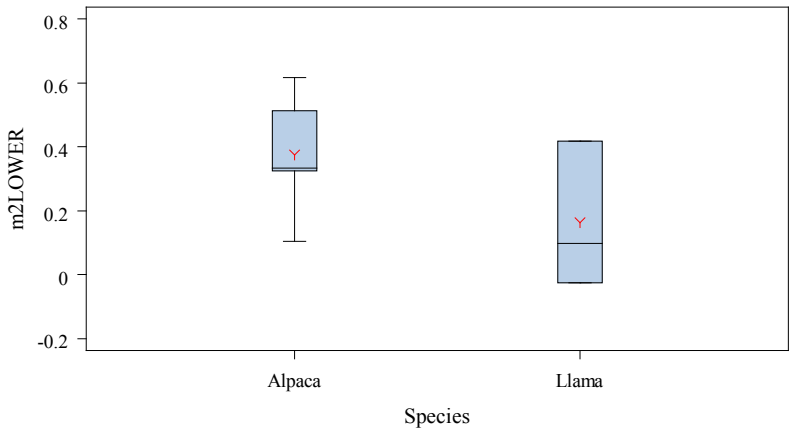

APPENDIX C: COMPOSITE MRI IMAGES OF ALPACA SPINES

This images were put together by Dr. John Wendel, and were used by Dr. Wendel and Dr. Suzanne Stiegar-Vanegas for assigning a degeneration rating using the Pfirrmann grade. The first image (below) is an exemplar of a grade 1 (top) through grade 5 (bottom), according to the Pfirrmann grade. The following images are of each of the 20 alpacas that was scanned, with one alpaca, named "SuzyQ," scanned twice.

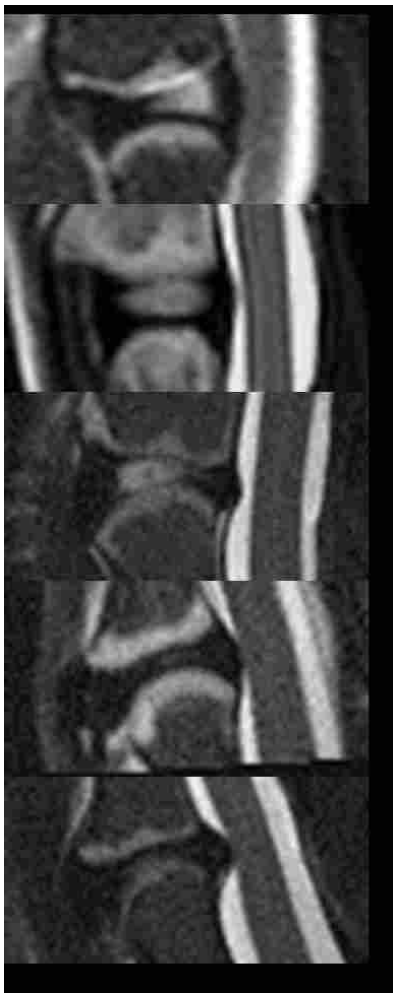


C1
C2
C3
C4
C5
C6
C7
T1
Dove
C1
C2
C3
C4
C5
C6
C7
T1
Breeze


C1
C2
C3
C4
C5
C6
C7
Anasette


C1
C2
C3
C4
C5
C6
C7
Mi Corazon

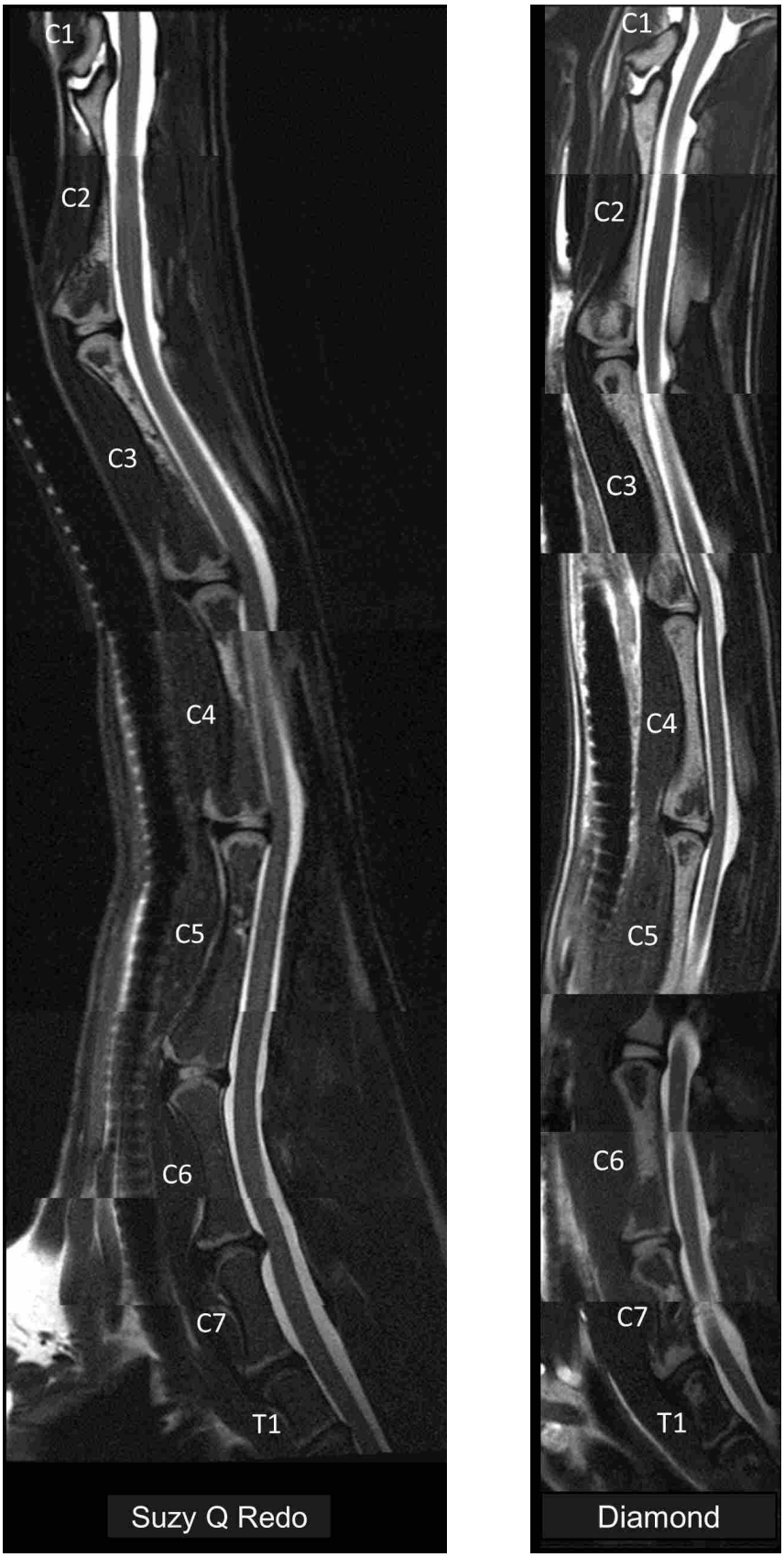
C1
C2
C3
C4
C5
C6
C7
T1
Suzy Q Redo
C1
C2
C3
C4
C5
C6
C7
T1
Diamond

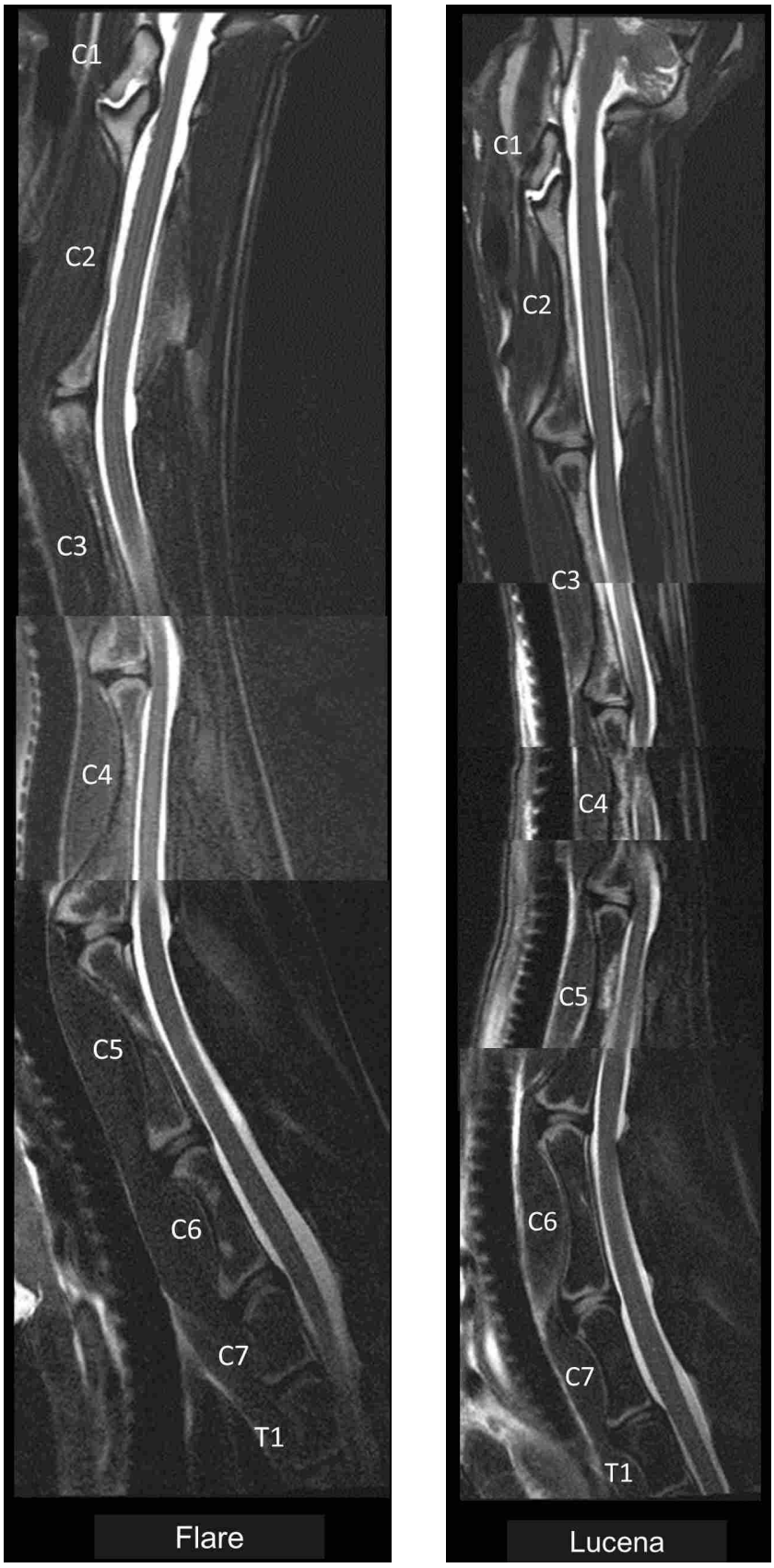
C1
C2
C3
C4
C5
C6
C7
T1
Flare
C1
C2
C3
C4
C5
C6
C7
T1
Lucena

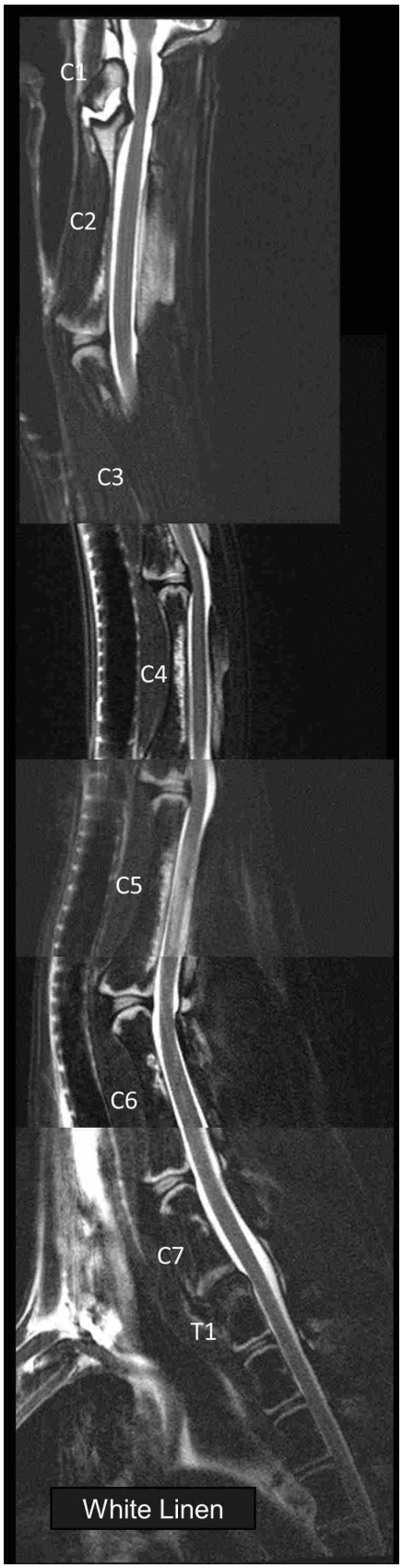
C1
C2
C3
C4
C5
C6
C7
T1
White Linen


C1
C2
C3
C4
C5
C6
C7
T1
Montero Elena

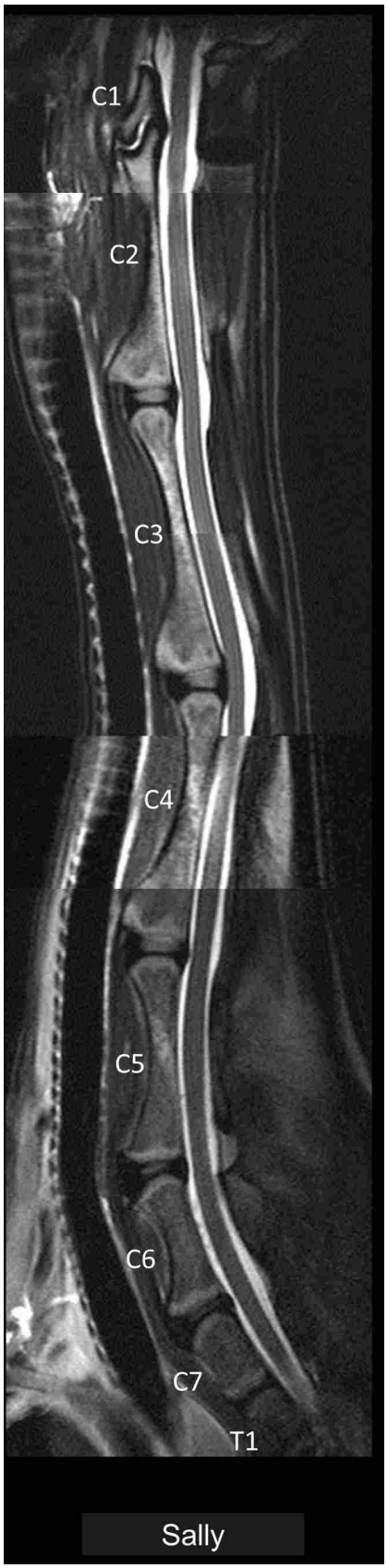
C1
C2
C3
C4
C5
C6
C7
T1
Sally

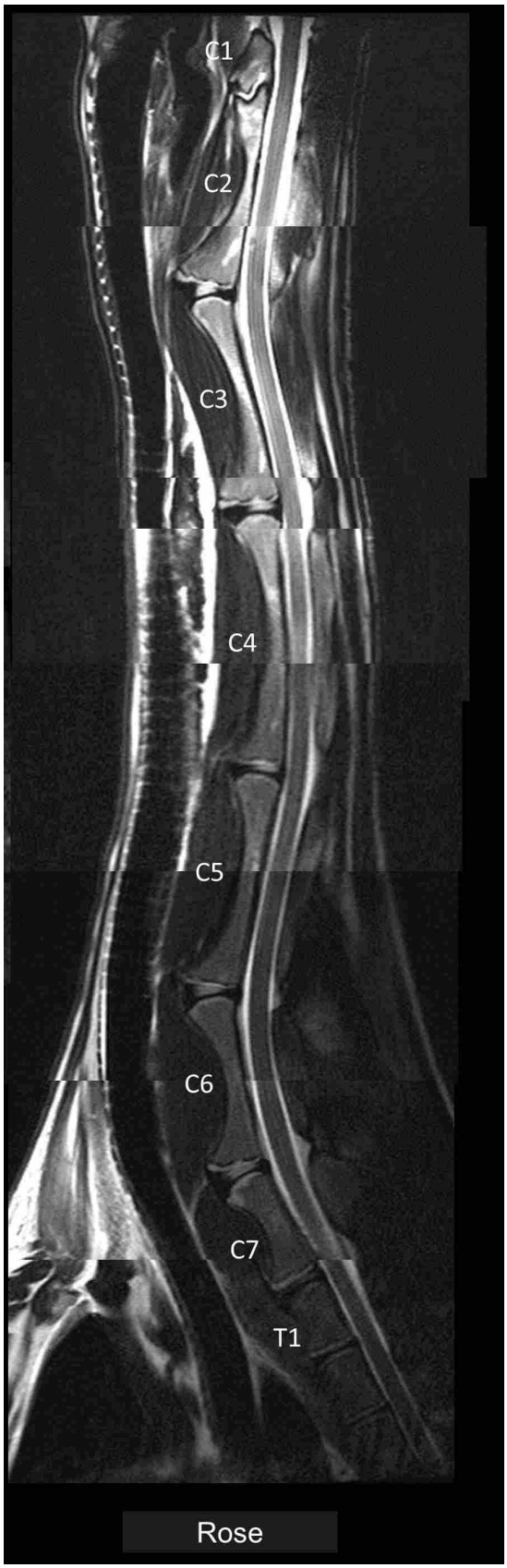
C1
C2
C3
C4
C5
C6
C7
T1
Rose


C1
C2
C3
C4
C5
C6
C7
T1
Allice
C1
C2
C3
C4
C5
C6
C7
T1
Fazenada


C1
C2
C3
C4
C5
C6
C7
T1
Claudette

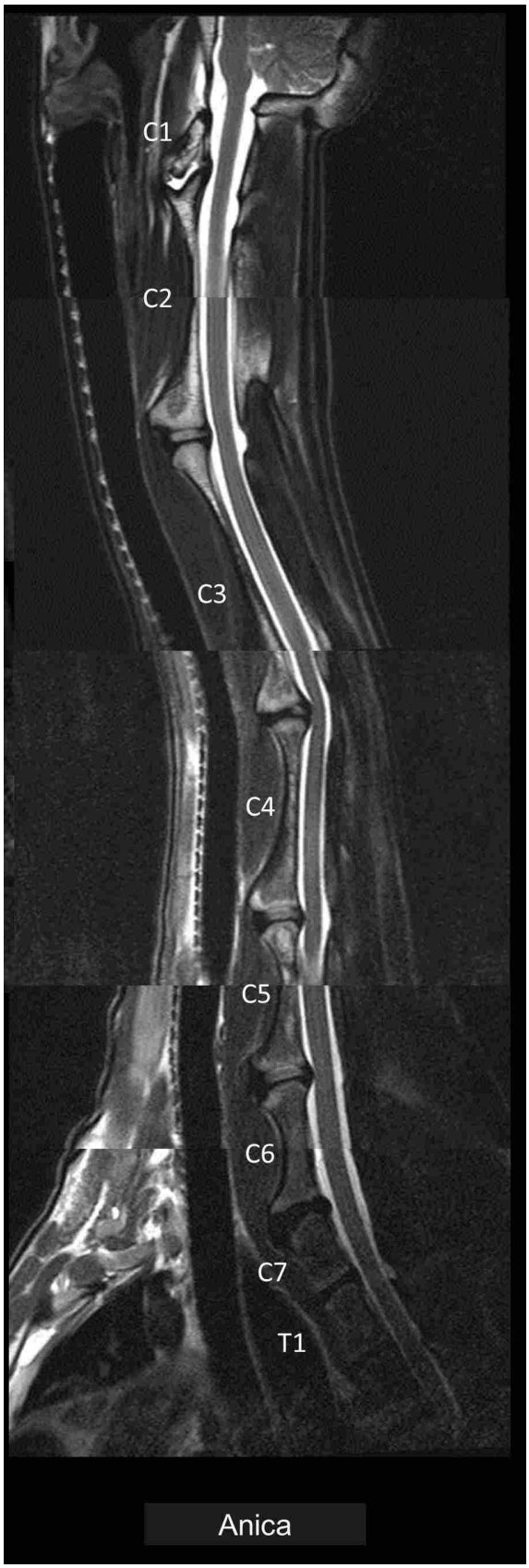
C1
C2
C3
C4
C5
C6
C7
T1
Anica

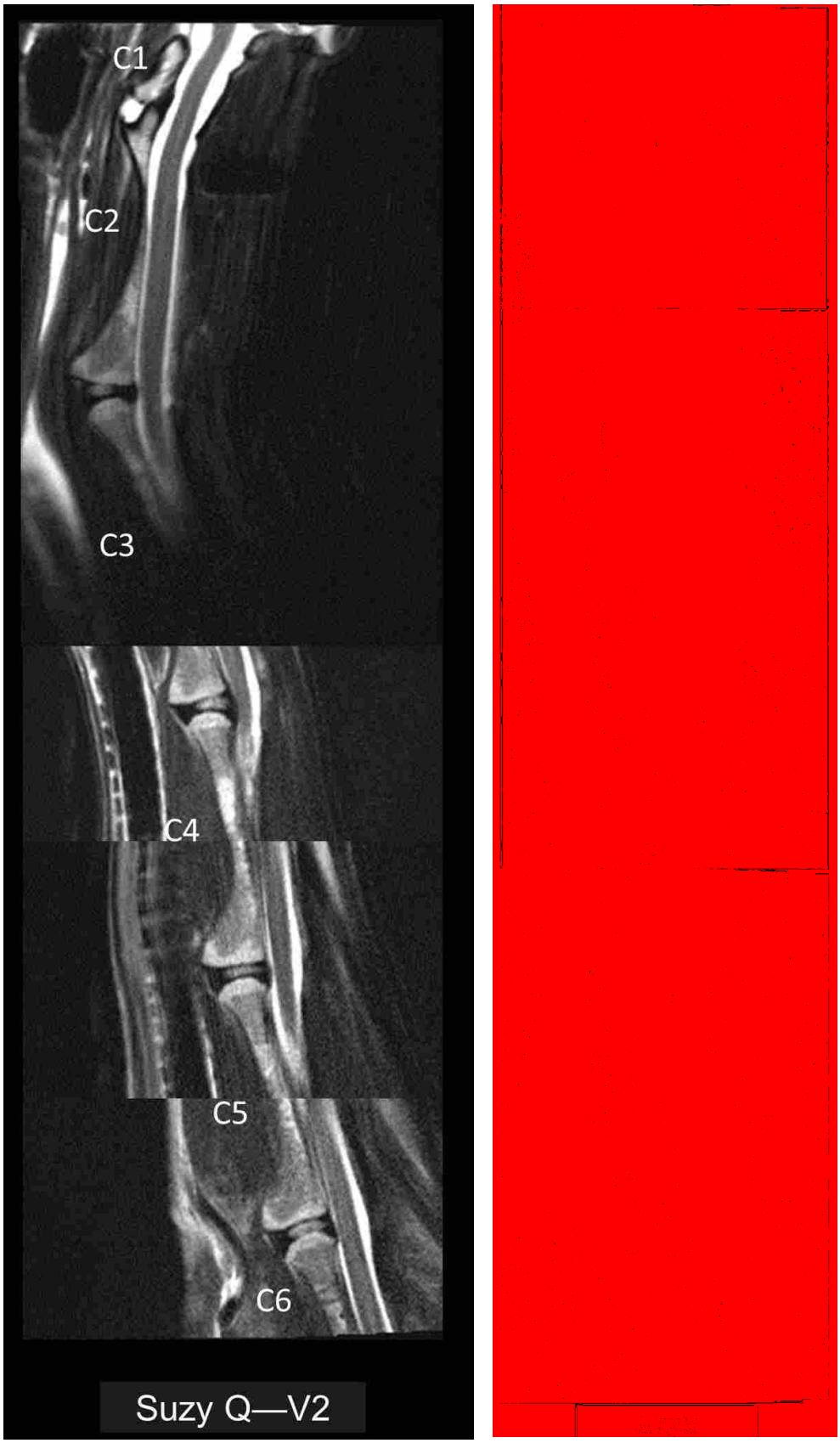
C1
C2
C3
C4
C5
C6
Suzy Q—V2

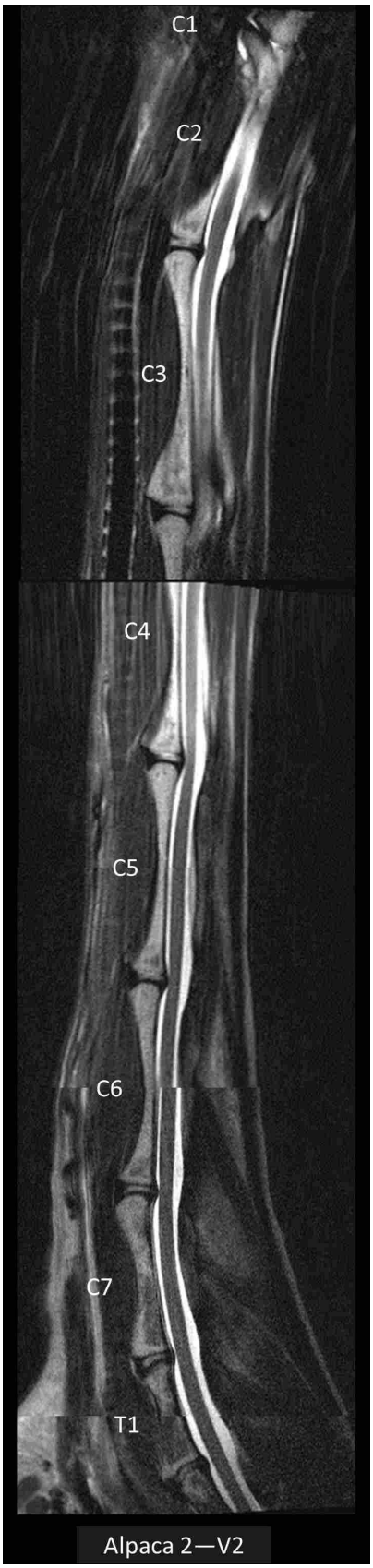
C1
C2
C3
C4
C5
C6
C7
T1
Alpaca 2—V2


C1
C2
C3
C4
C5
C6
C7
T1
Alpaca 1


C1
C2
C3
C4
C5
C6
C7
T1
Dona

APPENDIX D – DYNAMIC BIOREACTOR PROTOCOLS

D.1 FSU Retrieval

Materials

PBS-Solution
Dissection Mats
Latex/Nitrile Gloves
Safety Glasses
Face-Shield
Dissection Gown & booties
Band-saw or sawzall
Dremel-tool w/ wheel blades
Scalpels: handles & blades

Procedure

Immediately following the time of donor "death" (TOD), and obtaining the cervical spine

> *Note: Time of death may refer to the time that the animal/donor dies, or the time that a tissue sample was removed from a living donor. However, this must be exclusive for all samples in the test group (i.e., all the tissue samples must come from living donors, or all the samples must come from a donor following death) in order to maintain consistency in the supporting environment of the cell/tissue.*

1. In lab notebook, mark the TOD of animal.
2. Thoroughly wet the entire cervical spine with PBS solution.
3. Locate the IVD of interest using palpation techniques.
4. Using a saw (bandsaw, sawzall, or Dremel-tool w/ wheel blade), make a mid-transverse cut through the superior and inferior vertebra, adjacent to the IVD of interest, and remove the vertebra-IVD-vertebra section from the rest of the tissue.
5. Use the bandsaw or scalpel to remove any peripheral soft-tissue that may contribute stiffness to the IVD joint.

****The FSU is now clean and ready for Flexibility Studies or see additional prep for culture and/or staining.***

D.2 IVD Preparation (For Static Culture or Live/Dead Staining)

Materials

PBS-Solution
Dissection Mats
Latex/Nitrile GlovesSafety Glasses
Face-Shield
Dissection Gown & bootiesBand-saw or sawzall
Dremel-tool w/ wheel blades
Scalpels: handles & blades

Procedure

1. Using a saw (bandsaw, sawzall, or Dremel-tool w/ wheel blade), remove bony vertebrae down to the endplate.
2. Place the IVD in a beaker with a solution of DMEM + Pen/Strep (antiseptic) and transport to a clean facility.
3. Drop the IVD into a small beaker containing ethanol and retrieve using the long forceps.
4. Transfer the IVD into the large, sterile fume hood.
5. Tap off the excess ethanol before passing the disk over a flame (with long forceps) to burn off all impurities and contaminants.

The disk is now clean and must not leave the sterile zone (i.e., fume hood).

6. Clean off all musculature and bony endplate whilst in the hood using a sterile scalpel.
    a. Make a transverse cut through the superior bony vertebral endplate.
        i. Remove as much of the bony endplate as safely possible
    b. Make a transverse cut through the inferior bony vertebral endplate.
        i. Using a various cutting tools (e.g., scalpel, Dremel®), remove as much of the bony endplate as safely possible**

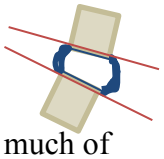

7. Use the dremel tool (sanitized/clean) and a sterile end-mill bit to remove the bony endplate, leaving only the cartilage endplate.
8. Use sterile saline to rinse off shavings/debris from cuts.
9. ***The disk is now ready for culture or staining.***
    a. ***For static culture…***Place the disc into the IVD culture medium
    b. ***For live/dead staining…*** Place the disc into the live/dead stain solution.

D.3 IVD Preparation (For Dynamic Bioreactor Culture)

Materials

PBS-Solution
Dissection Mats
Latex/Nitrile Gloves
Safety Glasses
Face-Shield
Dissection Gown & booties
Band-saw or sawzall
Dremel-tool w/ wheel blades
Scalpels: handles & blades

Procedure

Immediately following the time of donor "death" (TOD), and obtaining the cervical spine

Note: Time of death may refer to the time that the animal/donor dies, or the time that a tissue sample was removed from a living donor. However, this must be exclusive for all samples in the test group (i.e., all the tissue samples must come from living donors, or all the samples must come from a donor following death) in order to maintain consistency in the supporting environment of the cell/tissue.

1. Use the bandsaw or scalpel to remove any peripheral soft-tissue that may interfere with cuts through the superior/inferior endplates.
2. Place the IVD in a beaker with a solution of DMEM + Pen/Strep (antiseptic) and transport to clean facility for cell culture or staining
3. Drop the IVD into a small beaker containing ethanol and retrieve using the long forceps.
4. Transfer the IVD into the large, sterile fume hood.
5. Tap off the excess ethanol before passing the disk over a flame (with long forceps) to burn off all impurities and contaminants.

****The disk is now clean and must not leave the fume hood.***

6. Clean off all musculature whilst in the hood using a sterile scalpel.
7. Using the Dremel End-mill tool (sterilized), remove the anterior and posterior vertebral bodies (caudal and cephalic). Using this access point
    a. Remove as much of the bony endplate as safely possible
    b. Using the Dremel End-mill tool (sterilized), or other various cutting tools (sterilized) (e.g., scalpel, Dremel®), remove as much of the bony endplate as safely possible**

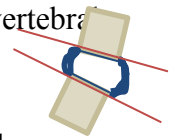

It is advised that the cartilage endplate be left intact as much as possible to discourage swelling of the disk

8. Using the PBS-solution (sterile) clean the IVD to remove any blood, and bone-fragments

You should now have a whole, single IVD.

9. Once cleaned, the disk can be placed onto the stand within the Dynamic Bioreactor and covered with culture medium.
10. Remove bioreactor from the fume hood and transport to a 5% CO_2 incubator.

****All lids and openings of the bioreactor must be tightly closed while transported out of the fume hood, once within the incubator lids must be loosened to allow for flow of Co_2 into the bioreactor.***

11. Change the medium in the bioreactor approximately every 3 days to continue optimal nutrient flow through the disk.
12. Batteries connected to the bioreactor need to be swapped at least once a day so the pump never stops.

*****The small battery is charged at the outlet by the sink within the clean room, the large battery is charged at the outlet by the refrigerator in the lab area.***

Note: the pump should be on the lowest setting to have a relaxed medium flow through the bioreactor.

D.4 Live/Dead Stain Solution

Stain Ingredients

- 30mL DMEM
- 6 µL Cell-Tracker Green
- 30 µL Propidium Iodide

Staining Procedure

1. Spray the bioreactor and wipe off the excess ethanol with kimtech wipes before bringing under the sterile hood.

Tighten the lids of the bioreactor before removing from incubator

2. Under the hood, remove disk from the bioreactor using sterile forceps and transport into the beaker of dye previously prepared under the hood
3. Remove the beaker from the fume hood (at this point contamination is of no concern)

4. Pump the disk within the medium for 5 minutes before incubating; induce loading in both lateral bending and flexion extension ranges of motion for even distribution of dye.
5. Cover the entire beaker with aluminum foil to keep light from disrupting the proteins within the dye
6. Transport to a 37˚ incubator for 45 minutes
7. After incubating wash the disk briefly with PBS solution to remove excess dye; , induce loading in both lateral bending and flexion extension ranges of motion for even washing
8. Wrap in aluminum foil
9. Flash freeze the disk in liquid nitrogen for 10 seconds by placing the disk in a plastic box within the storage racks, and submerging within the liquid nitrogen.
10. Once flash frozen the disk can be bound to a cryostat using OCT tissue solution.
11. Samples from the disk can now be taken using the cryostat and placed on slides by gently pressing the slide on top of the sample cut from the disk within the cryostat.
12. View samples under the fluorescent microscope in the RIC facility on the 8th floor of the WIDB.

D.5 IVD Culture Medium Preparation(for Static Culture or Dynamic Bioreactor)

Ingredients

- 500 mL high-glucose DMEM (w/ 4500 mg Glucose/L + 0.584 g L-glutamine /L + 3.7 g $NaHCO_3$ /L).
- 100 mL FBS (20%)
- 12.5 mL HEPES
- 12.5 uL ascorbate (L-ascorbic acid)
- 1.0 mL Pen/Strep
- 500 uL Gentamycin
- 3 mL Fungizone
- 55 mg Sodium Pyruvate
- 1403 mg NaCl (added 40 mM)

Sterile Requirements

Note: It is important that the medium remain sterile throughout this process so the final product and various chemicals involved stay free from contaminants.

- ❖ Containers and instruments must be autoclaved before use and not opened until within the fume hood to keep sterile.
- ❖ All ingredients must be mixed within a sterile fume hood in the clean room

- Anything exposed to air within the lab (or clean room) is considered unsterile
- Everything brought into the fume hood must be sprayed with 70% ethanol for sterilization .
- The person mixing the medium must wear gloves that were sterilized with ethanol before brought to work under the hood.

❖ Although it is considered clean within the fume hood, care must be taken in case contaminants are present
❖ Pipet tips must be replaced before using a different chemical.
❖ The pipette-er must take great care not to touch the pipette tip to anything throughout the process to ensure the tip remain sterile:if contact is made to potentially unsterile objects, change the pipette tip.
❖ Avoid the lips of containers when retrieving chemicals as that is the most likely place for contaminants to reside (It may help to tip bottles in order to access the chemicals without inserting the pipette fully into the container).

Mixing Procedure

Strictly observing the sterile requirements (above), mix all ingredients within the DMEM container

1. Thaw FBS, Pen/Strep, [other frozen ingredients].
    a. Place in zip-loc bags to avoid direct contact with water
    b. Submerge chemicals in a 37° incubation bath until the chemicals have thawed completely
2. Using the large (25 mL) pipette, transfer 100-mL FBS to DMEM
3. Using the large (10 mL)pipette, transfer 12.5 mL HEPES to DMEM
4. Using the 20 uL pipette, transfer 12.5 uL ascorbate to DMEM
5. Using the 1000 uL pipette, transfer 1 mL penn/strep to DMEM
6. Using the 1000 uL pipette, transfer 500 uL gentamycin to DMEM
7. Using the 1000 uL pipette, or the lare (5 mL) pipette, transfer 3 mL fungizone to DMEM
8. Once all the sterile chemicals have been mixed into DMEM, remove container from the sterile fume hood to add the potentially unsterile powder chemicals to the solution
    a. Measure 55 mg of sodium pyruvate and 1403 mg NaCl on an accurate weight scale, using clean weigh boats and spatulas to transfer and weigh chemicals to avoid excess contaminants
    b. Add chemicals into DMEM outside of the fume hood and carefully swill the bottle to dissolve the powders
9. Sterilize the DMEM and filter package with ethanol before bringing into the fume hood

10. Assemble the filter and attach the vacuum pump under the fume hood (making sure all containers on the filter are tight to allow for a tight vacuum and fast filtration)
11. Pour the medium into the top container and turn on the vacuum pump from beneath the fume hood to begin filtration
12. Once the medium has been pulled through the filter into the container below, remove filter and screw on the sterile lid contained within the filter package
13. Parafilm the seam around the lid of the container and label the bottle BABEL before storing in the fridge until needed